ENERGY DENSIFICATION OF CARBOHYDRATE-DERIVED CHEMICAL PLATFORMS BY CATALYTIC HYDROGENATION AND ESTERIFICATION REACTIONS

Thesis

Submitted in partial fulfilment of the requirements for the degree of

DOCTOR OF PHILOSOPHY

by

NIVEDHA VINOD

DEPARTMENT OF CHEMISTRY

NATIONAL INSTITUTE OF TECHNOLOGY KARNATAKA,

SURATHKAL, MANGALURU-575025

JANUARY, 2024

ENERGY DENSIFICATION OF CARBOHYDRATE-DERIVED CHEMICAL PLATFORMS BY CATALYTIC HYDROGENATION AND ESTERIFICATION REACTIONS

Thesis

Submitted in partial fulfilment of the requirements for the degree of

DOCTOR OF PHILOSOPHY

by

NIVEDHA VINOD

Reg. No: 197025CY005

DEPARTMENT OF CHEMISTRY

NATIONAL INSTITUTE OF TECHNOLOGY KARNATAKA,

SURATHKAL, MANGALURU-575025

JANUARY, 2024

DECLARATION

By the Ph.D. Research Scholar

I hereby *declare* that the Research Thesis titled **"Energy densification of carbohydrate-derived chemical platforms by catalytic hydrogenation and esterification reactions,"** which is being submitted to the ***National Institute of Technology, Karnataka, Surathkal,*** in partial fulfilment of the requirements for the award of the *Degree* of ***Doctor of Philosophy*** in ***Chemistry*** is *a bonafide report of the research work carried out by me*. The materials contained in this Research Thesis have not been submitted to any University or Institution for the award of any degree.

NIVEDHA VINOD
Registration No.: 197025CY005
Department of Chemistry

Place: NITK Surathkal
Date: 15-01-2024

CERTIFICATE

This is to *certify* that the Research Thesis titled **"Energy densification of carbohydrate-derived chemical platforms by catalytic hydrogenation and esterification reactions,"** submitted by **NIVEDHA VINOD** (Registration Number: 197025CY005) as the record of the research work carried out by her, is *accepted* as the *Research Thesis submission* in partial fulfilment of the requirements for the award of the degree of ***Doctor of Philosophy***.

Saikat Dutta
18/01/2024

Dr. Saikat Dutta
Supervisor
Associate Professor
Department of Chemistry
NITK Surathkal-575025

19/01/2024
Chairman - DRPC

विभागाध्यक्ष / H.O.D.
रसायन शास्त्र विभाग/ Chemistry Dept.
राष्ट्रीय प्रौद्योगिकी संस्थान कर्नाटक, सुरत्कल
NITK SURATHKAL
मंगलूरु-५७५ ०२५, कर्नाटक
MANGALURU-575 025, KARNATAKA

ACKNOWLEDGEMENT

I am privileged to thank my research supervisor, Dr. Saikat Dutta, for giving me this excellent opportunity to work under his supervision. I am greatly indebted to him for his enthusiasm, guidance, and constant support throughout the course of my Ph.D.

I am grateful to my Research Progress Assessment Committee members, Dr. Sib Sankar Mal, Department of Chemistry, and Dr. Kartick Tarafder, Department of Physics, for their timely evaluation and valuable suggestions on my work. I would like to thank the HOD, Department of Chemistry, Prof. Darshak R Trivedi. I am thankful to NITK for providing financial assistance in terms of scholarship and research contingency during my Ph.D. I am grateful to all faculties, students, and staff members in the Department of Chemistry, NITK, for all the support I received during my Ph.D. I thank the Central Research Facility, NITK, and Mangalore University for supplying the analytical and spectral data.

I would like to extend my sincere thanks to Dr. Harshitha N Anchan, Mr. Gopikrishnan K., Mr. Poornachandra S. P., Mr. Abhishek Kumar Yadav, Mr. Sandeep Kumar Yadav, Ms. Megha B. N., Mr. Prajwal Naik C, and Mr. Panchakshari Swami. Many thanks to Dr. Navya Subray Bhat and Dr. Rasmi Bhaskaran P. who have always been there for me throughout my Ph.D. journey. I would like to thank Dr. Neethu Ravindran M., Dr. Anjana A.V., Dr. Sukanya Maity, and Dr. Subhasmita Ray for their continuous support.

I am thankful to my parents and family for their support and encouragement. Many thanks to all those who have made this happen.

Nivedha Vinod

ABSTRACT

Biomass-derived abundant and non-food polymeric carbohydrates (e.g., cellulose) have been identified as suitable biogenic carbon to synthesize transportation fuels, organic chemicals, and polymers. Catalysis remains at the heart of biorefinery research, which ensures energy efficiency, affords high product selectivity and yield, lessens materials input, and minimizes waste generation. The acid-catalyzed hydrolysis and dehydration of heavily functionalized and oxygenated biopolymers like cellulose into 5-(hydroxymethyl)furfural (HMF) is an elegant chemocatalytic value addition pathway of biomass. Other carbohydrate-derived compounds formed under acid hydrolysis conditions include furfural (FF) and levulinic acid (LA). Isosorbide (IS) can be formed from cellulose by catalytic steps involving hydrolysis, hydrogenation, and dehydration reactions. HMF, FF, LA, and IS have been identified as renewable chemical platforms for synthesizing wide classes of compounds of commercial significance. The value addition pathways often involve removing oxygen atoms and adding more hydrogen and carbon atoms in the structure for higher energy density. Humin, a complicated furan-based polymer, is formed as a side product during the acid-catalyzed dehydration of carbohydrates. Significant research has focused on minimizing humin formation and developing value-addition pathways of this waste material. This work developed solid acid and noble metal-based catalysts supported on humin-derived activated carbon (HAC) for the synthetic value addition of FF, HMF, and LA. γ-Butyrolactone (GBL) and γ-valerolactone (GVL), with potential applications as fuel oxygenates and green solvents, have been produced by catalytic hydrogenation of their precursors (i.e., 2-furanone and angelica lactone) using the Pd/HAC catalyst. Ethyl levulinate (EL), a potential diesel additive, has been produced by the esterification of LA and ethanolysis of furfuryl alcohol, respectively, using phosphotungstic acid supported on HAC. Various mono- and diesters of IS, with potential applications as renewable surfactants and plasticizers, have been reported using the transesterification reaction in the presence of an anhydrous K_2CO_3 catalyst. All the catalysts and the synthesized products were characterized extensively.

Keywords*: Biomass valorization; Heterogeneous catalysis; Humin; Activated carbon; Alkyl levulinates; γ-Butyrolactone; γ-Valerolactone; Isosorbide esters.*

TABLE OF CONTENTS

LIST OF FIGURES

CHAPTER 1

CHAPTER 3

CHAPTER 6

LIST OF SCHEMES

CHAPTER 1

CHAPTER 3

CHAPTER 4

CHAPTER 5

CHAPTER 6

LIST OF TABLES

CHAPTER 2

CHAPTER 3

CHAPTER 4

CHAPTER 5

CHAPTER 6

LIST OF ABBREVIATIONS

AC	Activated carbon
AGL	α-Angelica lactone
AL	Alkyl levulinate
ASTM	American society for testing and materials
BJH	Barrett–Joyner–Halenda
BTBAC	Benzyltributylammonium chloride
BL	Butyl levulinate
BET	Brunauer-Emmett-Teller
DCE	1,2-Dichloroethane
DI	Deionized
EDX	Energy dispersive X-ray analysis
EL	Ethyl levulinate
FAL	Furfuryl alcohol
FESEM	Field emission scanning electron microscopy
FF	Furfural
FTIR	Fourier-transform infrared
GBL	γ-Butyrolactone
GVL	γ-Valerolactone
HAC	Humin-derived activated carbon
HMF	5-(Hydroxymethyl)furfural
HPA	Heteropoly acid
HR-TEM	High resolution transmission electron microscopy
II	Isoidide
IIDB	Isoidide-2,5-dibenzoate
IIDF	Isoidide-2,5-difuroate
IIMB	Isoidide-2-monobenzoate
IIMF	Isoidide monofuroate

IM	Isomannide
IMDAr	Isomannide diacrylate
IMDB	Isomannide-2,5-dibenzoate
IMDL	Isomannide dilevulinate
IMDO	Isomannide dioleate
IMML	Isomannide monolevulinate
IMMO	Isomannide monooleate
IMMB	Isomannide-2-monobenzoate
IMMF	Isomannide monofuroate
IN	Iodine number
IS	Isosorbide
ISDA	Isosorbide-2,5-diacetate
ISDAr	Isosorbide diacrylate
ISDB	Isosorbide-2,5-dibenzoate
ISDF	Isosorbide-2,5-difuroate
ISDL	Isosorbide dilevulinate
ISMB	Isosorbide monobenzoate
ISMF	Isosorbide monofuroate
ISDO	Isosorbide dioleate
ISML	Isosorbide monolevulinate
ISMO	Isosorbide monooleate
LA	Levulinic acid
ML	Methyl levulinate
PL	Propyl levulinate
PTA	Phosphotungstic acid
PXRD	Powder X-ray diffraction
TCD	Thermal conductivity detector
TGA	Thermogravimetric analysis
THF	Tetrahydrofuran
TPD	Temperature-programmed desorption

LIST OF SYMBOLS

α	Alpha
Å	Angstrom
β	Beta
cc	Cubic centimeter
°C	Degree Celsius
δ	Delta
eq.	Equivalent
γ	Gamma
g	Gram
h	Hour
Hz	Hertz
kV	Kilovolt
L	Liter
M	Molar
mg	Milligram
MHz	Megahertz
min	Minute
mL	Milliliter
mmol	Millimole
mol%	Mole percent
nm	Nanometer
ppm	Parts per million
%	Percentage
cm^{-1}	Reciprocal centimeters
s	Second
θ	Theta
wt.%	Weight percent

CHAPTER 1

GENERAL INTRODUCTION

1.1 INTRODUCTION

Over the past century, substantial research on petrorefinery has furnished the processes increasingly competent and established petroleum as the primary resource for transportation fuels, chemicals, and materials (He et al. 2023). However, the increasing gap between demand and supply of petroleum-derived fuels, chemicals, and materials creates volatility in the market due to geopolitical tensions and exacerbated environmental complications caused by the excessive release of anthropogenic carbon into the biosphere (Okolie et al. 2022). According to the United States Department of Energy (US-DOE), crude oil production in the USA reached a new record of 12.4 million per day in 2023 and surpassed the previous 12.3 million per day in 2019 (Figure 1.1). Crude oil prices are increasing over time due to the disparity between demand and supply, aggravated by depleting petroleum reserves and geopolitical complications over the global supply chain. Moreover, the excess addition of carbon dioxide in the biosphere creates a kinetic imbalance leading to serious environmental complications, such as global warming and climate shift. Therefore, securing an economically viable and sustainable carbon-based feedstock that can substitute petroleum in producing transportation fuels, organic chemicals, and synthetic polymers is the need of the day.

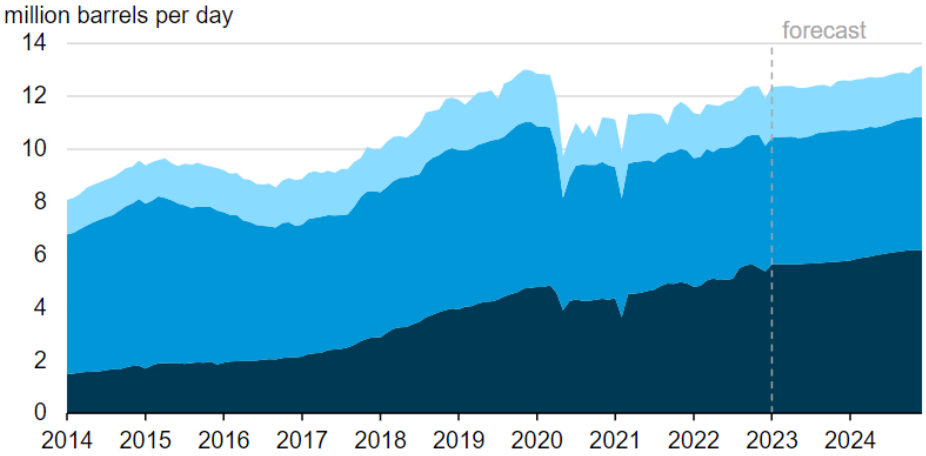

Figure 1.1 Crude oil production in the USA (2014-2024) according to the United States Department of Energy (https://www.eia.gov/todayinenergy/detail.php?id=55299#).

The aim for a sustainable future that was once primarily driven by stricter environmental regulations and the public outlook is now also supported by economic incentives. This has led to the search for alternative renewable feedstocks for producing

fuels and chemical building blocks. In this regard, biomass has shown promise as a renewable feedstock to supplant petroleum in the transportation sector and organic chemical industries (Wang et al. 2023a). Adopting biomass-derived fuels and chemicals would help relieve the economic and environmental distresses triggered by the excessive use of petrofuels and petrochemicals. Biomass in the form of cellulosic waste and terrestrial lignocellulosics is abundant, inexpensive, geographically diverse, renewable, and carbon–neutral (Devi et al. 2022). The suitable integration of renewable, carbon-neutral biomass in the chemical industry would be a giant step toward their long-anticipated sustainability. However, the choice of biomass feedstock is critical so as not to compete with the animal and human food chain (Thompson 2012). Furthermore, the suitable integration of renewable, carbon-neutral biomass in the chemical industry would be an indispensable step toward their long-anticipated sustainability (Haq et al. 2021). However, selecting biomass feedstock is critical to not compete with the animal and human food supply chain (Shen et al. 2020). In this regard, cellulosic biomass has been suitable for producing fuels and chemicals. Only a fraction of around 180 billion tons of lignocellulosic biomass produced worldwide per year is utilized.

The main components of lignocellulosic biomass are cellulose (40-50%), hemicellulose (25-30%), and lignin (15-20%) (Figure 1.2). Other minor fraction includes ash and extractive components (Gautam et al. 2022). Cellulose is a crystalline, unbranched polymer of D-glucose units stitched together by the β-1-4-glycosidic bonds. It is the primary structural constituent of plant cell walls and the most abundant natural organic polymer in the world (Wu et al. 2023). Hemicellulose is a branched heteropolymer containing different sugar units, pentoses (xylose and arabinose) along with hexoses (glucose, mannose, galactose, and rhamnose), and acetylated sugars. The degree of polymerization of hydrophilic hemicellulose fractions is low compared to the complex cellulosic moieties (Chen et al. 2022). Lignin is an amorphous branched chain polymer with monomer units p-coumaryl, coniferyl, and sinapyl alcohol. Lignin is often regarded as the 'glue' that binds the various components of lignocellulosic biomass together, rendering it insoluble in water (Lobato-Peralta et al. 2021).

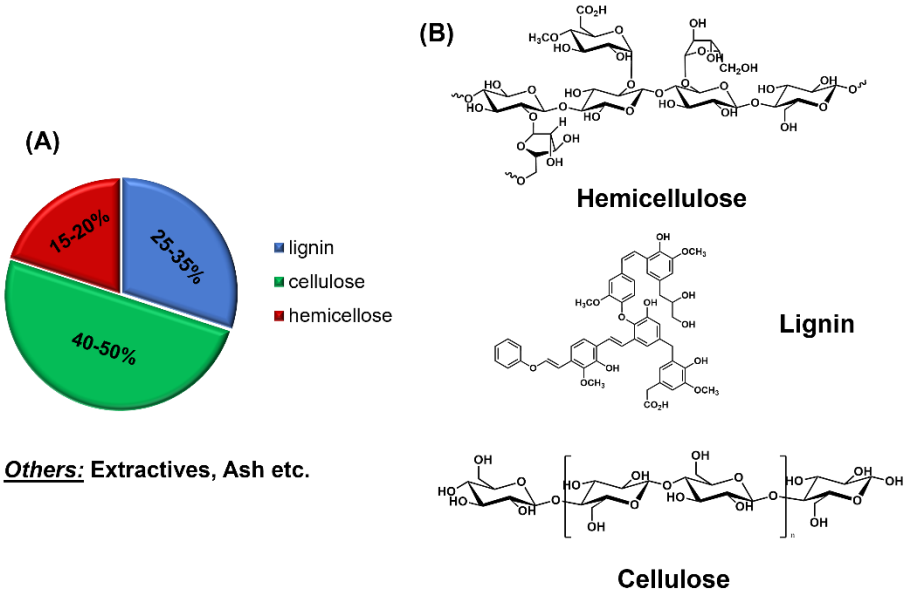

Figure 1.2 (A) The composition of lignocellulosic biomass and (B) structural representation of hemicellulose, cellulose, and lignin.

The major challenge in the value addition of biomass is to selectively depolymerize, defunctionalize, and deoxygenate the biopolymers into simple molecules with desired structural features and physicochemical properties. Various new technologies have been explored for the pretreatment of lignocellulosic biomass. However, the capital cost for these techniques is high, and the efficiency of these processes is unsatisfactory. In this regard, the catalytic value addition of biomass is advantageous since the processes are fast, selective, biomass agnostic, and could benefit from the existing petrorefinery infrastructure (Geboers et al. 2011; Hara et al. 2015).

The acid-catalyzed hydrolysis of cellulose and lignocellulose fractions in lignocellulosic biomass to pentose and hexose sugars followed by dehydration of the latter into furfural (FF), 5-(hydroxymethyl)furfural (HMF), and levulinic acid (LA) are well-documented in the literature. The sequential elimination of three molecules of water from a molecule of glucose forms HMF under acid catalysis (Tomishige et al. 2022). The elegant process decreases the oxygen content of glucose by 50 mol% without C-C bond cleavage reactions or producing toxic byproducts. Similarly, the acid-catalyzed dehydration of xylose produces FF. LA is produced by the acid-catalyzed rehydration followed by the furan ring-opening of HMF. FF, HMF, and LA

have elaborate derivative chemistry with a multitude of established and emerging commercial applications of those derivatives (Figure 1.3) (Rosatella et al. 2011).

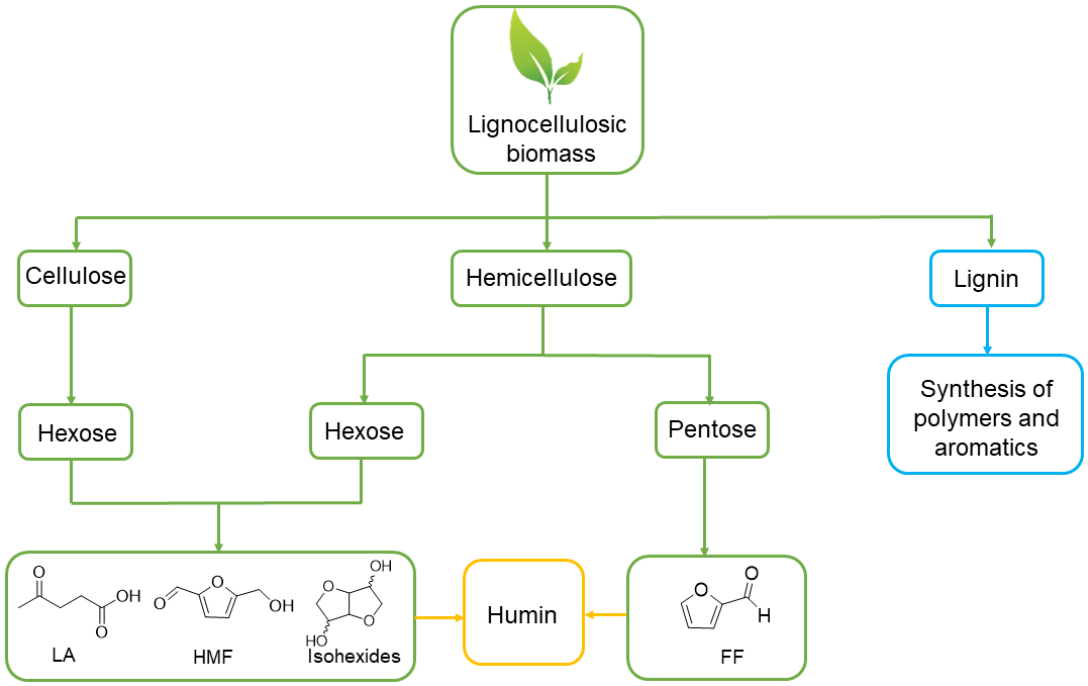

Figure 1.3 Various pathways for the transformation of lignocellulosic biomass.

Biomass-derived chemical platforms have oxygen-containing reactive functionalities that often render them unsuitable for direct use as fuel. However, synthetic upgrading makes them more stable and often reduces the oxygen content, improving their higher heating value. Energy densification involves altering the molecular structure to store more energy per unit weight than the starting material. It will increase the calorific value for compounds that have applications as fuels. For example, LA can be esterified into ethyl levulinate (EL) by esterification reaction. LA cannot be used directly as fuel or fuel additive due to the presence of a carboxylic acid group. On the other hand, EL is a promising fuel oxygenate with a higher calorific value than LA. The calorific value is also increased by catalytic hydrogenation. Some products reported in the thesis were produced by catalytic hydrogenation and possessed higher calorific values than their corresponding starting material.

The preparation of FF and HMF was reported more than a century ago, but the process gained renewed attention only in the 1990s and has been perfected over the years since then. A wide range of product classes of commercial significance, including

fuels and fuel additives, solvents, surfactants, plasticizers, polymers, agrochemicals, and pharmaceuticals, have been produced using HMF and FF as renewable molecular scaffolds (Takkellapati et al. 2018). The biomass to HMF and FF transformation is typically carried out in the aqueous or a polar medium (e.g., ionic liquid) in the presence of an acid catalyst (Scheme 1.1). Though mineral acid catalysts have been extensively studied, the current focus is on developing inexpensive, selective, recyclable, and eco-friendly heterogeneous acid catalysts to prepare HMF directly from lignocellulosic biomass. In general, satisfactory yields of HMF are obtained from simple sugars under relatively mild conditions. However, the high-yielding preparation of HMF from untreated cellulosic biomass often requires special reaction conditions that raise questions about the economic feasibility of the process scale-up.

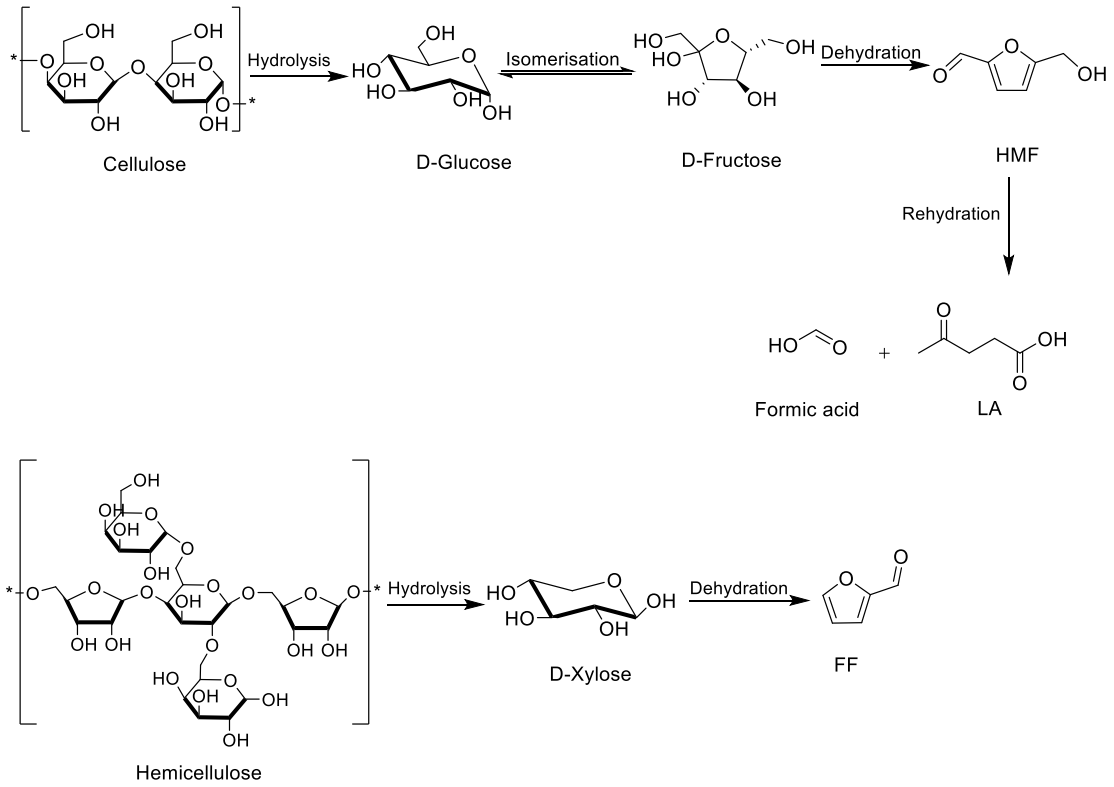

Scheme 1.1 Transformation of cellulose and hemicellulose into HMF, FF, and LA.

Biomass can also be converted into hydrogen by using various technologies. The gasification of biomass feedstock and steam reforming are viable options. The biological conversion of biomass, such as fermentative hydrogen production and biocatalyzed electrolysis, are also promising technologies. The chemocatalytic

conversion of biomass to hydrogen is an emerging field. Sourcing molecular hydrogen and furfurals for downstream energy densification could be a self-sufficient and sustainable chemical technology.

1.2 5-(HYDROXYMETHYL)FURFURAL (HMF)

HMF is one of the top value-added chemical intermediates that link biomass-based carbohydrate chemistry with petroleum-based industrial chemical technology. HMF and its derivates can replace voluminously consumed petroleum-based building blocks, but the high cost of production limits the industrial applications. The synthesis of HMF was first reported in the 19th century by heating inulin with an oxalic acid solution under pressure. Many detailed reviews are available on the synthesis of HMF involving fructose, glucose, and polysaccharides (sucrose, inulin, or cellulose). The acid catalysts examined for producing HMF from carbohydrates include mineral acids, solid acids, zeolites, and ion exchange resins. HMF production has been investigated in various solvent systems. The aqueous system was eco-friendly compared with other solvents, but the selectivity was low due to LA and humin formation. Lewis and Brønsted acid active sites are pivotal in the synthesis of HMF since they promote the isomerization of glucose to fructose and fructose dehydration (Scheme 1.2) (Mascal and Dutta 2014; Wang et al. 2014).

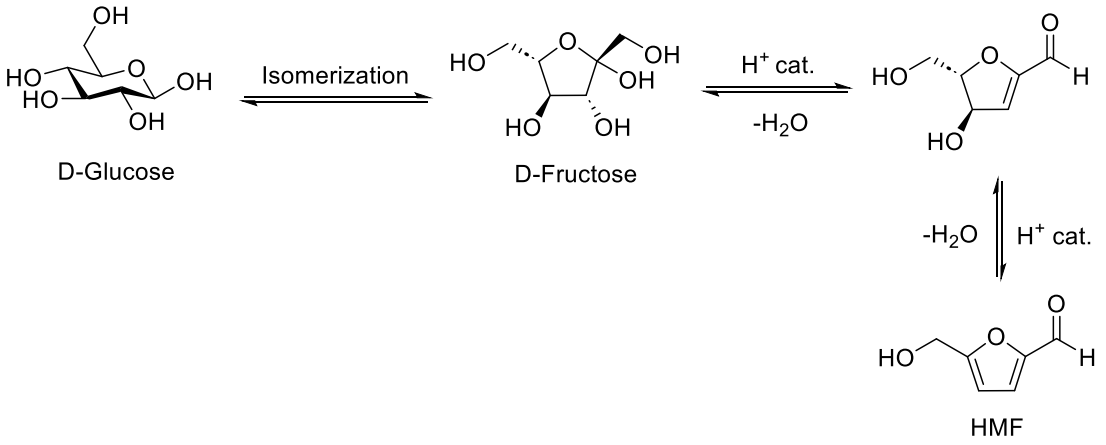

Scheme 1.2 The mechanistic pathway of acid-catalyzed dehydration of glucose to HMF.

The highly reactive hydroxymethyl group, aldehyde group, and furan ring make HMF reactive and synthetically versatile. It can be transformed into a series of bio-fuels

such as 2,5-dimethylfuran (DMF), EL, 5-(ethoxymethyl)furfural (EMF), and C_9-C_{15} alkanes and industrially important chemicals such as LA, 2,5-furandicarboxylic acid (FDCA), 2,5-diformylfuran (DFF), and 2,5-dihydroxymethylfuran (DHMF). FDCA is the precursor for synthesizing polyethylene furoate (PEF), a potential replacement for petroleum-derived polyethylene terephthalate (PET). DFF is used as a monomer and a starting material for synthesizing antifungal agents, drugs, and nematocides. It is also used for metal electroplating and in analytical chemistry (Scheme 1.2) (Dutta and Bhat 2021; Halliday et al. 2003; Xu et al. 2020a).

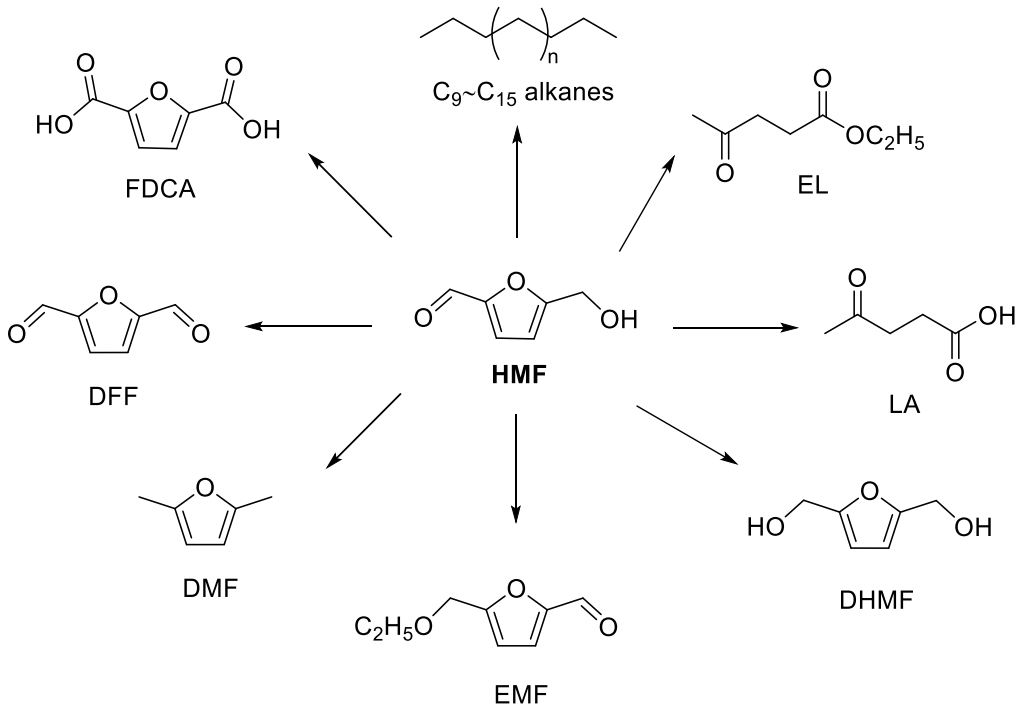

Scheme 1.3 Value-added chemicals derived from HMF.

Selective hydrogenolysis of the hydroxymethyl arm of HMF forms 5-methylfurfural (5MF), which has potential applications as a fuel oxygenate and a chemical intermediate (Scheme 1.3). Further reduction of 5MF leads to 2,5-dimethylfuran (DMF). DMF is a promising biofuel with similar physicochemical properties to those of gasoline (like high energy density (31.5 MJ/L), a high-octane number (119), and low volatility) and a green solvent. DMF has also been demonstrated as a crucial chemical intermediate to produce *p*-xylene for terephthalate polymers. Hydrogenation of the furan ring in DMF produces 2,5-dimethyltetrahydrofuran (DMTHF). DMTHF is a promising fuel oxygenate and a renewable substitute for

tetrahydrofuran (Grochowski et al. 2012; Hu et al. 2014). The other hydrogenated products of HMF include (5-methyltetrahydrofuran-2-yl)methanol (MTHFM), 5-methyltetrahydrofuran-2-carbaldehyde (MTHFC), (5-methylfuran-2-yl)methanol (MFM), and 2,5-dihydroxymethyltetrahydrofuran (DHMTHF) (Scheme 1.4).

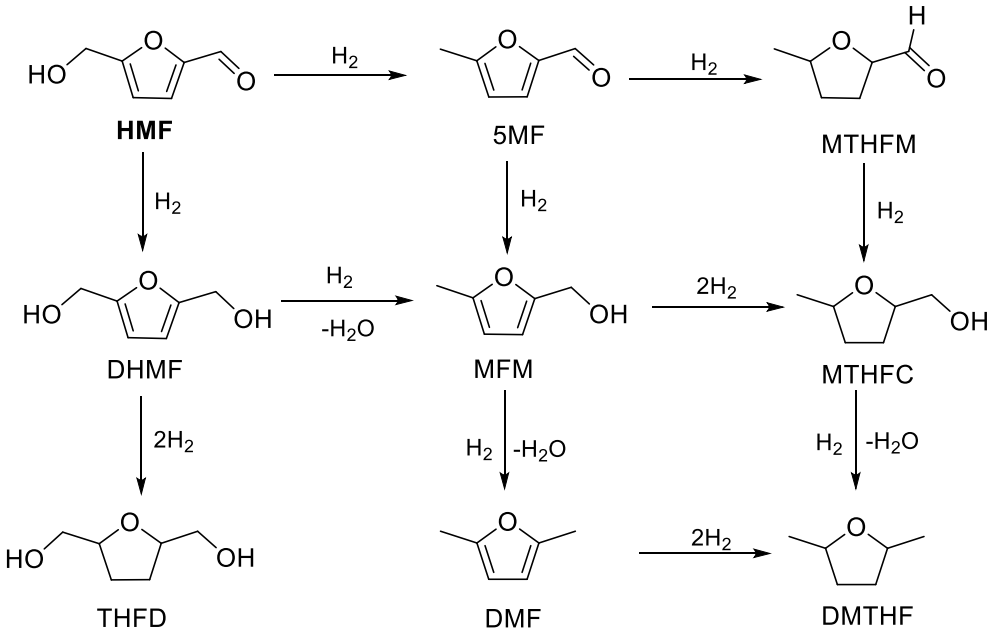

Scheme 1.4 Hydrogenated derivatives of HMF.

1.3 FURFURAL (FF)

FF, identified by the US Department of Energy (DOE) as one of the top 12 value-added products, is a crucial platform chemical produced in lignocellulosic biorefineries that can be transformed into fuels and several chemical intermediates (Yong et al. 2022). FF is obtained by acid-catalyzed dehydration of pentoses (xylose and arabinose) (Scheme 1.1) and is present in bio-oil obtained from fast pyrolysis of biomass. FF has been established as a promising, carbohydrate-derived chemical platform for synthesizing biofuels and biochemicals of commercial significance (Jaswal et al. 2022). FF is used as a selective flavoring agent in food products and beverages. FF can be upgraded to fuel components by removing the polarity of the aldehyde to blend in hydrocarbons and by reducing the volatility to blend in diesel. Hydrogenation with acid-catalyzed rearrangement or etherification, acid-base catalyzed coupling, and metal-catalyzed decarbonylation can achieve the above transformations (Li et al. 2018; Shen et al. 2020).

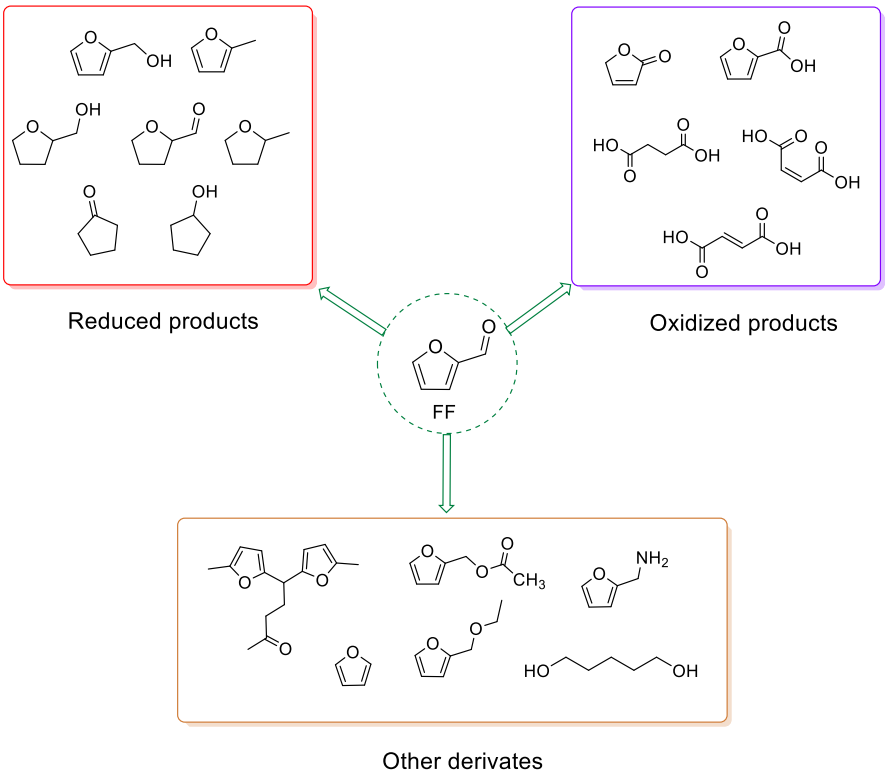

Scheme 1.5 Derivative chemistry of FF.

FF can be converted into several high-value chemical intermediates (Scheme 1.5) like 2-furanone, furoic acid, fumaric acid, succinic acid, and maleic acid via catalytic oxidation (Li et al. 2018). Hydrogenation of 2-furanone resulted in forming γ-butyrolactone (GBL), which is one of the most promising chemical platforms for producing fuels and value-added chemicals (Scheme 1.6).

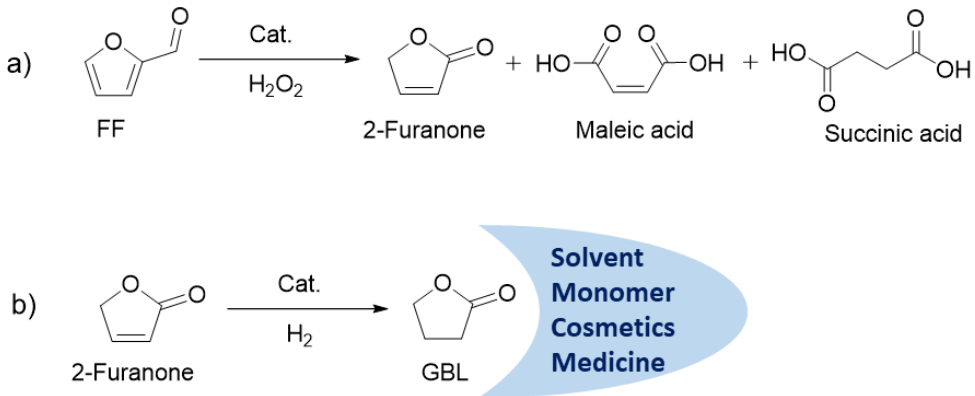

Scheme 1.6 a) Oxidation of FF to 2-furanone, b) Hydrogenation of 2-furanone to GBL.

Oligomerization of 2-furanone, followed by complete hydrodeoxygenation of the intermediates, can form gasoline-like hydrocarbons. The decarbonylation of FF

followed by hydrogenation of the ring results in the formation of tetrahydrofuran (THF), used as a solvent or monomer in both chemical and pharmaceutical industries. Furfuryl alcohol (FAL) is an essential chemical in the polymer industry, mainly used to synthesize resins, and 2-methylfuran (2MeF) provides excellent gasoline blending properties (Yan et al. 2014). Tetrahydrofurfural (THFF), tetrahydrofurfuryl alcohol (THFAL), and 2-methyltetrahydrofuran (MTHF) are the ring-hydrogenated products of FF (Scheme 1.7).

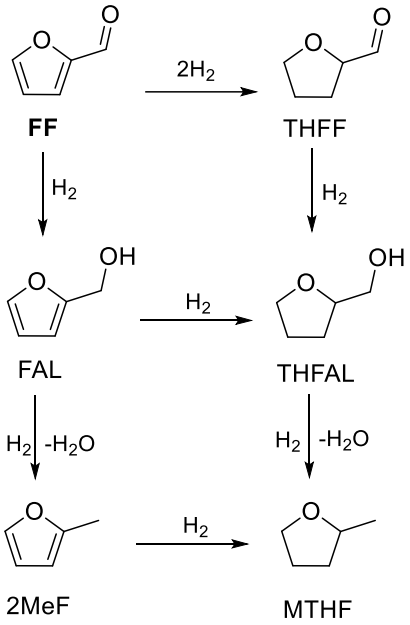

Scheme 1.7 Partially hydrogenated products of FF.

1.4 LEVULINIC ACID (LA)

LA (4-oxopentanoic acid) is a promising chemical intermediate for synthesizing various chemicals with potential applications as fuel additives, solvents, fragrances, and plasticizers. LA is obtained through the hydrolysis of HMF in an acidic solution with formic acid as the byproduct (Bazoti et al. 2023). Intramolecular dehydration of LA leads to angelica lactone (α and β isomers), a renewable intermediate whose base-catalyzed dimerization and trimerization lead to gasoline range alkanes. LA and its esters draw special attention due to their high potential to substitute petroleum feedstocks (Sajid et al. 2021). The reduction of ketone and carboxylic acid functionalities of LA forms 1,4-pentanediol (1,4-PDO) and 2-methyltetrahydrofuran (MTHF), used as a monomer and green solvent, respectively (Figure 1.4). δ-

Aminolevulinic acid (DALA) serves as a precursor molecule in the cellular production of tetrapyrroles and a natural herbicide (Kang et al. 2018a; Pileidis and Titirici 2016).

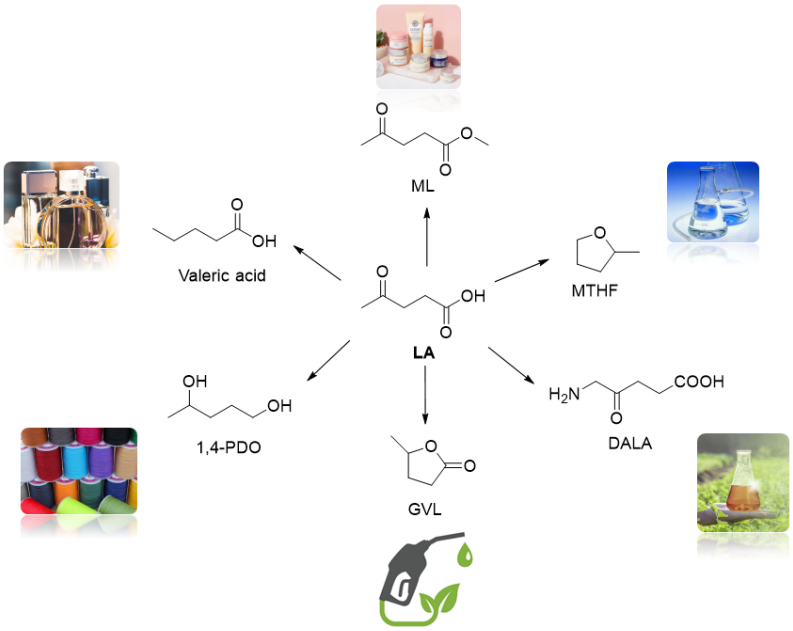

Figure 1.4 Derivates of LA and its applications.

Diphenolic acid, a condensation product of LA with two molecules of phenol, is widely used in polycarbonate and epoxy-resin industries. Selective transformation of LA forms γ-valerolactone (GVL) with potential applications as a fuel oxygenate and renewable solvent. Many studies focus on the direct conversion of LA to GVL via metal-catalyzed hydrogenation, for which two routes have been proposed (Liu et al. 2020). Either LA is hydrogenated to γ-hydroxyvaleric acid and then lactonized to GVL, or LA is lactonized to α-angelica lactone (AGL) and then hydrogenated to GVL (Scheme 1.8).

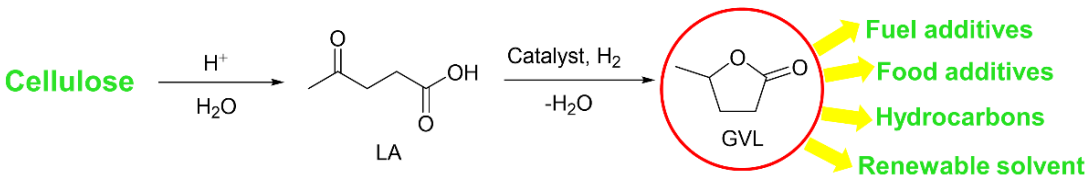

Scheme 1.8 Renewable synthesis of GVL from cellulose-derived LA and its potential applications.

Alkyl levulinates (ALs) are important derivatives of LA due to their specific physicochemical properties and find applications as specialty chemicals in industries

(Figure 1.5). Lower yields limit the direct synthesis of ALs from carbohydrates (Démolis et al. 2014). ALs are typically prepared by the esterification of LA, alcoholysis of FAL, or from FF by catalytic hydrogenation followed by alcoholysis. Esterification of LA with monohydric alcohols has become highly desirable since the EL produced can be used as gasoline and biodiesel additive (Kim and Han 2021). EL is an excellent octane booster for gasoline and serves as a cold flow improver in biodiesel.

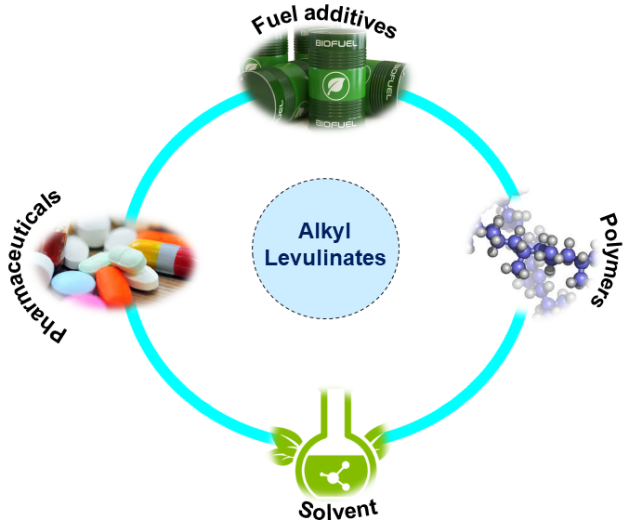

Figure 1.5 Potential applications of alkyl levulinates as a carbohydrate-derived chemical intermediate.

1.5 ISOHEXIDES

The depolymerization of cellulose to glucose has been studied extensively. Glucose is one of the main biomass-based feedstock for chemical-catalytic and biotechnological conversion into fuels, chemicals, and polymeric materials (Rose and Palkovits 2012). Hydrogenation of glucose to sorbitol, followed by acid-catalyzed double dehydration of the latter, forms isosorbide (IS) (Scheme 1.9).

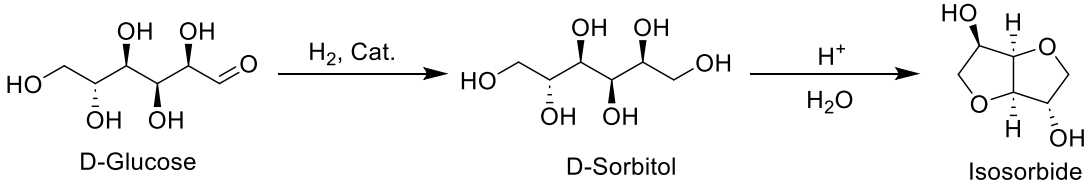

Scheme 1.9 Synthesis of isosorbide from D-glucose.

IS is a chiral, rigid, nontoxic renewable molecule with two secondary hydroxyl groups in *endo* and *exo* configurations. Because of its high stability, and two hydroxyl groups, IS is a versatile platform that finds applications as a monomer for the preparation of polyesters that act as plasticizers, surfactants, and intermediates for the synthesis of pharmaceuticals (Saska et al. 2021). Isomannide (IM) and isoidide (II) are stereoisomers of IS that can be synthesized from mannose and idose. These three isomers constitute isohexides (Figure 1.6).

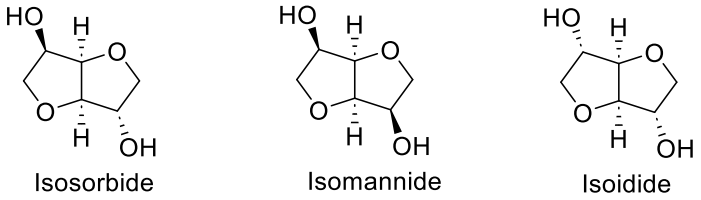

Figure 1.6 The structures of isohexides.

IS has been efficiently converted to value-added products, including biopolymers, pharmaceuticals, surfactants, plasticizers, and renewable solvents. Isosorbide-5-mono nitrate is used as a commercial vasodilator and is preferred over isosorbide-2-mononitrate and isosorbide-dinitrate because of its advantageous pharmacokinetics (Ragno et al. 2021). The diesters of IS have potential application as a plasticizer. The mono- and diesters of IS have potential applications as renewable solvents, plasticizers, and surfactants. IS can also be used as a comonomer in existing polymers like polyethylene terephthalate providing superior properties (Figure 1.7).

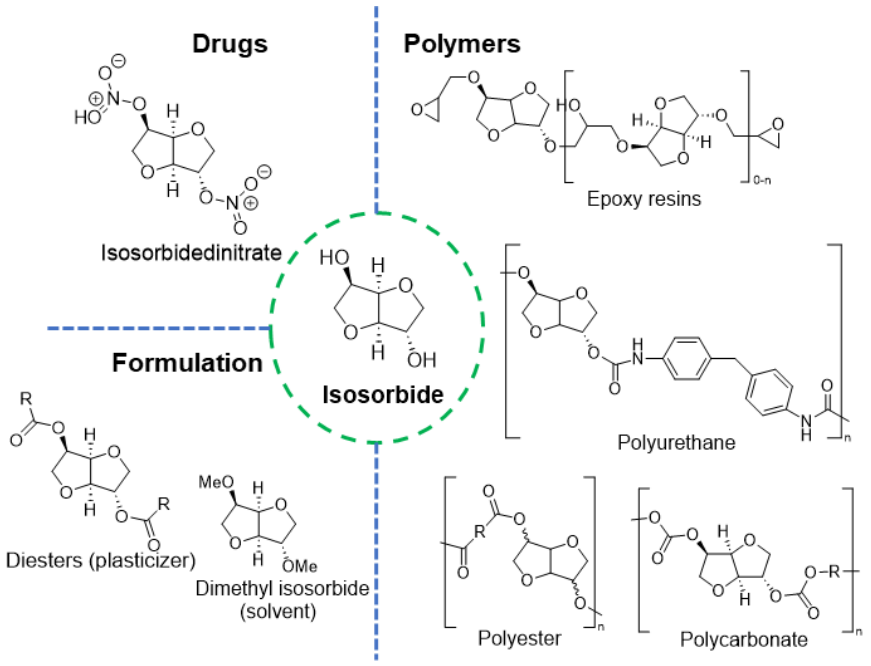

Figure 1.7 Applications of isosorbide derivatives (Dussenne et al. 2017).

1.6 CARBONIZATION OF HUMIN

Humins are a complex furanic resin that forms inadvertently during the acid-catalyzed hydrolysis of biomass-derived sugars. They are carbon-rich furanic polymers that constitute 50-66 wt.% of carbon. The structure of humin consists of an extensive network of furan rings with aldehyde and ketone functionalities (Patil and Lund 2011). Using humin as a reinforcing material, adsorbent, and catalyst support has attracted significant attention in the recent years. The elemental composition and morphology of humins are similar to hydrochar, starting material for activated carbon (AC) production. High surface area, pore volume, and adsorption properties make AC robust. Humin is considered the potential feedstock for the synthesis of AC, which finds applications as a support for several catalysts, electrode materials, and sorbents.

Carbonization aims to increase the C/O ratio in humin by a series of deoxygenation reactions, such as dehydration, decarbonylation, and decarboxylation (Figure 1.8). Generally, preparing AC carbon includes carbonization of the precursor followed by activation. Activation can be done either by physical or chemical means. In the physical method, the precursor is first carbonized in an inert atmosphere and activated using steam or CO_2. In the chemical method, the precursor is activated using activating agents, carbonized in an inert atmosphere, and requires less temperature than

physical activation (Chernyshev et al. 2017). Chemical activation is advantageous over the other methods owing to high surface area and uniform pore size distribution of the AC produced. The pore sizes are categorized into micropore (<2 nm), mesopore (between 2 and 50 nm), and macropore (>50 nm).

Chemical activating agents, such as KOH, NaOH, K_2CO_3, H_3PO_4, and $ZnCl_2$, have been used widely for the production of AC with well-developed porosity and high specific surface area (Yakout and Sharaf El-Deen 2016). It has been reported that KOH widens the micropore, $ZnCl_2$ develops mesoporosity, and H_3PO_4 leads to a more heterogeneous pore size distribution (Sych et al. 2012). H_3PO_4 has been used as a chemical activating agent for preparing AC from various biomass feedstock because of its lesser environmental constraints than $ZnCl_2$ and lower activation temperature than KOH and NaOH (İzgi et al. 2019).

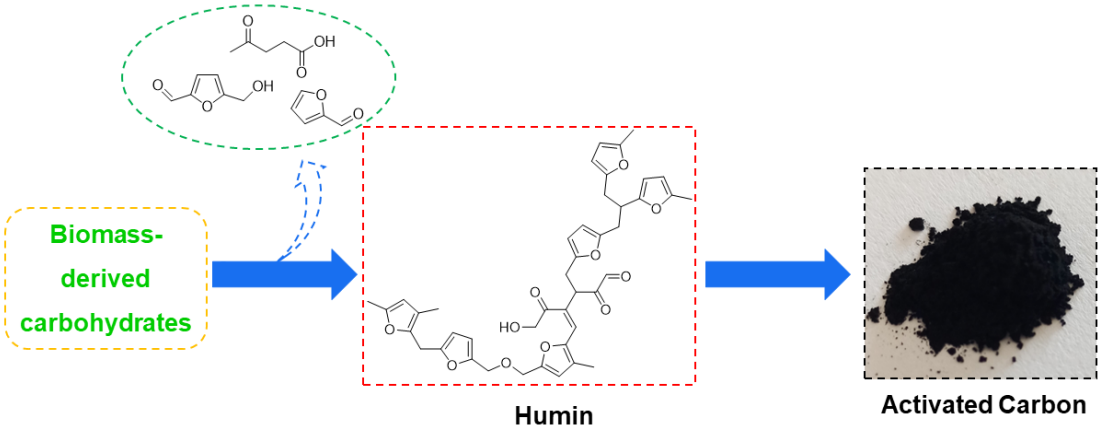

Figure 1.8 Formation of AC from biomass-derived carbohydrates.

CHAPTER 2

LITERATURE REVIEW, SCOPE, AND OBJECTIVES OF THE WORK

2.1 LITERATURE REVIEW

There are numerous research publications on the catalytic transformation of biomass-derived platform chemicals via hydrogenation, esterification, and transesterification reactions, and the works have been periodically reviewed. This chapter outlines existing methods, process optimization, opportunities, and challenges in this research field.

2.1.1 Literature review of the preparation of activated carbon (AC) from humin

Kang et al. (2018) reported the activation of humin and solid waste produced from acid hydrolysis to activated carbon (AC) by the KOH activation method. The BJH pore volume and BET surface area of ACs produced at high temperatures are typically high (~1975 m^2/g), and they have superior phenol, N_2, and methylene blue adsorption capacities (Kang et al. 2018a). The same group reported the preparation of AC from humin, obtained during levulinic acid (LA) synthesis starting from glucose, employing phosphoric acid as the activating agent. The humin obtained after the acid hydrolysis of glucose was mixed with phosphoric acid and heated in a temperature range of 300-700 ℃ in a nitrogen atmosphere. The prepared samples were washed several times with deionized water and dried. The characterization studies revealed that the surface area of the carbon material increased by a thousandfold after activation. The BET surface area and BJH pore volumes of the synthesized ACs were 1358-2375 m^2/g and 0.25-0.88 cm^3/g, respectively. The adsorption capacity of the material was also examined using methylene blue (Kang et al. 2018b).

Humin obtained during the acid hydrolysis of fructose to 5-(hydroxymethyl)furfural (HMF) was used to prepare AC. Chemical activation using KOH as the activating agent, physical activation by CO_2, and pyrolysis in an inert atmosphere, were the different activation methods used to prepare AC. Among the synthesized ACs, chemically activated humin at 900 ℃ showed the highest BET surface area of 862 m^2/g. The AC possessed micro and mesoporous structures and was used as an electrode material for supercapacitor applications (Chernysheva et al. 2018).

Yang et al. developed a solid acid catalyst by sulfonating humin produced during glucose dehydration (Yang et al. 2020). Humin was pyrolyzed at 200 °C for 3 h and then sulfonated at 150 °C to introduce SO_3H groups. The catalyst was further

employed for the esterification of LA to butyl levulinate (BL) (ca. 95% yield). The catalyst exhibited good recyclability for four catalytic cycles. A decline in the catalytic activity in consecutive cycles was attributed to the loss of acidic sites from the carbon matrix.

2.1.2 Literature review of transesterification and esterification of biomass-derived intermediates

Several homogeneous and heterogeneous catalysts were developed to synthesize esters from biomass-derived intermediates. Despite various catalytic systems developed to date, challenges associated with large-scale processing and purification methods of the ester product still need to be solved.

Badgujar et al. (2023) published a review on the synthesis of alkyl levulinates (ALs) by the catalytic valorization of carbohydrates via alcoholysis. The study emphasized the recent advancements in the production of ALs from carbohydrates and their fuel-blending properties. Different catalytic systems were used to valorize the carbohydrates into ALs that perform isomerization, depolymerization, solvolysis, hydration, and hydrolysis reaction. Several factors, such as the nature of feedstock, solvent, type of catalyst, and Lewis and Brønsted sites present in the catalyst, can influence the yield of ALs. The ALs can increase the fuel blending properties by reducing the emission of pollutant gases, improving fuel efficiency and performance (Badgujar et al. 2023). The same group reviewed the catalytic synthesis of ALs, from LA and elaborated on the mechanistic approach for the synthesis (Badgujar et al. 2020). They detailed the influence of reaction temperature, various solvents, product separation, reactant mole ratio, and substrate structure on the yield of ALs.

Di Bucchianico et al. elaborated on the production of ALs from carbohydrates and chemical intermediates like furfural (FF), LA, and furfuryl alcohol (FAL) (Di Bucchianico et al. 2022). The review focuses on various processes for synthesizing ALs, highlights industrial technologies, and suggests an environmentally and economically conscious approach for synthesizing the same. Furthermore, the review discusses separation and purification techniques, including distillation, absorption, adsorption, and liquid-liquid extraction.

Appaturi et al. elaborated on the recent developments in the esterification of LA using heterogenous catalysts (Appaturi et al. 2022). The review provides insight into the catalyst preparation, properties, structural modifications, and mechanisms. The influence of various reaction parameters, such as temperature, catalyst loading, duration, reaction medium, and the molar ratio of reactants, on the yield of ALs was also elaborated.

In 2021, Bhat et al. reviewed the synthesis of ALs from carbohydrates and biomass-derived chemical platforms such as LA, FAL, HMF, and α-angelica lactone (AGL) using heteropoly acid catalysts (Bhat et al. 2021). They elaborated on the preparation of ALs from various feedstocks and compared the selectivity of ALs synthesized using homogeneous and heterogeneous catalysts. The review focused on the catalyst design and selection of support that can enhance the acidic nature, porosity, and other synergistic interactions, improving the yield of ALs. Furthermore, the review summarizes the potential opportunities and challenges associated with developing an efficient catalyst to synthesize ALs.

Liu et al. elaborated on the different approaches employed for the production of ALs from various biomass-derived intermediates (Liu et al. 2020). The esterification of LA to ALs is often performed using solid acid catalysts, metal oxides, zeolites, and sulfonic acid-supported materials. The review also focused on preparing ALs from feedstocks such as FAL, 5-(chloromethyl)furfural, mono-, di-, and polysaccharides. In addition, the review highlights various biomass-pretreatment steps, the texture and properties of the catalyst, mechanisms, and the reaction intermediates formed during the synthesis of ALs.

Yan et al. discussed the transformation of LA and ALs into biofuels and value-added chemicals such as GVL, 2-methyltetrahydrofuran, 1,4-pentanediol, valeric acid, and N-substituted pyrrolidinones (Yan et al. 2017). The size of metal particles, surface morphology, and acidity are some factors that affect the catalytic performance of heterogeneous catalysts. Molecular hydrogen and formic acid are the conventional sources of hydrogen. In contrast, CTH reactions using alcohol as a source of hydrogen have gained attention due to the ease of recovery of the alcohol reagent from the

reaction mixture via distillation. The review summarized the development of non-noble metal catalysts for hydrogenating biomass-derived intermediates.

Rose and Palkovits reviewed the developments in the production of isosorbide using different catalytic systems and the chemical transformations of isosorbide (IS) into useful derivates (Rose and Palkovits 2012). Functionalization of the hydroxyl groups in IS, IM, and II via esterification, acetylation, and tosylation has been investigated.

Table 2.1 The representative literature reports on the synthesis of ALs from biomass-derived intermediates via esterification and transesterification.

Substrate	**Catalyst**	**Reaction Conditions**	**Product**	**Yield (%)**	**Reference**
LA	SFCB-4 (27 wt.%)	60 °C, 6 h, ethanol (excess)	EL	97.6	(Gong et al. 2023)
LA	MSA-SG (8 wt.%)	120 °C, 8 h, LA/n-propanol (1:15)	PL	93	(Vinod et al. 2023)
LA	TNP (8.6 wt.%)	120 °C, 8 h, LA/n-butanol (1:10)	BL	77.6	(Zhou et al. 2022)
LA	HPW-TiO_2 (40 wt.%)	120 °C, 2 h, LA/ethanol (1:42)	EL	81	(Ahmad et al. 2022a)
LA	$Sn_{1.5}PW_{12}O_{40}$ (0.6 mol%)	60 °C, 6 h, LA/ethanol (1:18),	EL	~85	(Da Silva et al. 2021)
LA	UCC-S (20 wt.%)	80 °C, 4 h, LA/ethanol (1:20)	EL	90	(Zainol et al. 2021)
LA	Nb-TCPP-SBA-15-AM (4.3 wt.%)	60 °C, 6 h, LA/methanol (1:5)	ML	43.6	(Anjali et al. 2021)
LA	10ZrPM(DS-E)	70 °C, 5 h, LA/ethanol (1:5)	EL	69.2	(Shestakova et al. 2021)

	(2.5 wt.%)				
LA	STA-AlSBA-15 (20 wt.%)	75 °C, 5 h, LA/ethanol (1:10)	EL	87.4	(Lucas et al. 2019)
LA	Sn T-4 (8.6 wt.%)	120 °C, 4 h, LA/n-butanol (1:5)	BL	95	(Pachamuthu et al. 2019)
LA	WO_3-SBA-16 (3 wt.%)	120 °C, LA/ethanol (1:7), fixed bed reactor	EL	95	(Enumula et al. 2017a)
FAL	SBA-15/H-ZSM-5 (0.8 g)	110 °C, 5 h, ethanol (excess)	EL	89	(Prajapati et al. 2023)
FAL	PMAC (100 wt.%)	140 °C, 3 h, ethanol (excess)	EL	63	(Chhabra et al. 2022)
FAL	A-15 (30 wt.%)	110 °C, 3 h, FAL/n-butanol (1:20)	BL	78	(Chung et al. 2022)
FAL	Sn_1-TPA/K-10 (20 wt.%)	110 °C, 5 h, FAL/n-butanol (1:20)	BL	98	(Tiwari et al. 2020)
FAL	AC (0.1 g)	170 °C, 5 min, MW, methanol (excess)	ML	78	(Wang et al. 2020)
FAL	Al/DFNS/Pr-SO_3H (14 wt.%)	130 °C, 3 h, n-butanol (excess)	HL	93.5	(Mohammad bagheri and Chermahini 2019)
FAL	H-ZSM-5-50	170 °C, methanol (excess),	ML	80	(Zhao et al. 2018)

	(0.2 g)	continuous flow reactor			
FAL	$Ti_{0.75}$TPA (2.25 wt.%)	120 °C, 0.5 h, FAL/n-propanol (1:53), sealed tube	PL	90	(Srinivasa Rao et al. 2018)
FAL	Fe/USY (3 wt.%)	130 °C, 4 h, ethanol (excess)	EL	90.6	(Kong et al. 2017)
AGL	WO_3/ZrO_2 (5 wt.%)	75 °C, 5 h AGL/n-butanol (1:1)	BL	47.6	(Ciptonugroho et al. 2023)
AGL	$HClO_4$-SiO_2 (0.55 mol%)	90 °C, 2 h, ethanol (excess)	EL	91	(Onkarappa et al. 2020)
AGL	MWCNT-$[C_2mim][OTf]$-$Al(OTf)_3$ (0.1 mol%)	60 °C, 1 h AGL/n-butanol (1:1)	BL	99	(Latos et al. 2019)
AGL	$Ch_2H_4P_2W_{18}O_{62}$ (20 wt.%)	75 °C, 1 h AGL/n-butanol (1:1)	BL	79.4	(Yi et al. 2017)
IS	$Sc(OTf)_3$ (0.02 wt.%)	RT, 4 h, IS/methacrylic anhydride (1.5/1.0 eq.)	ISMAr	32	(Nonque et al. 2021)
IS	$ZnCl_2$ (1.23 eq.)	40 °C, overnight, IS/acrylic acid (1.5/1.0 eq.)	ISMAr	17	(Nonque et al. 2020)

IS	A15 (5 wt.%)	111 °C, 24 h, acetic acid (excess), toluene	ISDA	90	(Inayat et al. 2018)
IS	Dowex 50W×2 (1 mol%)	reflux, 24 h, acetic acid (excess)	ISDA	78	(Fraile and Saavedra 2017)

Abbreviations: UCC-S: Sulfonated carbon cryogel catalyst; STA: Silicotungstic acid; TNP: Titania nanoparticles; HPW: Phosphotungstic acid; ML: Methyl levulinate, EL: Ethyl levulinate, PL: Propyl levulinate, BL: Butyl levulinate, HL: Hexyl levulinate; ISMAr: Isomannide monoacrylate, ISDA: Isosorbide diacetate, PMAC: Phosphomolybdic acid supported on activated carbon; DFNS: Dendritic fibrous nanosilica; Fe/USY: Iron modified zeolite catalyst; A-15: Amberlyst-15; SBA-15/H-ZSM-5: Alumino-silicate composite; MSA-SG: Methanesulfonic acid supported on silica gel; MWCNT: Multiwalled carbon nanotube; TPA: Tungstophosphoric acid; TCPP: meso-tetra-(4-carboxyphenyl)-porphyrin; SBA-AM: Surface amine groups on functionalized SBA-15; 10ZrPM(DS-E): Zr(IV) substituted Keggin polyoxometalate grafted on mesoporous silica; Sn T-4: mesoporous stannosilicates.

Several catalysts have been developed to synthesize ALs under straightforward reaction conditions. Even though satisfactory results were obtained in many cases, there is plenty of scope in developing inexpensive, efficient, and environmentally friendly catalysts for synthesizing ALs. The ease of recovery of a heterogeneous catalyst over its homogeneous counterpart makes the former more advantageous.

2.1.3 Literature review of hydrogenation of levulinic acid (LA) to γ-valerolactone (GVL)

GVL is routinely synthesized by the liquid- or vapor-phase hydrogenation of LA in a hydrogen-donor solvent or under an overpressure of hydrogen gas in the presence of a suitable metal catalyst. Catalysts used in this transformation include noble metals, non-noble metals, and bimetallic catalysts. Numerous literature reports were published over the past decade on preparing GVL using various metal catalysts. Therefore, this section briefly discusses a few important published reviews and tabulates the representative literature on the catalytic hydrogenation of LA to GVL (Table 2.2).

Maumela et al. reviewed the superior catalytic activity of Ru-based catalysts toward GVL synthesis (Maumela et al. 2021). he activity of Ru-based catalysts relies on the nature of support, preparation method, and reaction conditions. The Ru-based catalysts are preferred due to their intrinsic ability to hydrogenate the carbonyl functionality of LA at temperatures below 150 °C. The carbon-based supports proved to be best owing to their stability and uniform dispersion of Ru nanoparticles. Alloying Ru catalysts with Ni and Sn significantly improved the catalytic activity and selectivity toward GVL. Modification of the support improved the catalyst stability, metal-support interaction, and activity.

Seretis et al. elaborated on the recent advances in the Ru catalyzed hydrogenation of LA to various value-added chemicals (Seretis et al. 2020). The hydrogenation of LA into GVL, valeric acid, 2-methyltetrahydrofuran, 1,4-pentanediol, 2-butanol, and 2-pentanol using various organic and aqueous solvents was discussed. Remarkably, Ru-based catalytic systems are extensively employed for the above transformations due to the ability of Ru to hydrogenate the carbonyl functionality of LA selectively to hydroxyl functionality under mild reaction conditions. The 4-hydroxyvaleric acid intermediate thus formed undergoes dehydration followed by cyclization to form GVL. Several precious and non-noble metal-based catalytic systems have been developed in which water as the solvent facilitated the quantitative conversion of LA.

Yu et al. published a review on the effect of solid acid support on the catalytic hydrogenation of LA to GVL (Yu et al. 2020a). Acidic supports such as ZSM-5 resulted in over-hydrogenated products like valeric acid due to the high Brønsted acidity of the support. Mainly metal oxides were employed as the catalyst support in formic acid-mediated hydrogenation of LA, which promotes the dehydration of LA to form AGL. Whereas, in the case of molecular sieves and acidic resins, the GVL selectivity decreased on prolonged reaction time due to ring opening reactions. MOF-derived carbon supports are gaining attention due to high metal dispersion and strong metal-support interaction, but metal leaching from the support remains a challenge. The effect of catalyst loading, metal dispersion, coke formation, and Lewis and Brønsted acidity of the catalyst were also well documented.

Yu et al. published a mini-review on the hydrogenation of LA to GVL using formic acid as the source of hydrogen (Yu et al. 2020b). Higher formic acid concentration resulted in a decline in the GVL selectivity due to the formation of over hydrogenated products and catalyst deactivation. Precious metal catalysts such as Ru and Au are superior to non-precious metal catalysts owing to their catalytic efficiency and selectivity toward GVL. Bimetallic catalysts with a combination of precious and non-precious metals can effectively catalyze the hydrogenation of LA. The effects of heterogeneous catalysts and reaction parameters such as temperature, LA to formic acid molar ratio, time duration, and solvent on the catalytic performance were summarized.

Dutta et al. detailed the advancements in the design of non-noble metal catalysts for the hydrogenation of LA to GVL (Dutta et al. 2019). Non-noble metals have garnered attention owing to their high abundance, low cost, ease of separation, and recyclability. The review discussed the mechanisms and prevailing technologies utilized in producing GVL. The study examined the structural characteristics of the catalyst, the role of solid support, and the effect of various reaction parameters. They summarized the hydrogenation of LA via the CTH process, in which 2-propanol and formic acid were used as the source of hydrogen.

Table 2.2 Literature reports on hydrogenation of LA to GVL.

Substrate	**Catalyst**	**Reaction Conditions**	**Yield (%)**	**Reference**
LA	Ni/O-clay450N (30 wt.%)	140 °C, 5 h, 3 MPa H_2, 1,4-dioxane	100	(Kamble et al. 2023)
LA	Ni/Ru@WOMC (50 wt.%)	160 °C, 2 h, 3 MPa H_2, 2-propanol	100	(Wang et al. 2023b)
LA	NiCOK-12 (1 g)	250 °C, 0.1 MPa H_2, fixed bed reactor	~98	(Dosarapu et al. 2023)
LA	$Co_{0.5}$-LCS@500 (2.6 wt.%)	200 °C, 1 h, 2 MPa H_2, water	99.8	(Xu et al. 2023b)

LA	TY700 (100 wt.%)	175 °C, 12 h, 3 MPa H_2, 2-propanol	94	(Jayakumari and Krishnan 2023)
LA	ZrO_2/SBA-15 (0.1 g)	150 °C, 2-propanol, continuous flow reactor	80	(Merenda et al. 2023)
LA	CuCo@C (5 wt.%)	220 °C, 4 h, 1 MPa H_2,	100	(Ibrahim et al. 2023)
LA	Ni-Zn@OMC (31 wt.%)	140 °C, 2 h, 3 MPa H_2, water	78.6	(Tang et al. 2023)
LA	$Ru_{0.18}/Al_2O_3$/NC (1 wt.%)	150 °C, 3 h, 5.8 MPa H_2	99.7	(Liu et al. 2023)
LA	Zr-FDCA-15HPWO (32 wt.%)	180 °C, 2 h, 3 MPa H_2, 2-propanol	95.4	(Huang et al. 2023)
LA	Ni–Mn/SiO_2 (20 wt.%)	140 °C, 5.5 h, 2 MPa H_2, 1,4-dioxane	100	(Chen et al. 2023)
LA	Ni_1Co_1-BTC (20 wt.%)	160 °C, 3 h, 4 MPa H_2, 1,4-dioxane	95.2	(Xu et al. 2023a)
LA	Ru/C (0.01 g)	100 °C, 1 h, 1 MPa H_2, water	92	(Bounoukta et al. 2023a)
LA	Ru/CNF-APTMS (0.02 g)	100 °C, 2 h, 1 MPa H_2, water	99	(Bounoukta et al. 2023b)
LA	Cu-Re/TiO_2 (10 wt.%)	180 °C, 4 h, 4 MPa H_2, 1,4-dioxane	100	(Liu et al. 2022b)
LA	Pt-HT (20 wt.%)	40 °C, 24 h, 5 MPa H_2, water	100	(Siddiqui et al. 2022)
LA	Ni_2Co_1P (2.3 wt.%)	180 °C, 4 h, 3 MPa H_2	100	(Raguindin et al. 2022)

LA	Ru/HPNC (2 wt.%)	100 °C, 2 h, 2.5 MPa H_2	100	(Li et al. 2022)
LA	Co@NC (10 wt.%)	190 °C, 2 h, 1.9 MPa H_2, 1,4-dioxane	100	(Wang et al. 2022)
LA	$Pt/Sn_{0.8}Mn_1O$ (8.6 wt.%)	120 °C, 6 h, 2 MPa H_2, 1,4-dioxane	99	(Lu et al. 2022)
LA	CuNi-1Al/AC (1 wt.%)	220 °C, 2 h, 2-propanol	97.2	(Yu et al. 2022)
LA	Ru-PPP-S (0.064 mol%)	100 °C, 3 h, 5 MPa H_2, water	99.8	(Sorokina et al. 2022)
LA	Ru/TiO_2@CN (17 wt.%)	30 °C, 14 h, 6 MPa H_2, water	100	(Zhang et al. 2021a)
LA	HPW@MOF808 (43 wt.%)	160 °C, 6 h, 2-propanol	86	(Li et al. 2021)
LA	Co^RNC/SMCNF (11 wt.%)	180 °C, 2 h, 4.5 MPa H_2, water	99	(Shao et al. 2021)
LA	Ru/UCN (34 wt.%)	100 °C, 4 h, 2-propanol	99.8	(Cai et al. 2021)
LA	15%Ni-15%Co/Al_2O_3 (33 wt.%)	110 °C, 2 h, 3 MPa H_2, 2-propanol	99.5	(Bai et al. 2021)
LA	Ni/Al_2O_3-CN-600 (34 wt.%)	130 °C, 3 h, 1 MPa H_2, THF	~99	(Jiang et al. 2021)
LA	Sn/Al-SBA-15 (100 wt.%)	200 °C, 3 h, 2-propanol	99	(Kumaravel et al. 2020)
LA	Ni_3P-$CePO_4$ (10 wt.%)	180 °C, 2 h, 2-propanol	89.9	(Yu et al. 2020c)

LA	Fe-Re/TiO_2 (10 wt.%)	180 °C, 4 h, 4 MPa H_2, water	95	(Huang et al. 2020)

Abbreviations: O-clay450N: Organoclay calcined at 450 °C in nitrogen atmosphere; WOMC: Walnut shell lignin-based ordered mesoporous carbon; COK-12: Ordered mesoporous silica; LCS: Lignin-metal coordinated colloidal nanospheres; TY700: Thermally dealuminated NH_4Y zeolite; OMC: Ordered mesoporous carbon; NC: Nitrogen-doped carbon; FDCA: 2,5-Furandicarboxylic acid; HPWO: Phosphotungstic acid; HT: Hydrotalcite; HPNC: N-doped carbon nanosphere; CN: N-doped carbon; BTC: Benzene-1,3,5-tricarboxylic acid; CNF: Carbon nanofibers; APTMS: Amine propyltrimethoxysilane; AC: Activated carbon; PPP-S: Acid functionalized pyridylphenylene polymers; HPW: Phosphotungstic acid; MOF: Metal-organic framework; SMCNF: Nitrogen-doped mesoporous carbon nanofibers; UCN: Graphitized carbon nitride support from urea.

Most studies used a noble-metal-based catalyst, with Ru and Ni being the most used metals. Pd and Au-based catalysts have also shown promising results. Emphasis has now been placed on developing inexpensive but efficient transition-metal-based catalysts. Nearly quantitative yields of GVL were achieved in many cases using robust catalysts with excellent recyclability. Although numerous heterogeneous catalysts have been screened for the hydrogenation of LA to GVL, developing a stable, active heterogeneous catalyst remains challenging. Catalyst deactivation over time due to coke formation and leaching of the metallic species from the support are the main factors that limit the catalytic activity. More focus is required to account for the influence of support on catalyst activity and deactivation pathways.

2.1.3 Literature review of hydrogenation of biomass-derived lactones

Catalytic hydrogenation of the olefinic group in furanone is limited in the literature. The major target is to develop inexpensive but efficient catalysts concerning their stability, selectivity, and recyclability. This section discusses the existing literature on the catalytic hydrogenation of AGL to γ-butyrolactone (GBL) (Table 2.3).

Li et al. reported the selective hydrogenation of 2-furanone to GBL over Ni-based bimetallic catalysts (Li et al. 2018). Out of several metals used (Fe, Cu, Zn, and Co), Ni-Fe/SiO_2 catalyst showed high selectivity toward GBL (ca. 89.5% yield).

Compared to the monometallic Ni/SiO_2, the bimetallic catalyst showed the best results owing to the high reaction rate constant of $Ni\text{-}Fe/SiO_2$. The formation of Ni-Fe alloy on the surface of the support also enhanced the yield of GBL. The same group studied the effect of different oxide support on Pt-Ni metal sites toward the hydrogenation of 2-furanone (Li et al. 2019). $Pt\text{-}Ni/SiO_2$ furnished a high yield of GBL compared with other oxide supports (Al_2O_3, ZrO_2, and TiO_2). The distribution of metallic species over the supports was uniform, but the variation in the yield of GBL is attributed to their acidity.

Zhang and coworkers reported the hydrogenation of AGL under mild reaction conditions using $Pd\text{-}NiO/SiO_2$ catalysts (Zhang et al. 2016a). The catalyst was prepared by wet impregnation and deposition-precipitation-reduction method. NiO was loaded on silica by the wet impregnation method, whereas Pd by the deposition-reduction method. A set of catalysts with different Pd and Ni loadings were prepared and employed for the hydrogenation reaction. The catalyst with 0.2% Pd and 9.9% NiO loading afforded quantitative conversion of AGL. The catalyst recyclability was tested for six consecutive cycles with marginal loss in the yield of GVL.

Al Shaal et al. reported the solvent-free hydrogenation of AGL to GVL over Ru/C catalyst (Al-Shaal et al. 2014). They studied the influence of reaction parameters such as temperature, pressure, and time duration on the hydrogenation of AGL. The GC analysis of the reaction mixture revealed the formation of a trace amount of valeric acid along with GBL under optimized reaction conditions. A quantitative conversion of AGL was obtained at room temperature and atmospheric pressure of hydrogen gas under solvent-free conditions. Under optimized reaction conditions (50 °C, 1 h, 2.4 MPa H_2), they reported 97% of GVL starting from AGL.

Cao et al. reported using ionic liquids as a solvent for the hydrogenation of AGL to GVL in the presence of a Pd/C catalyst (Cao et al. 2014). Various ionic liquids were employed for the above transformation, in which $[Bmim]PF_6$ furnished GVL in high yields. No decrease in the yield of GVL was observed after ten consecutive cycles. The kinetic study revealed that the hydrogenation of AGL is a first-order reaction in $[Bmim]PF_6$ under optimized reaction conditions.

Table 2.3 The catalytic hydrogenation of 2-furanone to GBL and AGL to GVL.

Substrate	Catalyst	Reaction Conditions	Product	Yield (%)	Reference
2-Furanone	Ni4.0–Fe1.0/SiO_2 (2.5 wt.%)	80 °C, 3.5 MPa H_2, methanol	GBL	89.5	(Li et al. 2018)
2-Furanone	Pt-Ni/SiO_2 (2.5 wt.%)	80 °C, 3.5 MPa H_2, methanol	GBL	79	(Li et al. 2019)
AGL	Ru/C (6 wt.%)	50 °C, 1 h, 2.4 MPa H_2	GVL	92.7	(Al-Shaal et al. 2014)
AGL	0.2Pd–9.9NiO/SiO_2 (0.025 g)	30 °C, 0.5 h, 0.3 MPa H_2, water	GVL	82	(Zhang et al. 2016)
AGL	Pd/C (2 wt.%)	RT, 20 min, 4.0 MPa, [Bmim]PF_6	GVL	99.9	(Cao et al. 2014)

Abbreviations: [Bmim]PF_6: Ionic liquid.

2.2 SCOPE OF THE WORK

Humin, the insoluble carbonaceous solid waste formed from the acid hydrolysis of biomass, is considered a potential feedstock for producing AC. AC is an important industrial raw material with remarkable properties such as high surface area and rich porosity. AC can be prepared by activating the humin using phosphoric acid or KOH in a temperature range of 200-700 ℃. The synthesized AC has remarkable properties such as high pore volume, surface area, and excellent adsorption properties and can be used as a supporting material for heterogeneous catalysts. The selective hydrogenation of angelica lactone to GVL and 2-furanone to GBL are of great interest due to the wide applications of the synthesized molecules. Several noble and non-noble heterogeneous catalysts were employed for the above transformation, but catalyst stability and deactivation remained unresolved. However, designing efficient support can improve activity, stability, and recyclability. The production of ALs from LA, FAL, LA-derived AGL, and even directly from carbohydrates by reacting with C1-C4 monohydric alcohols under acid-catalyzed esterification and alcoholysis is well explored. ALs have

garnered immense attention due to their existing and emerging applications as biofuels, green solvents, and chemical intermediates for downstream synthetic value addition. Even though several efficient catalysts have been developed over the years, there is still a constant search for more efficient (e.g., activity, selectivity), inexpensive, recyclable, and eco-friendly catalyst candidates for synthesizing ALs under economically amenable reaction parameters. However, catalysts that function equally well with multiple feedstocks to form ALs following a general synthetic protocol are limited. Furthermore, the catalytic hydrogenation of LA leads to GVL. The synthesis of a noble metal catalyst with inexpensive carbon support can effectively upgrade LA to GVL.

Base-catalyzed transesterification of biomass-derived intermediates has been employed as a convenient and scalable strategy for synthesizing biorenewable esters of commercial significance. The diesters of glucose-derived IS can be used as novel surfactants and plasticizers. According to the literature reports, the base-catalyzed transesterification of IS resulted in a moderate yield of monoesters and a trace amount of diesters. Therefore, a systematic study of the base-catalyzed transesterification of all three isohexides under straightforward and scalable process conditions is warranted.

2.3 OBJECTIVES OF THE PRESENT WORK

Based on the literature survey, the primary objectives of the present work are as follows:

1. Synthesis and characterization of activated carbon from biomass and using them as catalyst support for the energy densification of biomass-derived intermediates.
2. Catalytic hydrogenation of biomass-derived angelica lactone and 2-furanone to GVL and GBL, respectively.
3. Synthesis and characterization of alkyl levulinates from renewable chemical intermediates like furfuryl alcohol, levulinic acid, and α-angelica lactone using an acid catalyst.
4. One-pot transformation of levulinic acid to γ-valerolactone using a metal-based catalyst.
5. Base-catalyzed transesterification of biomass-derived isohexides under solvent-free conditions.

The present work elaborates on synthesizing value-added chemicals from biorenewable intermediates using humin-derived activated carbon as catalyst support. Also, base-catalyzed transesterification isohexides are reported under solvent-free conditions. The thesis comprises seven chapters; details of each are outlined below:

CHAPTER 1 covers a general introduction to biomass, including its catalytic value-addition into sustainable production fuels, chemicals, and materials. **CHAPTER 2** briefly overviews the recent advances in the chemo-catalytic transformation of biomass-derived carbohydrates and humin into value-added products of commercial interest. The research gaps associated with the existing literature have been highlighted. The chapter outlines the scope and objectives of the present work. **CHAPTER 3** reports the production of ALs from carbohydrate-derived chemical intermediates using phosphotungstic acid supported on humin-derived activated carbon (PTA/HAC) as a recyclable catalyst. Humin obtained during the acid-catalyzed hydrolysis of xylose was used to prepare AC. ALs were prepared in good to excellent yields by the acid-catalyzed esterification of LA and by the alcoholysis of carbohydrate-derived chemical platforms, such as FAL and AGL. The reaction was optimized on the reaction temperature, duration, and catalyst loading. The catalyst recyclability was tested for five consecutive cycles with a marginal loss in the yield of ALs. **CHAPTER 4** discusses the base-catalyzed transesterification of isohexides into the mono- and diesters under solvent-free conditions. This chapter describes a solvent-free, high-yielding, and scalable pathway for producing the monoesters and diesters of IS by transesterification reaction using K_2CO_3 as an efficient, inexpensive, and recyclable base catalyst. Alkyl, aryl, vinyl esters of isohexides, and unsymmetrical diesters were synthesized and characterized. **CHAPTER 5** describes the renewable synthesis of GBL from biomass-derived 2-furanone using palladium supported on humin-derived activated carbon (Pd/HAC) as a heterogeneous catalyst. Using HAC as catalyst support, biomass-derived 2-furanone and AGL were hydrogenated to GBL and GVL, respectively. Different solvents were screened for the catalytic hydrogenation of 2-furanone to GBL, and THF gave the best results under optimized reaction conditions. **CHAPTER 6** describes the one-pot transformation of LA to GVL using heterogeneous catalysts (mono- and bifunctional catalysts). Heterogeneous catalysts (Ru/HAC and Ru-PTA/HAC) were prepared,

characterized, and used to transform LA into GVL. The catalytic activities of synthesized catalysts were studied in detail for LA to GVL transformation. The reaction parameters such as temperature, duration, hydrogen pressure, and catalytic amount were studied. Ru/HAC showed the best activity under optimized reaction conditions. **CHAPTER 7** summarizes the conclusions drawn from the present work and emphasizes future research scope.

CHAPTER 3

PRODUCTION OF ALKYL LEVULINATES FROM CARBOHYDRATE-DERIVED CHEMICAL INTERMEDIATES USING PHOSPHOTUNGSTIC ACID SUPPORTED ON HUMIN-DERIVED ACTIVATED CARBON (PTA/HAC) AS A RECYCLABLE HETEROGENEOUS ACID CATALYST

Abstract

This work reports a straightforward and high-yielding synthesis of alkyl levulinates (ALs), a class of promising biofuel, renewable solvent, and chemical feedstock of renewable origin. ALs were prepared by the acid-catalyzed esterification of levulinic acid (LA) and by the alcoholysis of carbohydrate-derived chemical platforms, such as furfuryl alcohol (FAL) and α-angelica lactone (AGL). Phosphotungstic acid (PTA) was chosen as the solid acid catalyst for the transformation, which was heterogenized on humin-derived activated carbon (HAC) for superior recyclability. Using HAC as catalyst support expands the scope of valorizing humin, a complex furanic resin produced inevitably as a side product (often considered waste) during the acid-catalyzed hydrolysis/dehydration of sugars and polymeric carbohydrates. Under optimized conditions (150 °C, 7 h, 25 wt.% PTA/HAC-600 catalyst), ethyl levulinate (EL) was obtained in an 85% isolated yield starting from FAL. Using the general synthetic protocol, EL was isolated in 88% and 84% yields from LA and AGL, respectively. The PTA/HAC-600 catalyst was successfully recovered from the reaction mixture and recycled for five cycles. A marginal loss in the yield of ALs was observed in consecutive catalytic cycles due to the partial leaching of PTA from the HAC support.

Graphical abstract

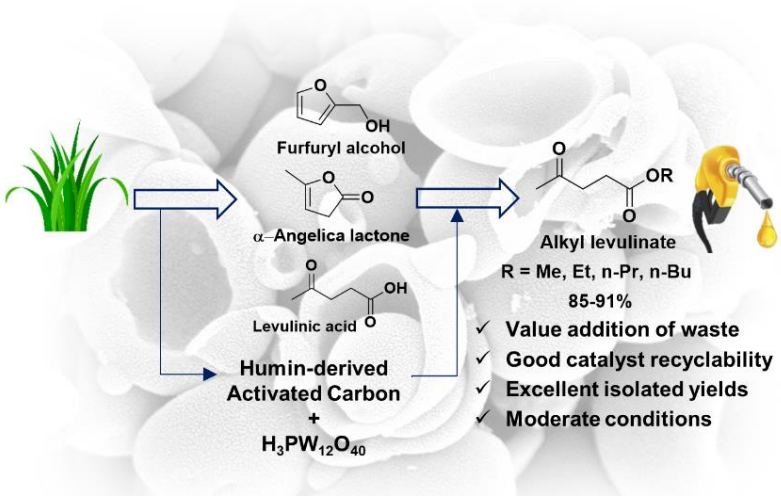

3.1 INTRODUCTION

The acid-catalyzed transformations are astounding from a green chemistry perspective since water is produced as the sole innocuous byproduct, and no

stoichiometric reagent is warranted. Furfural (FF) production from biomass has been commercialized, and many of its derivatives have established markets (Mariscal et al. 2016). For example, furfuryl alcohol (FAL), produced by the partial reduction of FF under catalytic hydrogenation conditions, has major applications in the paint and resin industry (Eseyin and Steele 2015). The production of 5-(hydroxymethyl)furfural (HMF) and its derivatives have a significant presence in the literature, and thousands of publications are added every year on their production, derivative chemistry, and applications (Xu et al. 2020a). Not surprisingly, FF and HMF have been recognized globally as the most promising carbohydrate-derived renewable chemical platforms for synthesizing products of commercial interest (Dusselier et al. 2014). HMF and FAL can be transformed into levulinic acid (LA) by hydrolysis at elevated temperatures under acid catalysis (Tian et al. 2021). LA has received significant attention as a carbohydrate-derived chemical platform to synthesize numerous renewable chemicals of commercial significance (Dutta and Bhat 2021). Commercial ventures, such as the Biofine process, demonstrated the direct transformation of lignocellulose into LA in acceptable yields and promising production costs (Hayes et al. 2005). Alkyl levulinates (ALs) can be produced from LA, FAL, LA-derived α-angelica lactone (AGL), and even directly from carbohydrates by reacting with C1-C4 monohydric alcohols under acid-catalyzed esterification and alcoholysis (Di Bucchianico et al. 2022). ALs have garnered immense attention due to their existing and emerging applications as biofuels, green solvents, and chemical intermediates for downstream synthetic value addition (Démolis et al. 2014). An acid catalyst of some sort is routinely used for these transformations, including mineral acids, solid Brønsted and Lewis acids (supported and unsupported), acidic resins, and acidic ionic liquids (Di Bucchianico et al. 2022). Even though several efficient catalysts have been developed over the years, there is still a constant search for more efficient (e.g., activity, selectivity), inexpensive, recyclable, and eco-friendly catalyst candidates for synthesizing ALs under economically amenable reaction parameters. However, catalysts that function equally well with multiple feedstocks to form ALs following a general synthetic protocol are rare.

In this regard, heteropoly acids (HPAs), the protonated versions of heteropolyoxometalates, are increasingly used in chemical-catalytic biomass value-addition pathways and sustainable chemistry (Ahmad et al. 2022b; Gao et al. 2023;

Zhang et al. 2021b). HPAs are considered a greener alternative to mineral acids and many other solid acid catalysts due to various advantageous properties, such as strong Brønsted acidity, low corrosivity, no volatility, high thermal stability, and tunable solubility (Luo et al. 2020). HPAs have already been explored as an acid catalyst in synthesizing ALs, and the works have recently been reviewed (Bhat et al. 2021). HPAs are often heterogenized by partially replacing the protons with suitable cations (e.g., Cs^+, quaternary ammonium) or supported on solid materials (e.g., SiO_2, zeolite) to assist their convenient recovery from the reaction mixture and recycling (Wu et al. 1996). Carbon is a promising heterogeneous supporting material for solid acids and metal catalysts due to its chemical resistance in acidic or basic reaction media, high thermal stability, low cost, and tailored morphology (Lam and Luong 2014; Lin et al. 2022). Interestingly, HPAs supported on activated carbon have also been reported for synthesizing ALs (Ayashi et al. 2022; Chhabra et al. 2022).

Humin is a complex furanic resin that forms as a side product when sugars and polymeric carbohydrates are dehydrated into FF, HMF, and LA (Patil et al. 2012). Recent studies have attempted to understand the mechanism of its formation so that the formation of this unwanted side product can be minimized (Xu et al. 2020b). Even though humin is typically combusted to produce process heat for other biorefinery processes, more profitable uses of humin, such as renewable materials and catalyst support, are being explored (Liu et al. 2022a). A carbonaceous solid acid catalyst derived from humin (produced during the dehydration of glucose) has been used as an efficient acid catalyst with a high surface area for synthesizing ALs and diesel fuel precursors from LA and FF (Yang et al. 2020). Humin-derived carbon is a promising catalyst support for HPAs as a heterogeneous acid catalyst in synthesizing ALs from carbohydrate-derived chemical intermediates. Value-adding humin as a supporting material for catalysts would be beneficial for improving the commercial appeal of an integrated biorefinery.

This work heterogenized the Keggin-type phosphotungstic acid (PTA, $H_3PW_{12}O_{40}$) on humin-derived activated carbon (HAC) to develop a heterogeneous acid catalyst. Humin used in this work was obtained by the acid-catalyzed dehydration of xylose into FF. The PTA/HAC-600 was then used as a heterogeneous acid catalyst for the alcoholysis of FAL with C1-C4 monohydric alcohols in a batch-type sealed

glass reactor. Moreover, other chemical intermediates such as LA and AGL have also been successfully converted into ALs in excellent isolated yields (Scheme 3.1). The PTA/HAC-600 catalyst was recovered from the reaction medium by centrifugation and successfully recycled for several cycles. The PTA/HAC-600 catalysts (fresh and recycled) were characterized by Fourier Transform Infrared Spectroscopy (FTIR), Powder X-Ray Diffraction (PXRD), Field Emission Scanning Electron Microscopy-Energy Dispersive X-Ray Analysis (FESEM-EDX), NH_3-Thermal Conductivity Detector (TCD), and Brunauer-Emmett-Teller (BET) surface area analyzer.

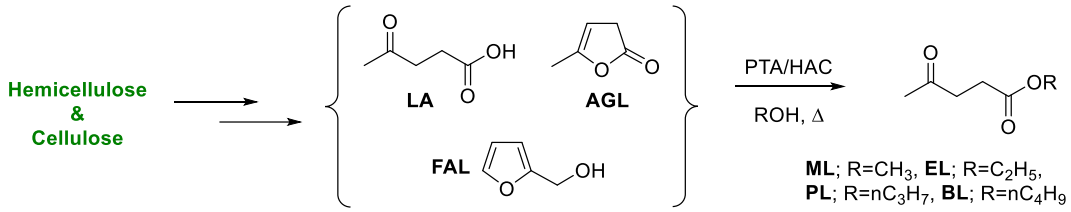

Scheme 3.1 Preparation of alkyl levulinates from levulinic acid and other chemical intermediates using phosphotungstic acid supported on humin-derived activated carbon as the acid catalyst.

3.2 EXPERIMENTAL PROCEDURE

3.2.1 Materials

Phosphotungstic acid hydrate was purchased from Sigma. HCl (aq., 35–38%) was purchased from Molychem. Xylose (99%), levulinic acid (LA, 98%), furfuryl alcohol (FAL, 98%), and benzyltributylammonium chloride (BTBAC, 99%) were procured from Spectrochem. n-Propanol (99.5%), n-butanol (99%), deionized (DI) water, 1,2-dichloroethane (DCE, extra pure), and sodium sulfate (anhydrous, 99%) were purchased from Loba Chemie Pvt. Ltd. Ethanol (99.9%) was procured from CSS. Methanol (99.9%) and chloroform (98%) were purchased from Finar. AGL was purchased from TCI. All the alcohols were used after drying over activated molecular sieves (4 Å) at room temperature for 12 h.

3.2.2 Preparation of Humin

Humin was obtained as the byproduct during the dehydration of xylose into FF in an aqueous-organic biphasic batch reaction setup (Bhat et al. 2020). In a round-bottomed glass pressure vessel fitted with a Teflon screw-top, xylose (2.00 g), HCl (20 mL, 20.2% aq.), DCE (20 mL), and BTBAC (10 wt.% of xylose) were introduced. The

reactor was sealed, placed in a preheated (100 °C) oil bath, and stirred magnetically at 400 rpm for 3 h. The biphasic reaction mixture slowly turned from colorless to yellow to dark brown. After 3 h, the reactor was lifted from the oil bath and cooled in air. The reaction mixture was filtered through filter paper under a vacuum. The black solid residue (humin) collected on the filter paper was washed with DCE (25 mL) to remove soluble organic residues, followed by excess deionized water. The humin was dried in a hot-air oven for 24 h at 80 °C.

3.2.3 Preparation of HAC

Humin was chemically activated using H_3PO_4. In a typical process, 2 g of humin was mixed intimately with 85% H_3PO_4 (1:3, *w*/*w*) in a silica crucible and kept for 2 h. The mixture was carbonized at 500 and 600 °C in a muffle furnace for 2 h under N_2 flow. When the mixture was carbonized at 700 °C, it combusted partially, even under nitrogen flow. After carbonized mass (500 and 600 °C) was cooled to RT, suspended in deionized water (100 mL), and ultrasonicated for 30 min. The suspension was then filtered under a vacuum and repeatedly washed with deionized water until the pH of the filtrate increased to 7. The prepared samples were dried at 60 °C for 12 h in a hot-air oven and further sonicated for 30 min in methanol for uniform dispersion. After removing methanol, the carbon was dried at 110 °C for 6 h, powdered in a mortar, and labeled as HAC-X, X corresponds to carbonization temperature.

3.2.4 Preparation of Catalyst

The catalyst was prepared by the incipient wetness impregnation method (Kozhevnikov et al. 1996). HAC-600 (0.4 g) was suspended in dry methanol (75 mL) and stirred for 30 min under room temperature. PTA (0.1 g) dissolved in methanol (10 mL) was added dropwise to the suspension under vigorous magnetic stirring, and the stirring was continued overnight at room temperature. After removing methanol under reduced pressure in a rotary evaporator, the catalyst was dried at 110 °C in a hot-air oven for 10 h. The catalyst was labeled as 20%PTA/HAC-600. The same preparative method was followed to prepare 20%PTA/HAC-500 using HAC-500 as the supporting material.

3.2.5 Characterization Methods of Catalyst

The surface morphology of the samples was investigated using field-emission scanning electron microscopy (FESEM) in 7610FPLUS (Jeol, Japan) and Gemini 300

Carl Zeiss, operating at an accelerating voltage of 15 kV. Powder X-ray diffraction (PXRD) spectra were recorded in a MiniFlex 600 (Rigaku, Japan) X-ray Powder Diffractometer using Cu Kα radiation as the source. Fourier-transform infrared spectroscopy (FTIR) of support and catalyst were recorded on a Bruker Alpha 400 FTIR spectrometer using the KBr pellet technique. The Brunauer–Emmett–Teller (BET) surface area of the samples was measured using Autosorb IQ-XR-XR, Anton Paar, employing N_2 adsorption at 77.35 K. The pore size distribution of the samples was determined from nitrogen desorption isotherms using the Barrett–Joyner–Halenda (BJH) method. The temperature-programmed desorption (TPD) measurement was performed using Quantachrome TPRWin v3.52 instrument. The sample was activated in helium gas with a flow rate of 30 mL min^{-1} at 200 °C for 110 min. After cooling, the sample was saturated with 10% NH_3 blended in He with a flow rate of 30 mL min^{-1} for 60 min. The analysis was carried out in the 100–800 °C temperature range with a heating rate of 10 °C min^{-1}.

3.2.6 Catalytic Conversion of Biomass-Derived FAL, LA, and AGL to ALs

In a typical reaction, FAL (0.5 g), methanol (5 mL), and 25 wt.% PTA/HAC-600 were charged into a 50 mL ACE glass pressure reactor fitted with a Teflon screw top and a magnetic stir bar. The glass pressure reactor was placed in a preheated oil bath (150 °C) and stirred magnetically for 7 h. After the reaction, the reactor was cooled to room temperature and opened. The excess methanol was evaporated in a rotary evaporated under reduced pressure. The leftover was then diluted in chloroform (20 mL) and the suspension was centrifuged to precipitate the catalyst. The catalyst was then washed with fresh chloroform (2 × 10 mL) and was then dried in a hot-air oven at 110 °C for 5 h before subjecting it to the next catalytic cycle. The chloroform solution was then evaporated in a rotary evaporator under reduced pressure to obtain the crude product. The crude product was chromatographed (silica gel, chloroform) to obtain pure methyl levulinate (ML, 0.58 g, 87%) as a clear liquid. For FAL and LA, the reaction duration was 7 h. In the case of AGL, the reaction was worked up after 9 h. The reaction procedure was extended for other alcohols such as ethanol, n-propanol, and n-butanol. The spectroscopic data of the synthesized compounds were matched with literature reports (Enumula et al. 2017b; Onkarappa et al. 2020).

3.3 CHARACTERIZATION OF SYNTHESIZED COMPOUNDS

The progress of a reaction, the identification of the product(s) formed, and even the purity of the same was confirmed by using different spectroscopic techniques. The FTIR is used to identify the functional group(s) present in the synthesized compounds. FTIR spectra were recorded on a Bruker Alpha 400 FTIR spectrometer equipped with silicon carbide as an IR source. All sample spectra were recorded using the ATR technique. The FTIR spectra were collected by performing 24 scans at a scanning rate of 4 cm^{-1}/s in the range between 500-4000 cm^{-1}. The ^{1}H-NMR spectra of the synthesized compounds were collected by dissolving the compounds in suitable deuterated solvent and then recording the data in a Bruker NanoBay® and Jeol (JNM-ECZ400/L1) instrument operating at 300 & 400 MHz. The ^{13}C-NMR spectra (broadband decoupling) were recorded in the same instrument at a calculated frequency of 75 & 100 MHz.

3.3.1 The FTIR, ^{1}H-NMR, and ^{13}C-NMR of Methyl levulinate (ML)

^{1}H-NMR ($CDCl_3$, 400 MHz) δ (ppm): 3.60 (s, 3H), 2.69 (t, 2H, *J* = 6.8 Hz), 2.50 (t, 2H, *J* = 6.4 Hz), 2.12 (s, 3H); ^{13}C-NMR ($CDCl_3$, 100 MHz) δ (ppm): 205.7, 172.2, 50.8, 36.9, 28.8, 26.7; FTIR (ATR, cm^{-1}): 2955, 2852, 1712, 1157.

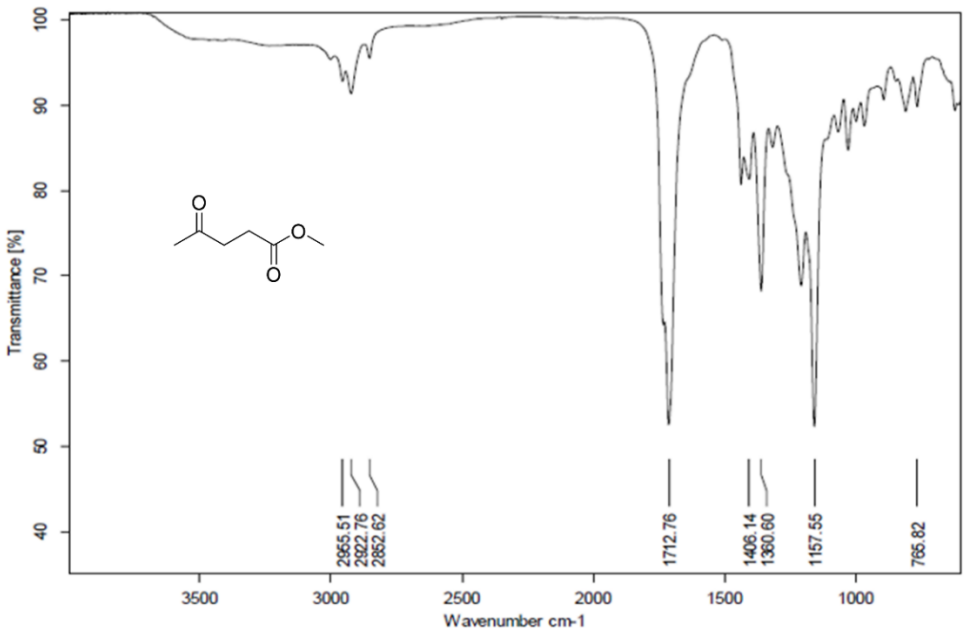

Figure 3. 1 The FTIR spectrum of methyl levulinate (ML).

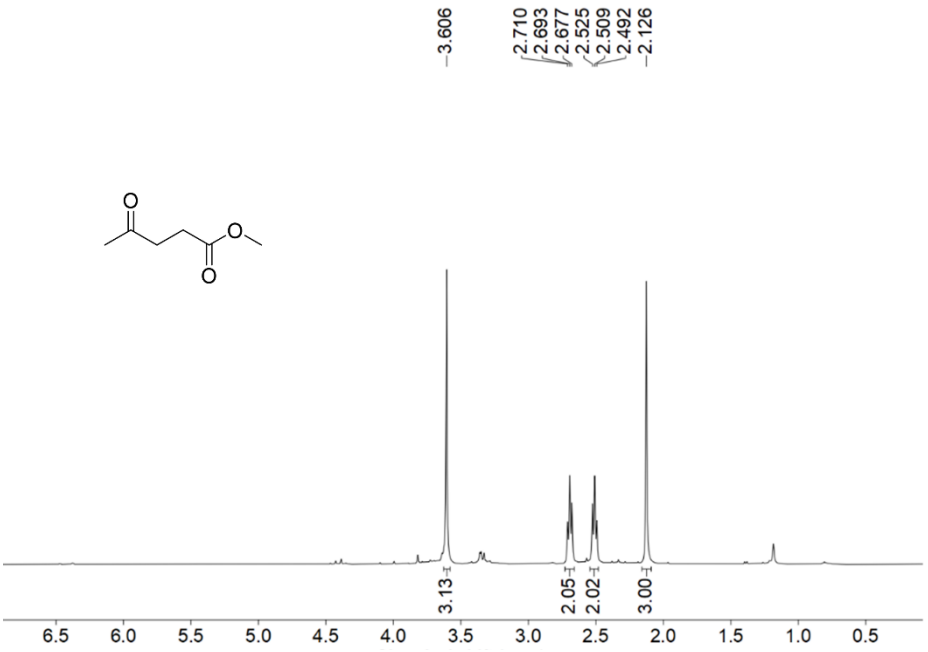

Figure 3.2 The ^{1}H-NMR spectrum of methyl levulinate (ML).

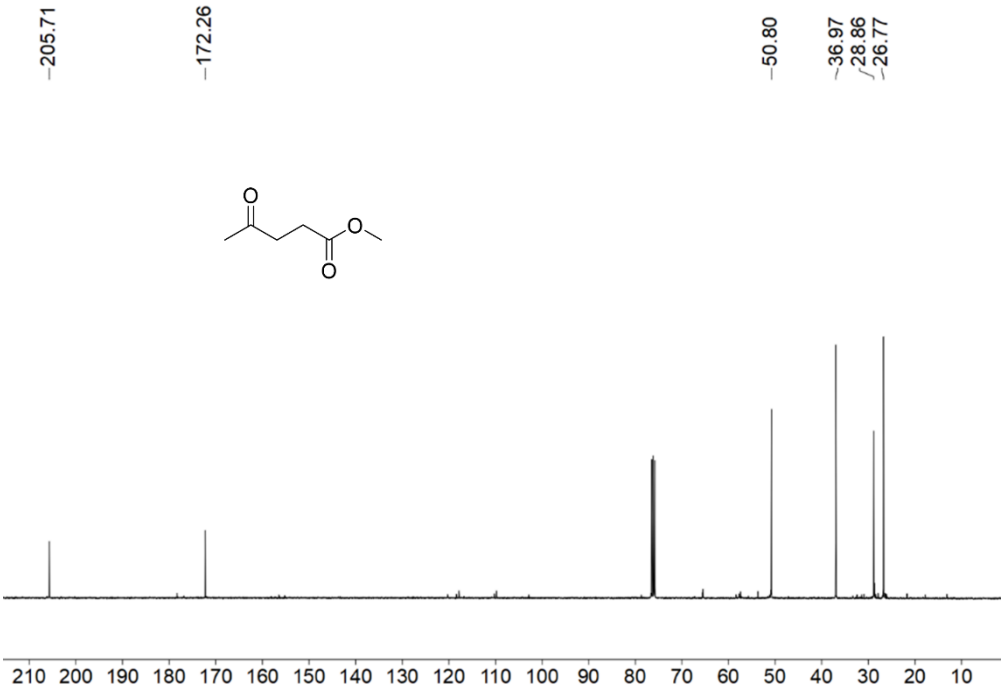

Figure 3.3 The ^{13}C-NMR spectrum of methyl levulinate (ML).

3.3.2 The FTIR, ^{1}H-NMR, and ^{13}C-NMR of Ethyl levulinate (EL)

^{1}H-NMR ($CDCl_3$, 400 MHz) δ (ppm): 4.05 (q, 2H, *J* = 7.2 Hz), 2.68 (t, 2H, *J* = 6.4 Hz), 2.49 (t, 2H, *J* = 6.4 Hz), 2.12 (s, 3H), 1.18 (t, 3H, *J* = 7.2 Hz); ^{13}C-NMR ($CDCl_3$, 100 MHz) δ (ppm): 205.7, 171.7, 59.5, 36.8, 28.8, 27.0, 13.08; FTIR (ATR, cm^{-1}): 2981, 2929, 1718, 1096.

3.3.3 The FTIR, ^{1}H-NMR, and ^{13}C-NMR of Propyl levulinate (PL)

^{1}H-NMR ($CDCl_3$, 400 MHz) δ (ppm): 3.95 (t, 2H, *J* = 6.4 Hz), 2.68 (t, 2H, *J* = 6.4 Hz), 2.49 (t, 2H, *J* = 6.4 Hz), 2.11 (s, 3H), 1.57 (m, 2H), 0.86 (t, 3H, *J* = 6.0 Hz); ^{13}C-NMR ($CDCl_3$, 100 MHz) δ (ppm): 206.6, 172.7, 66.1, 37.8, 29.7, 27.9, 21.8, 10.2; FTIR (ATR, cm^{-1}): 2965, 2880, 1719, 1156.

3.3.4 The FTIR, ^{1}H-NMR, and ^{13}C-NMR of Butyl levulinate (BL)

^{1}H-NMR ($CDCl_3$, 400 MHz) δ (ppm): 4.04 (t, 2H, *J* = 6.8 Hz), 2.72 (t, 2H, *J* = 6.8 Hz), 2.54 (t, 2H, *J* = 6.8 Hz), 2.16 (s, 3H), 1.57 (m, 2H), 1.35 (m, 2H), 0.90 (t, 3H, *J* = 7.6 Hz); ^{13}C-NMR ($CDCl_3$, 100 MHz) δ (ppm): 206.7, 172.9, 64.6, 38.0, 30.6, 29.9, 28.0, 19.1, 13.7; FTIR (ATR, cm^{-1}): 2961, 2875, 1717, 1069.

3.4 RESULTS AND DISCUSSION

3.4.1 Physicochemical Characterization

The adsorption capacities of the synthesized HACs were determined by iodine number (IN) using ASTM D 4607-94 standards (Table 3.1) (ASTM-D4607-14R21). The IN of HAC-500 and 600 were calculated to be 727 mg/g and 853 mg/g, respectively. The textural characterization of the synthesized HACs was studied using nitrogen adsorption–desorption analysis, and the samples exhibited type IV adsorption isotherm. As observed from the BJH pore size distribution curves, the pore size ranged between 2 nm and 40 nm, and a distinct peak at 4.25 nm confirms that the materials are mesoporous with relatively uniform pore size distribution (Figure 3.4). HAC-600 was used for the catalyst preparation because of its higher BET surface area than HAC-500 (Table 3.1). The high IN and BET surface area of HAC-600 makes it better catalyst support with a large micro- and mesoporous structure.

Table 3.1 Pore structure parameters of HAC-500, HAC-600, 20%PTA/HAC-500, and 20%PTA/HAC-600.

Sample	IN (mg/g)	S_{BET} (m^2/g)	V_{total} (cc/g)	D_{avg} (nm)
HAC-500	727	1203	0.32	3.4
HAC-600	853	1435	0.33	2.8
20%PTA/HAC-500	-	937	0.11	3.4

20%PTA/HAC-600	-	947	0.12	2.5

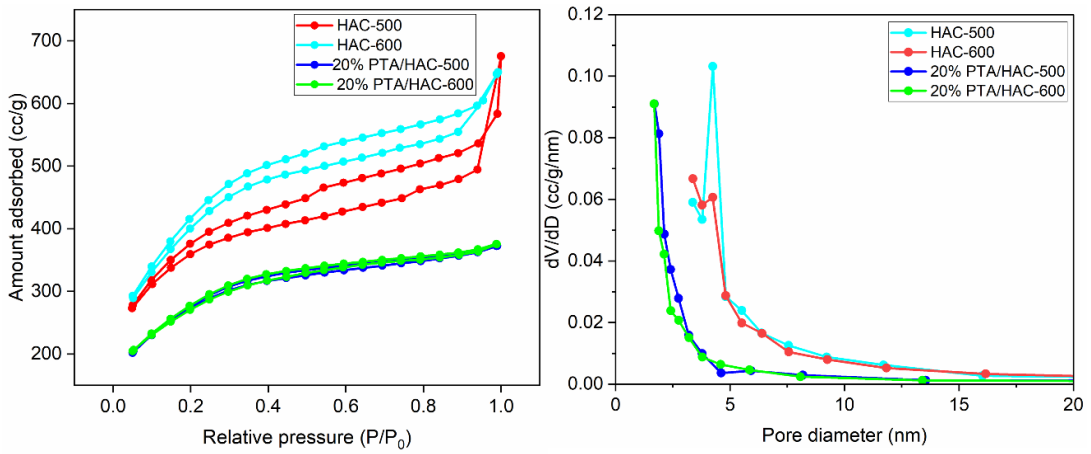

Figure 3.4 (**a**) N_2 adsorption isotherms and (**b**) BJH pore size distribution curves of HAC-500, HAC-600, and 20%PTA/HAC-600.

The surface morphology of the materials was determined using field-emission scanning electron microscopy (FESEM). The presence of constituent elements was confirmed by energy-dispersive X-ray analysis (EDX) (Figure 3.5). The elemental mapping of the catalyst further confirmed the uniform distribution of the constituent elements.

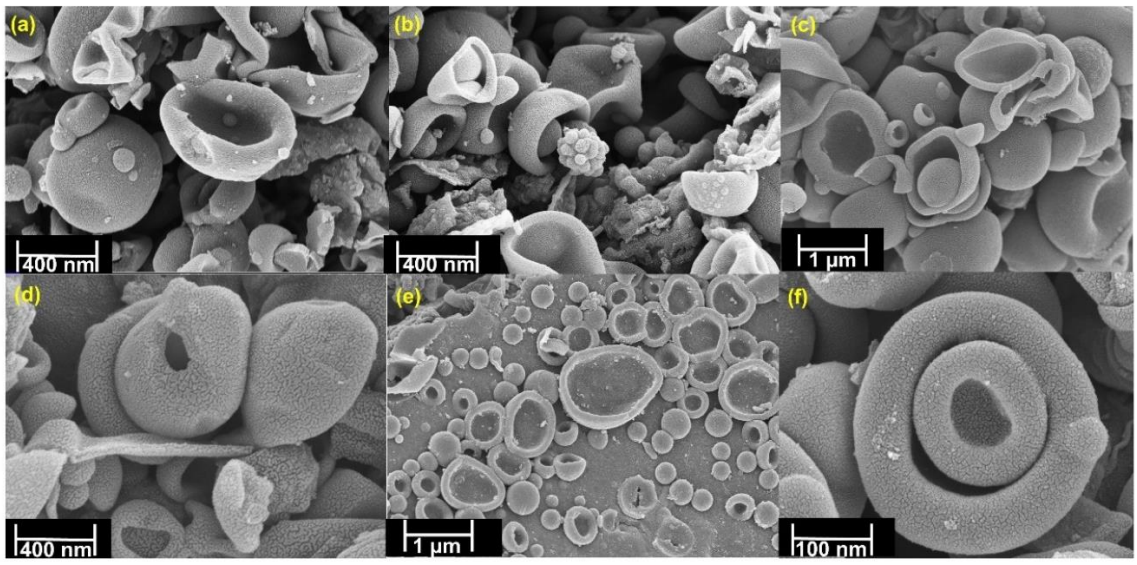

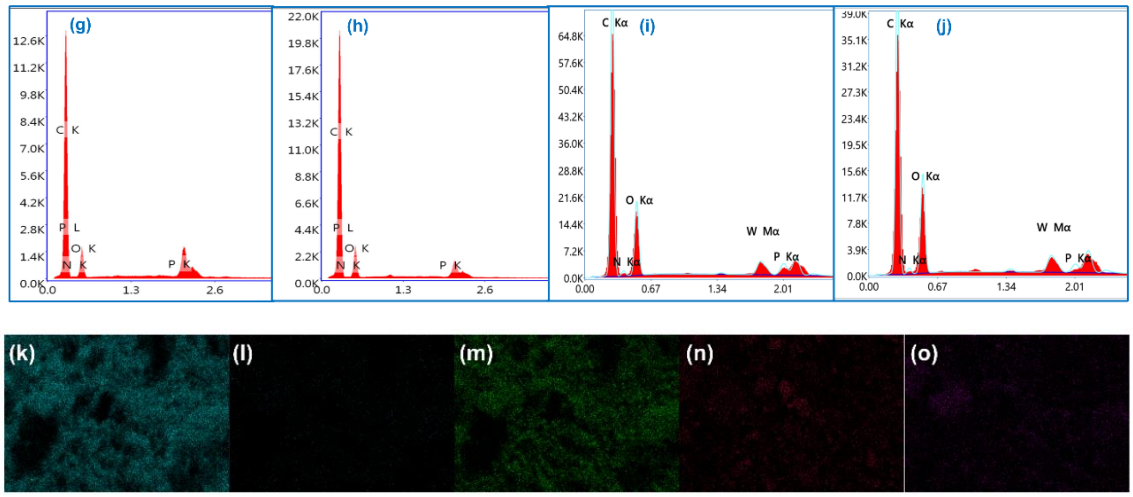

Figure 3.5 FESEM images of (a) HAC-500, (b) HAC-600, (c,d) 20%PTA/HAC-600, and (e,f) 20%PTA/HAC-600 recycled after the fifth cycle; EDX pattern of (g) HAC-500, (h) HAC-600, and (i) 20%PTA/HAC-600, and (j) 20%PTA/HAC-600 recycled after the fifth cycle; Elemental mapping of catalyst (k) C, (l) N, (m) O, (n) W, and (o) P.

The powder x-ray diffraction (PXRD) patterns of the HACs and catalyst are shown in Figure 3.6a. The scan was recorded in the 2θ range between 10–60°. A broad diffraction peak at 2θ = 23° confirms the amorphous nature of HAC. It is evident from the literature that peaks located at 2θ = 23° and 43° for AC-500 and 600 correspond to (002) and (101) planes of carbon. For PTA, peaks at 2θ = 10.8°, 18.3°, 23.5°, 25.6°, 29.9°, 35°, and 38.2° indicate the Keggin-type structure (JCPDS No. 50-0657). Distinct peaks of PTA are masked by the catalyst support (i.e., HAC) due to insufficient loading. The FTIR spectra of the HACs and the catalyst are shown in Figure 3.6b. The bands 2909 and 2838 cm^{-1} correspond to C-H asymmetric and symmetric stretching, whereas bands assigned 1612 and 1392 cm^{-1} correspond to C=C stretch and C-H bending vibrations. The peaks at 1079, 885, and 773 cm^{-1} correspond to P-O_a, W-O_c-W, and W-O_e-W vibrational frequencies. The O_a, O_t, O_c, and O_e atoms represent the internal, terminal, corner, and edge-shared oxygen atoms. The NH_3-TPD profile for the catalyst is shown in Figure 3.7. Based on the temperature at which adsorbed ammonia molecules desorb, the acidic sites in catalysts can be divided into several groups. Weak acidic sites desorb ammonia around 200–300 °C, moderate acidic sites around 300–450 °C and strong acidic sites above 450 °C. From Figure 3.7, it is evident that the catalyst

possesses weak and moderate acidic sites. The total acidity of the catalyst is calculated to be 1.7 mmol/g.

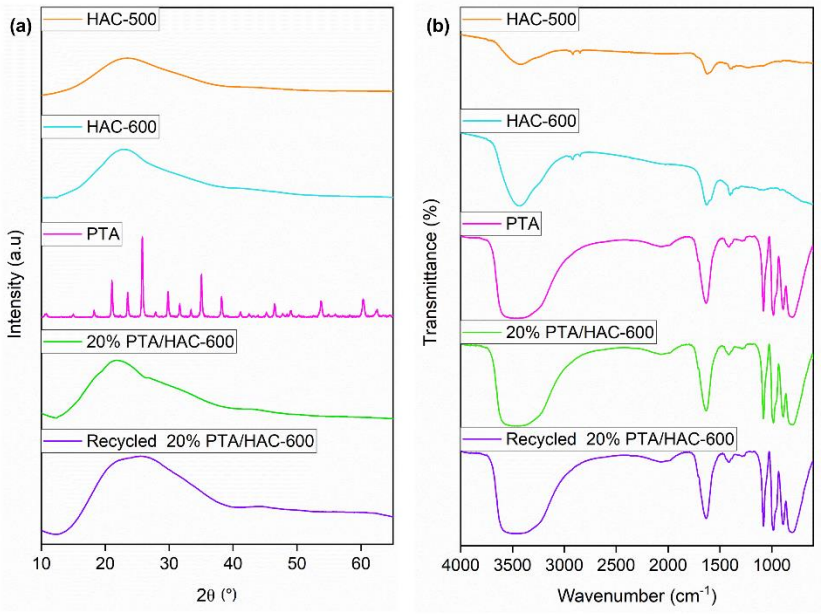

Figure 3.6 (a) PXRD patterns, and (b) FTIR spectra of HAC-500, HAC-600, PTA, 20%PTA/HAC-600, and recycled (5th cycle) 20%PTA/HAC-600.

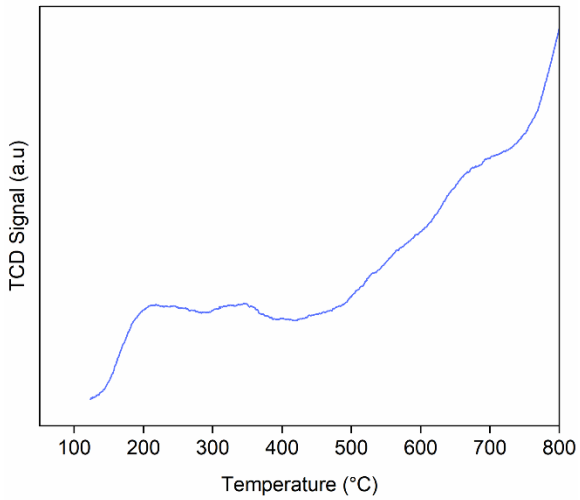

Figure 3.7 NH_3-TPD pattern of the 20%PTA/HAC-600 catalyst.

3.4.2 Catalytic Tests

The catalytic activity of the prepared 20%PTA/HAC-600 catalyst was evaluated towards the alcoholysis of FAL using excess methanol at 150 °C for the synthesis of ML. Firstly, the catalytic activity of 20%PTA/HAC-600 was compared with unsupported PTA and HAC-600. The use of the same amount of PTA (in comparison

with PTA/HAC-600) gave only a 25% yield of ML, and in the case of HAC-600, no conversion of FAL to ML was observed under identical reaction conditions (150 °C, 7 h). The results can be explained by the rapid decomposition of FAL in the presence of homogeneous PTA. Since HAC has no significant acidic sites, it failed to catalyze the methanolysis of FAL. Furthermore, the effect of reaction parameters such as temperature, time, and catalyst loadings on the yield of ML was studied using FAL as a model substrate. All the reactions were performed in triplicate, and the average yields of isolated and spectroscopically pure ALs are reported. The yield variation between the trials was only 2–3%.

Temperature is one of the profound reaction parameters affecting the conversion of the starting material and the yield of the desired product. When the reaction was carried out at lower temperatures (<150 °C), only moderate yields of ML (<70%) were obtained due to incomplete conversion of FAL (Figure 3.8). Quantitative conversion of FAL was ensured when the reaction was performed in a batch-type glass pressure reactor for 7 h at 150 °C, affording an 87% isolated yield of ML. However, further increasing the reaction temperature to 160 °C lowered the yield of ML due to the accelerated decomposition of FAL and ML.

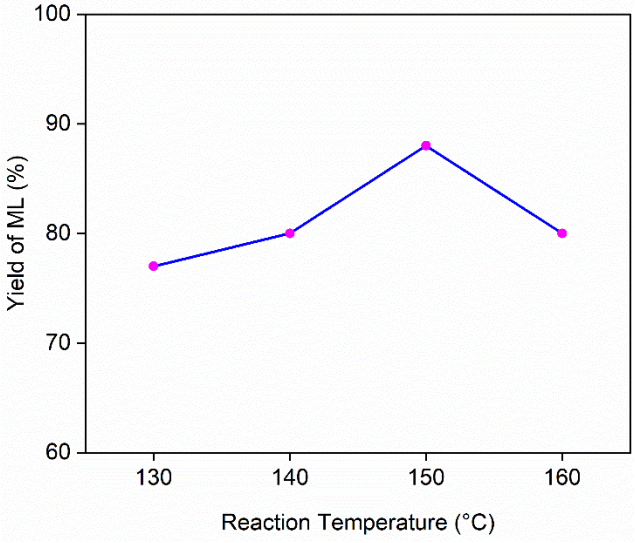

Figure 3.8 Effect of reaction temperature on the yield of ML.

Reaction conditions: FAL (0.5 g, 5.09 mmol), methanol (5 mL), 20%PTA/HAC-600 (25 wt.%, 0.125 g), 7 h.

The effect of reaction duration was studied by varying the time between 5–8 h (Figure 3.9a). When the reaction was conducted for 7 h, ML was obtained in an 87% isolated yield with the quantitative conversion of FAL. No perceptible increase in the yield of ML was observed by prolonging the reaction time to 8 h. However, lowering the duration to 6 h decreased the isolated yield of ML to 75%. The result may be explained by the incomplete conversion of FAL in 6 h. The catalyst loading was varied from 10 wt.% to 30 wt.% to see its influence on the yield of ML (Figure 3.9b). Lower catalyst loadings (10 wt.%) resulted in the low conversion of FAL. The slow reaction kinetics resulting from the low concentration of acid sites catalyzing the transformation can explain the result. A quantitative conversion of FAL with an 87% isolated yield of ML was obtained at 25 wt.% loading of 20%PTA/HAC-600. A further increase in the catalyst loading to 30 wt.% resulted in only a marginal increase (ca. 89%) in ML yield.

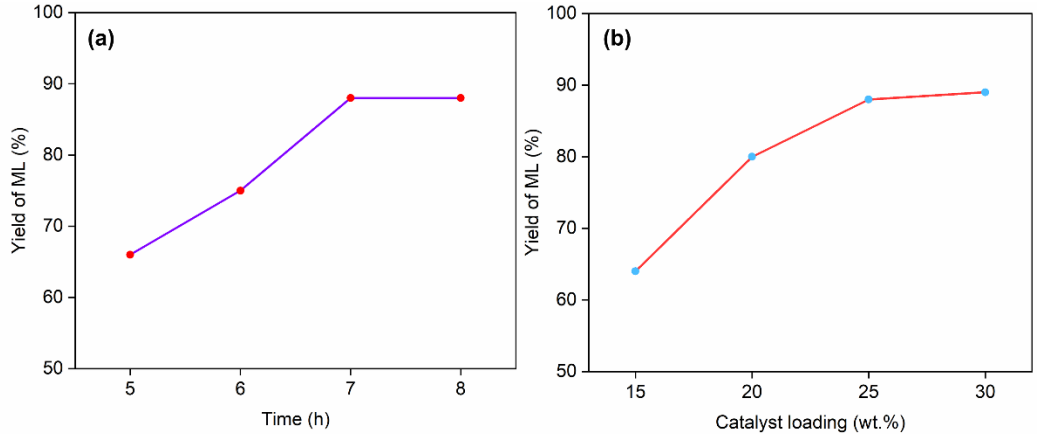

Figure 3.9 (a) Effect of reaction time on ML yield and (b) Effect of catalyst loading on the yield of ML.

Reaction conditions: (a) FAL (0.5 g, 5.09 mmol), methanol (5 mL), 20%PTA/HAC-600 (25 wt.%, 0.125 g), 150 °C and (b) FAL (0.5 g, 5.09 mmol), methanol (5 mL), 150 °C, 7 h.

Therefore, ML was isolated in an 87% yield at the quantitative conversion of FAL under optimized reaction conditions (150 °C, 7 h, 25 wt.% of PTA/HAC-600). The same optimized reaction conditions were applied to synthesize ALs using C1-C4 alcohols (Table 3.2). Under identical reaction conditions, EL, PL, and BL were isolated in 85%, 83%, and 85% yield, respectively, using 20%PTA/HAC-600 as a heterogeneous acid catalyst.

Table 3.2 Conversion of FAL to ALs.

Entry	Product	Yield (%)
1	ML	87
2	EL	85
3	PL	83
4	BL	85

Reaction conditions: FAL (0.5 g, 5.09 mmol), alcohol (5 mL), 20%PTA/HAC-600 (25 wt.%, 0.125 g), 150 °C, 7 h.

We envisaged that the synthetic protocol would work equally well for synthesizing ALs starting from biomass-derived intermediates, such as LA and AGL. Esterification of LA with n-propanol provided PL in a 90% isolated yield, whereas methanol, ethanol, and n-butanol gave 85%, 88%, and 87% of ML, EL, and BL, respectively (Table 3.3).

Table 3.3 Conversion of LA to ALs.

Entry	Product	Yield (%)
1	ML	85
2	EL	88
3	PL	90
4	BL	87

Reaction conditions: LA (0.5 g, 4.30 mmol), alcohol (5 mL), 20%PTA/HAC-600 (25 wt.%, 0.125 g), 150 °C, 7 h.

The same protocol was extended to synthesize ALs from AGL using C1-C4 alcohols (Table 3.4). When the reaction was carried out using methanol, 91% of ML was isolated. The use of ethanol provided 84% of EL, whereas n-propanol and n-butanol resulted in 86% PL and 88% BL, respectively, starting from AGL when the reactions were performed at 150 °C for 9 h using 20%PTA/HAC-600 (25 wt.% of AGL) catalyst.

Table 3.4 Conversion of AGL to ALs.

Entry	Product	Yield (%)
1	ML	91
2	EL	84
3	PL	86
4	BL	88

Reaction conditions: AGL (0.5 g, 5.09 mmol), alcohol (5 mL), 20%PTA/HAC-600 (25 wt.%, 0.125 g), 150 °C, 9 h.

The catalytic tests were further carried out using a 20%PTA/HAC-500 catalyst for the conversion of FAL using C1-C4 alcohols, and the results were compared with a 20%PTA/HAC-600 catalyst. A marginal decrease in the yields of ALs was only observed using a 20%PTA/HAC-500 catalyst. Under optimized reaction conditions, ML was obtained in 85% yield, whereas EL, PL, and BL were obtained in 85, 82, and 83% yields, respectively (Figure 3.10). The results may be explained by the better adsorption of PTA on HAC-600 when compared to HAC-500 due to better porosity and higher surface area of the former supporting material.

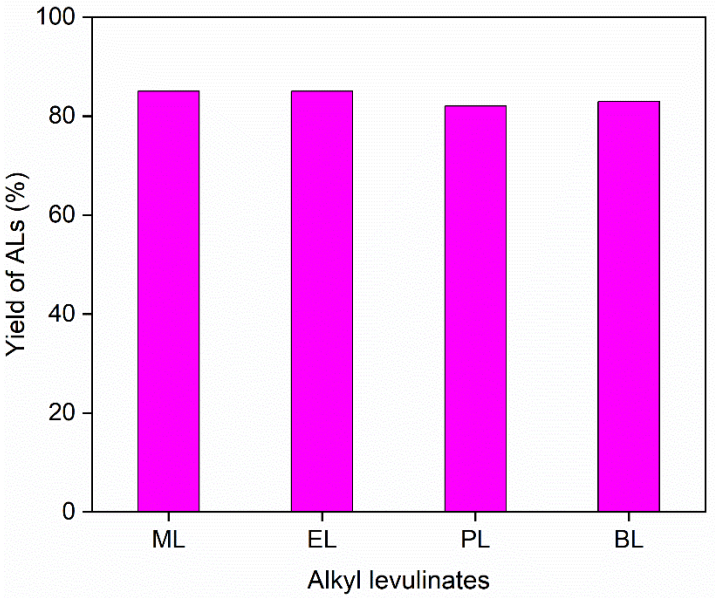

Figure 3.10 Conversion of FAL to various ALs using 20%PTA/HAC-500 catalyst. *Reaction conditions:* FAL (0.5 g, 5.09 mmol), alcohol (5 mL), 20%PTA/HAC-500 (25 wt.%, 0.125 g), 7 h.

3.4.3 Catalyst Recyclability

The recyclability of the PTA/HAC-600 catalyst used for transforming FAL into ML was studied (Figure 3.11). The trials were carried out under optimized reaction conditions (0.5 g FAL, 150 °C, 7 h, 25 wt.% catalyst, 5 mL methanol). After the reaction, the volatiles (i.e., excess methanol) were removed from the mixture under reduced pressure. The catalyst was centrifuged and washed with chloroform. The catalyst was dried at 110 °C for 5 h before using it in the next catalytic cycle. The catalyst was successfully recycled for five consecutive cycles with good conversion and selectivity towards ML. Since there was minor mass loss during the catalyst recovery, the starting amount of FAL was adjusted accordingly for consistency of catalyst loading in consecutive cycles. Up to the third cycle, the loss in yield of ML was nominal, whereas the fourth and fifth cycles showed a noticeable loss in yield.

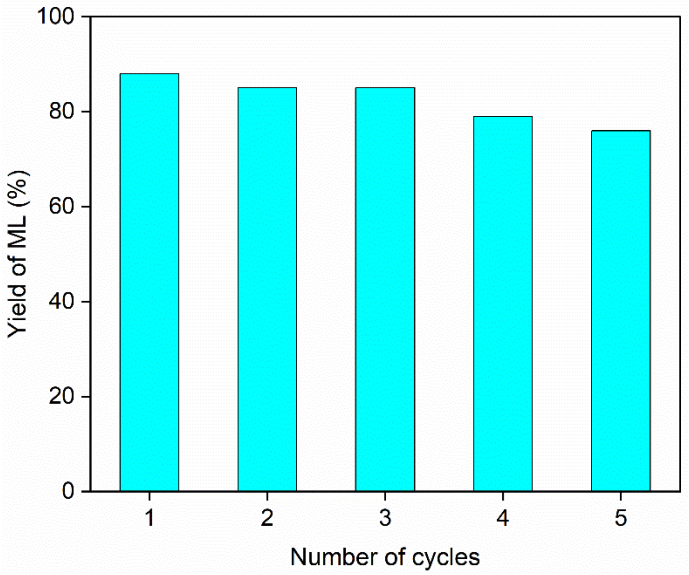

Figure 3.11 Catalyst recyclability test for the conversion of FAL to ML.
Reaction conditions: FAL (0.5 g, 5.09 mmol), methanol (5 mL), 20%PTA/HAC-600 (25 wt.%, 0.125 g), 150 °C, 7 h.

Whereas the fresh 20%PTA/HAC-600 catalyst afforded an 87% yield of ML, the catalyst for the fifth consecutive cycle gave a 76% yield. Marginal loss in ML yield can be due to the slight leaching of PTA from the HAC-600 support, a common occurrence in supported acid catalysts.

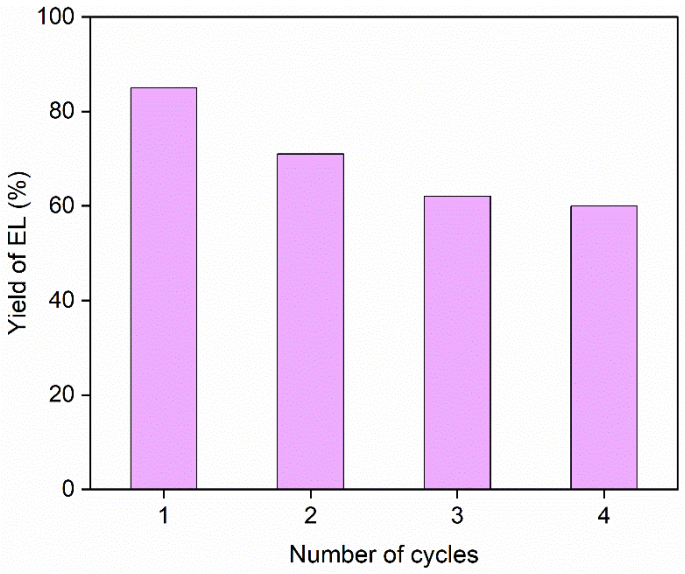

Figure 3.12 Catalyst recyclability test for the conversion of LA to EL.
Reaction conditions: LA (0.5 g, 4.30 mmol), ethanol (5 mL), 20%PTA/HAC-600 (25 wt.%, 0.125 g), 150 °C, 7 h.

The catalyst recyclability was also examined for esterifying LA with alkyl alcohols. The process is more challenging since water is formed as a byproduct, which may lead to increased leaching of PTA from the HAC-600 support. As predicted, the fresh catalyst provided an 88% yield of EL from LA, which decreased to 62% after the third catalytic cycle (Figure 3.12). However, the prior evaporation of polar volatiles (i.e., ethanol, water) before separating the catalyst assists in redepositing the leached PTA back into the HAC-600 support.

3.5 CONCLUSION

Humin worked as a promising feedstock for deriving activated carbon with high surface area with micro- and mesoporosity. HAC was successfully used as a supporting material for PTA to produce a heterogeneous acid catalyst. The PTA/HAC-600 catalyst produced alkyl levulinates in good to excellent isolated yields starting from carbohydrate-derived chemical intermediates, such as LA, FAL, and AGL. The catalyst was successfully recovered and recycled for five catalytic cycles. This work will create interest in the high-value application of humin, a waste product produced in the biorefinery. Future work will explore the efficiency of the PTA/HAC-600 catalyst towards other acid-catalyzed reactions for the catalytic value addition of biomass and sustainable organic synthesis in general.

CHAPTER 4

EFFICIENT PREPARATION OF THE ESTERS OF BIOMASS-DERIVED ISOHEXIDES BY BASE-CATALYZED TRANSESTERIFICATION UNDER SOLVENT-FREE CONDITION

Abstract

The monoesters and diesters of glucose-derived isosorbide (IS) have a number of applications, such as dispersants in pigments, surfactants in detergents, emulsifiers in cosmetics, monomers for biopolymers, and plasticizers in vinyl polymers. This work reports a solvent-free, high-yielding, and scalable pathway for producing the monoesters and diesters of IS by transesterification reaction using K_2CO_3 as an efficient, inexpensive, and recyclable base catalyst. Selectivity toward the exo-monoester of IS was higher than the endo-monoester due to relative thermodynamic stability of the former, which was supported by literature precedence. The methodology was successfully extended to synthesize the monoesters and diesters of the other two isohexides, i.e., isomannide and isoidide. The gram-scale preparation of alkyl, vinyl, and aryl esters of isohexides was optimized on the reaction temperature, duration, equivalence of the ester reagent, and catalyst loading. Under optimized conditions (180 °C, 6 h, 50 mol% K_2CO_3), various aryl and alkyl esters of the isohexides were isolated in excellent to good yields. The unsymmetrical diesters of isohexides have also been produced using step-wise transesterification.

Graphical abstract

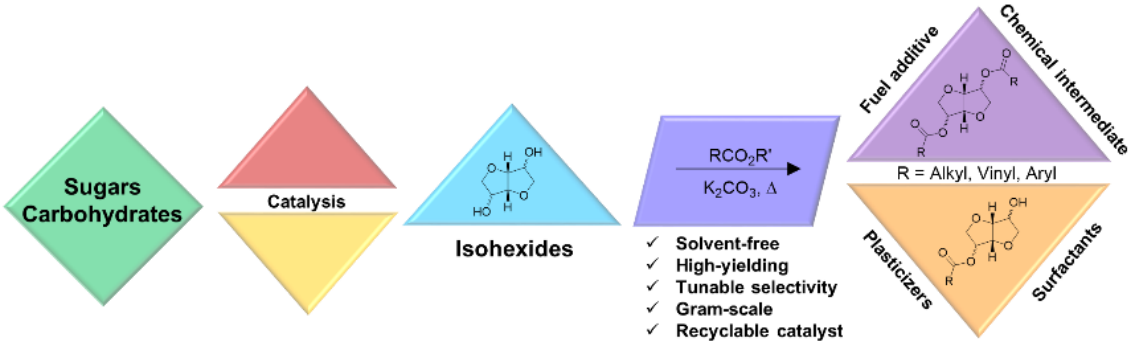

4.1 INTRODUCTION

As discussed in Chapter 1, 1,4:3,6-dianhydro-D-glucitol, commonly termed as isosorbide (IS), is one such cellulose-derived chemical platform that can be transformed into all major classes of products, including fuels, solvents, plasticizers, surfactants, polymers, and pharmaceuticals (Rose and Palkovits 2012). The molecular scaffold of IS has also been employed in asymmetric catalysis (Kadraoui et al. 2015). Cellulose is converted into IS in a series of catalytic steps involving hydrolysis, hydrogenation, and dehydration reactions (He et al. 2020). Glucose, produced by the acid-catalyzed

depolymerization of polymeric carbohydrates like starch and cellulose, is catalytically hydrogenated into sorbitol (Xiang et al. 2022). Sorbitol is then subjected to a double dehydration reaction under acid catalysis to form IS (Dussenne et al. 2017). The elegant process produces water as the sole byproduct and preserves all the biogenic carbon atoms in the parent sugar molecule, affording a 100% carbon economy. Many of the fascinating properties of IS originate from its V-shape geometry and dissimilar spatial orientation of the two hydroxyl groups. The two hydroxyl groups in IS (*exo*- and *endo*-) show differing reactivity due to electronic and steric factors (Zhang et al. 2020). Following analogous synthetic pathways, two other hexose sugars, mannose, and idose, can be converted into isomannide (IM) and isoidide (II) (Fenouillot et al. 2010). IS, IM, and II are termed isohexides, in which the two –OH groups are oriented in *exo-endo*, *endo-endo*, and *exo-exo* geometry, respectively (Marubayashi et al. 2017). Since mannose and idose are scarcer and significantly more expensive than glucose, there has been significant interest in the alternative synthetic pathways of IM and II using an abundant and inexpensive starting material. In this regard, the isomerization of IS into IM and II under catalytic hydrogenation conditions has received significant interest (Saska et al. 2021). The monoesters and diesters of isohexides have potential applications as renewable monomers, chemical intermediates, green solvents, surfactants, and plasticizers (Cui et al. 2016; Matt et al. 2018; Thiyagarajan et al. 2014). The monoesters and diesters of isohexides are routinely prepared by acid-catalyzed esterification of isohexides following the Fischer esterification protocol (Inayat et al. 2018). For example, a gram-scale preparation of isosorbide-2,5-diacetate (ISDA) has been reported using glacial acetic acid as the reagent and Amberlyst-15 as a heterogeneous acid catalyst (Fraile and Saavedra 2017). Although the process works reasonably well with aliphatic carboxylic acids used in excess, the aromatic acids do not provide satisfactory yields of the isohexide esters. In an alternative strategy, the isohexides are reacted with reactive carbonyl compounds, such as carbonyl chloride and acid anhydride, to form esters (Li et al. 2018; Thiyagarajan et al. 2014). However, the processes are less atom economical and produce significant waste streams. In a recent report, the esters of IS have been synthesized by oxidative esterification using aldehydes in the presence of an *N*-heterocyclic carbene catalyst (Ragno et al. 2021). The benzyl ether of IS has been converted into isosorbide-2,5-dibenzoate (ISDB) by

aerobic oxidation using a dye-sensitized semiconductor under visible light photocatalysis (Ren et al. 2017). Transesterification of IS with diphenyl carbonate and dimethyl carbonate have also been reported focusing on the theoretical and experimental understanding of the reactivity difference between the *exo*-OH and *endo*-OH groups (Qian et al. 2019; Zhang et al. 2020). Though these processes for synthesizing isosorbide esters are promising, they require multi-step synthesis and relatively expensive reagents and catalysts.

Base-catalyzed transesterification has been employed as a convenient and scalable strategy for synthesizing biorenewable esters of commercial significance (Rashid and Anwar 2008). Interestingly, transesterification of IS has been reported under microwave conditions in organic solvents using K_2CO_3 as the base catalyst (Limousin et al. 1998). However, only a decent yield of monoesters was reported, with diesters in only trace amounts. Therefore, a systematic study of the base-catalyzed transesterification of all three isohexides under straightforward and scalable process conditions is warranted. One of the primary challenges in base-catalyzed transesterification is identifying an efficient base catalyst for the transformation. This work reports anhydrous K_2CO_3 as an inexpensive, highly active, and recyclable base catalyst for the selective synthesis of various monoesters and diesters of isohexides (Scheme 4.1). The gram-scale synthesis afforded excellent isolated yields of the esters. The base catalyst worked equally well for both aliphatic and aromatic esters and afforded excellent isolated yields of the monoesters and diesters of isohexides. Biorenewable carboxylic acids, such as acetic acid, propionic acid, levulinic acid, and 2-furoic acid, have been used to produce entirely biorenewable esters of isohexides.

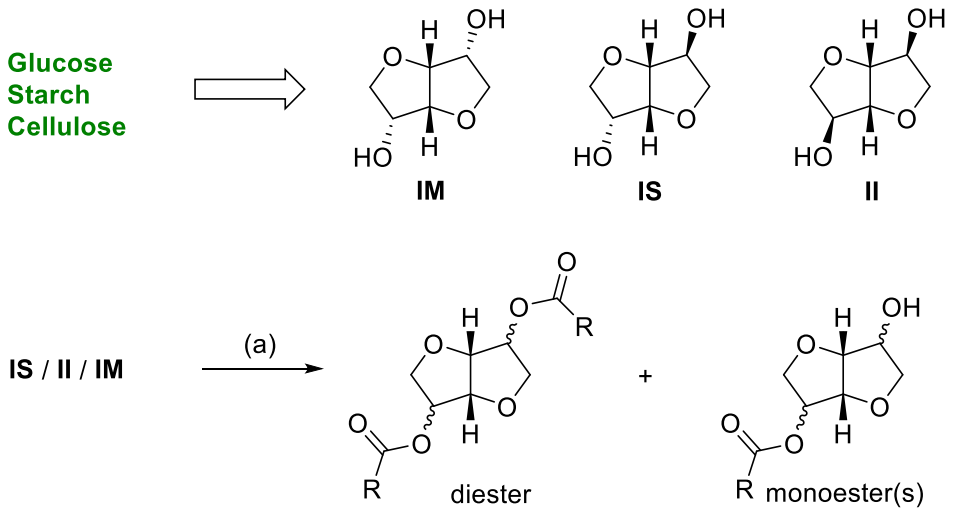

Scheme 4.1 The molecular structure of isohexides and the synthesis of isohexide esters (mono- and di-) by base-catalyzed transesterification reaction.

4.2 EXPERIMENTAL PROCEDURE

4.2.1 Materials

Ethyl acrylate (99%), sodium hydroxide (97%), silica gel (60-120), and potassium *tert*-butoxide (98%) were purchased from Spectrochem. Potassium phosphate tribasic (>98%) was purchased from Sigma Aldrich. Ethyl oleate (98%) and ethyl benzoate (99%) were purchased from Loba Chemie Pvt. Ltd. Sodium sulfate (99%, anhydrous), pet ether (60-80, 95%), and ethyl acetate (99%) were purchased from Finar. Isosorbide (> 98%), isomannide (>97%), and ethyl furoate (>98%) were purchased from TCI. Potassium carbonate anhydrous (99%) was purchased from Spectrum. All the reagents and solvents were used as received without additional purification.

4.2.2 Synthetic Procedure

IS (0.502 g, 3.42 mmol), ethyl benzoate (2.57 g, 17.11 mmol), and anhydrous K_2CO_3 (0.237 g, 50 mol%) were charged in a 50 mL round-bottomed flask. The mixture was placed in a pre-heated oil bath (open reactor) at the desired temperature and stirred magnetically for the stipulated time. After the reaction, the reaction mixture was cooled to room temperature. The reaction mixture was diluted with ethyl acetate (20 mL) and filtered using a Whatmann filter paper, and the ethyl acetate layer was washed with

water (10 mL). The ethyl acetate layer was dried over anhydrous Na_2SO_4 and evaporated in a rotary evaporator under reduced pressure. After evaporation, the crude product containing excess ethyl benzoate was chromatographed (silica gel, pet ether/ethyl acetate) to obtain pure mono- and diesters of IS. The same synthetic protocol was extended for synthesizing other mono- and diesters of all three isohexides. The spectroscopic data of the synthesized compounds were matched with literature reports (Fraile and Saavedra 2017; Ragno et al. 2021).

4.3 CHARACTERIZATION OF SYNTHESIZED COMPOUNDS

4.3.1 The FTIR, ^{1}H-NMR, and ^{13}C-NMR of isosorbide-2,5-dibenzoate (ISDB)

^{1}H-NMR ($CDCl_3$, 300 MHz) δ (ppm): 8.10-8.01 (m, 4H), 7.61-7.55 (m, 2H), 7.48-7.41 (m, 4H), 5.49 (d, 2H, *J*=3.0 Hz), 5.43 (q, 1H, *J*=5.4 Hz), 5.07 (t, 1H, *J*=5.1 Hz), 4.69 (d, 1H, *J*=4.5 Hz), 4.13-4.07 (m, 4H); ^{13}C-NMR ($CDCl_3$, 75 MHz) δ (ppm): 166.0, 165.7, 133.5, 133.4, 129.9, 129.8, 129.6, 129.5, 128.5, 86.3, 81.2, 78.6, 74.6, 73.6, 70.8; FTIR (ATR, cm^{-1}): 3138, 2983, 2879, 1722, 1578, 1014.

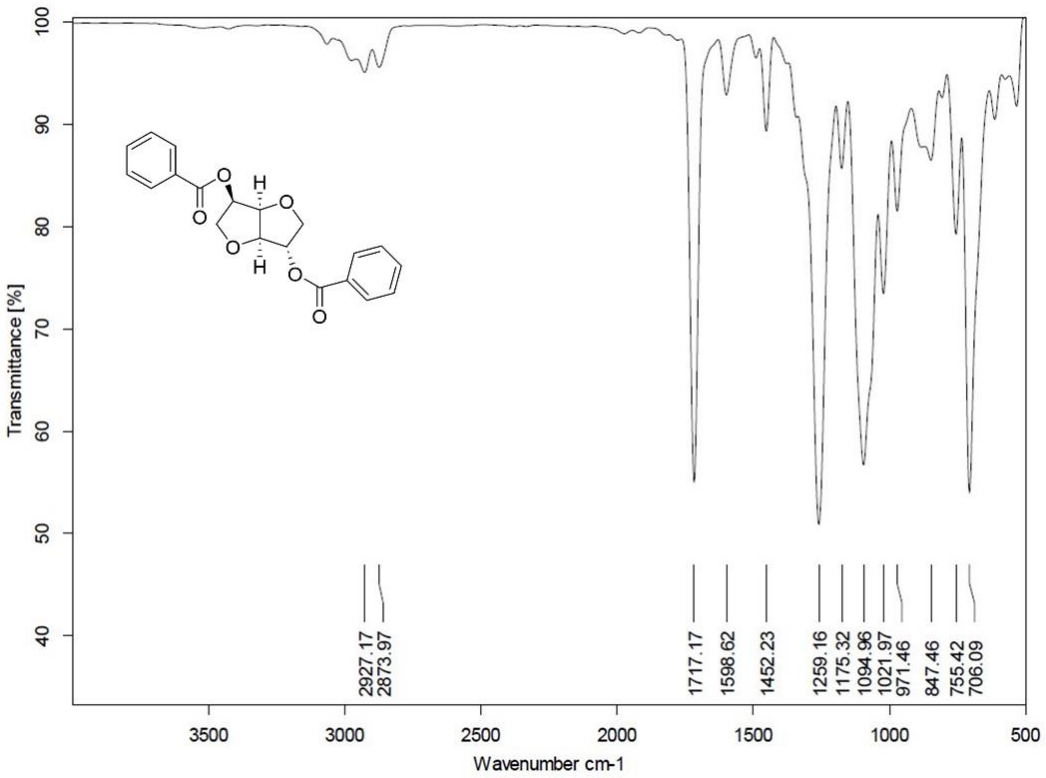

Figure 4.1 The FTIR spectrum of isosorbide-2,5-dibenzoate (ISDB).

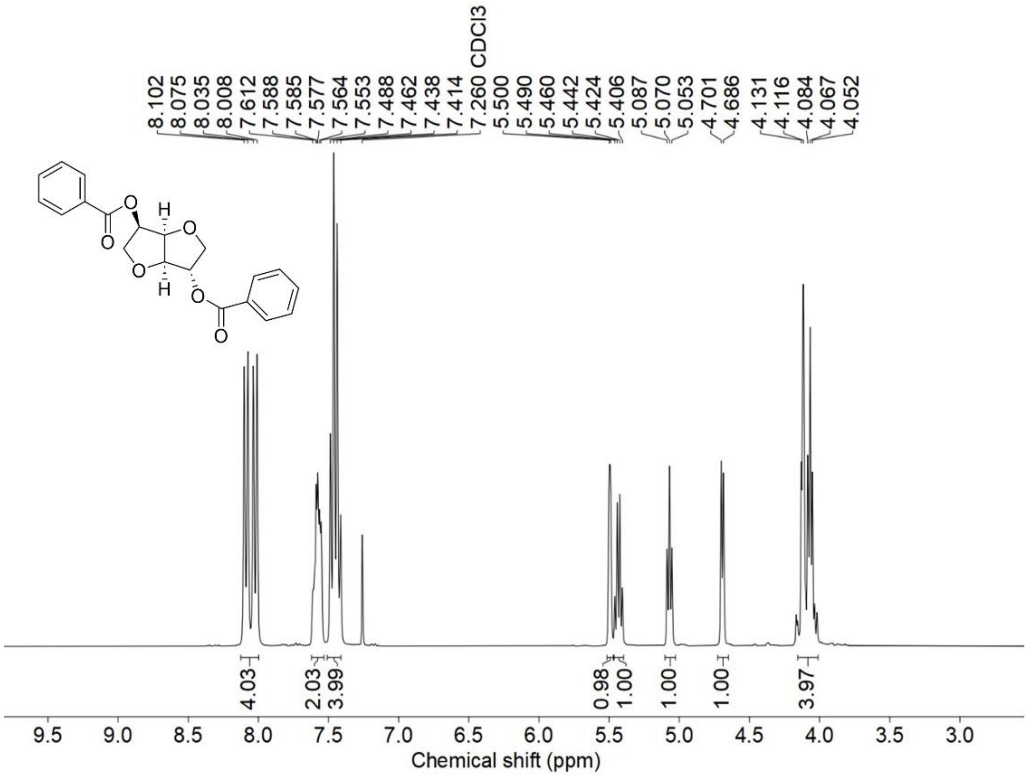

Figure 4.2 The ^{1}H-NMR spectrum of isosorbide-2,5-dibenzoate (ISDB).

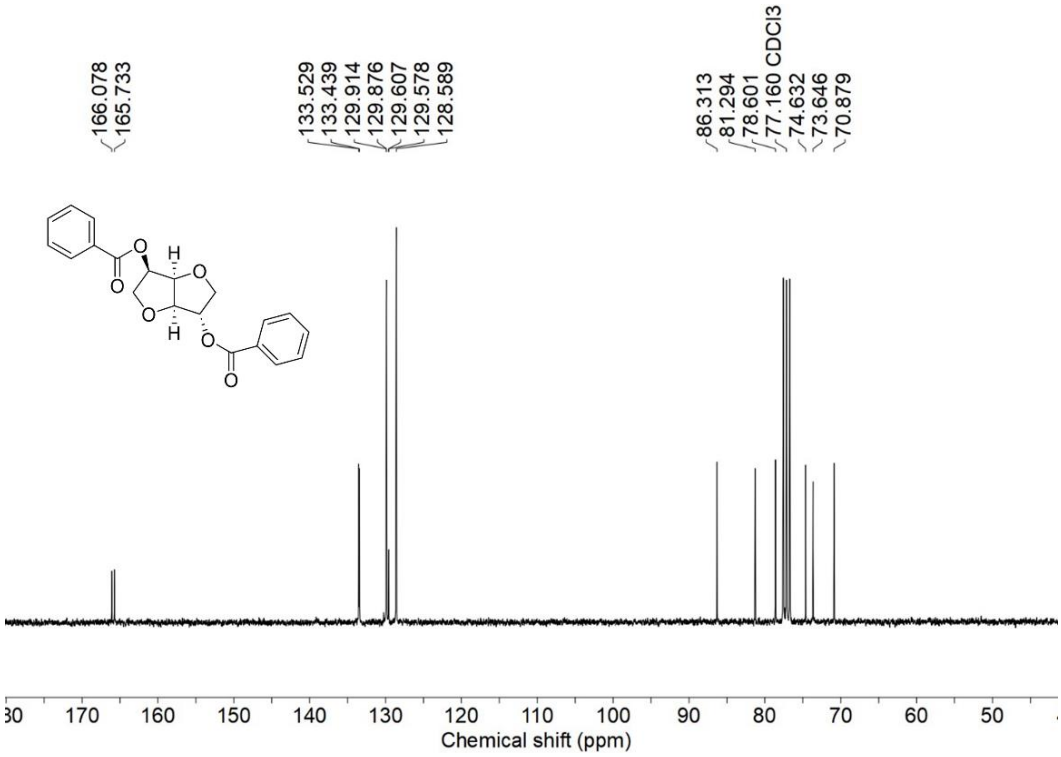

Figure 4.3 The ^{13}C-NMR spectrum of isosorbide-2,5-dibenzoate (ISDB).

4.3.2 The FTIR, ^{1}H-NMR, and ^{13}C-NMR of isosorbide *exo*-monobenzoate (*exo*-ISMB)

^{1}H-NMR ($CDCl_3$, 300 MHz) δ (ppm): 8.01 (d, 2H, *J*=8.4 Hz), 7.57 (t, 1H, *J*=6.9 Hz), 7.44 (t, 2H, *J*=7.5 Hz), 5.46 (d, 1H, *J*=3.6 Hz), 4.71 (t, 1H, *J*=4.8 Hz), 4.63 (d, 1H, *J*=4.5 Hz), 4.34 (q, 1H, *J*=5.7 Hz), 4.19-4.09 (m, 2H), 3.93 (dd, 1H, *J*=6.0, 6.0 Hz), 3.60 (dd, 1H, *J*=6.0, 6.0 Hz), 2.37 (bs, 1H); ^{13}C-NMR ($CDCl_3$, 75 MHz, δ ppm): 165.5, 133.4, 129.8, 129.6, 128.7, 85.8, 82.1, 78.9, 73.7, 73.6, 72.4; FTIR (ATR, cm^{-1}): 3462, 3066, 2955, 2875, 1716, 1451, 1071.

4.3.3 The FTIR, ^{1}H-NMR, and ^{13}C-NMR of isosorbide *endo*-monobenzoate (*endo*-ISMB)

^{1}H-NMR ($CDCl_3$, 300 MHz) δ (ppm): 8.06 (d, 2H, *J*=8.7 Hz), 7.57 (t, 1H, *J*=6.9 Hz), 7.44 (t, 2H, *J*=7.5 Hz), 5.39 (q, 1H, *J*=5.4 Hz), 4.98 (t, 1H, *J*=5.1 Hz), 4.45 (d, 1H, *J*=4.8 Hz), 4.36 (m, 1H), 4.03-3.86 (m, 4H), 1.93 (bs, 1H). ^{13}C-NMR ($CDCl_3$, 75 MHz, δ ppm): 166.1, 133.3, 129.9, 129.6, 128.5, 88.5, 80.8, 76.3, 75.6, 74.6, 70.8. FTIR (ATR, cm^{-1}): 3489, 1703, 1450, 1085.

4.3.4 The FTIR, ^{1}H-NMR, and ^{13}C-NMR of isomannide-2,5-dibenzoate (IMDB)

^{1}H-NMR ($CDCl_3$, 300 MHz) δ (ppm): 8.10 (d, 4H, *J*=8.4 Hz), 7.58 (t, 2H, *J*=7.8 Hz), 7.46 (t, 4H, *J*=8.4 Hz), 5.34 (q, 4H, *J*=6.6 Hz), 4.89 (d, 2H, *J*=4.2 Hz), 4.15 (dd, 2H, *J*=6.3, 6.3 Hz), 4.02 (dd, 2H, *J*=6.9, 6.9 Hz); ^{13}C-NMR ($CDCl_3$, 75 MHz) δ (ppm): 166.1, 133.4, 129.9, 129.5, 128.5, 80.8, 74.3, 70.8; FTIR (ATR, cm^{-1}): 3062, 2982, 2875, 1715, 1092.

4.3.5 The FTIR, ^{1}H-NMR, and ^{13}C-NMR of isomannide-2-monobenzoate (IMMB)

^{1}H-NMR ($CDCl_3$, 300 MHz) δ (ppm): 8.07 (d, 2H, *J*=8.4 Hz), 7.57 (t, 1H, *J*=7.5 Hz), 7.44 (t, 2H, *J*=7.8 Hz), 5.39 (q, 1H, *J*=6.3 Hz), 4.83 (t, 1H, *J*=5.1 Hz), 4.53 (t, 1H, *J*=5.4 Hz), 4.31 (q, 1H, *J*=6.6 Hz), 4.20 (dd, 1H, *J*=6, 5.4 Hz), 3.99-3.94 (m, 2H), 3.60 (t, 1H, *J*=7.5 Hz), 2.41 (bs, 1H); ^{13}C-NMR ($CDCl_3$, 75 MHz) δ (ppm): 165.9, 133.3, 129.8, 129.4, 128.4, 81.6, 80.7, 74.5, 73.8, 72.2, 71.2; FTIR (ATR, cm^{-1}): 3468, 3078, 2944, 1716, 1584, 1086.

4.3.6 The FTIR, ^{1}H-NMR, and ^{13}C-NMR of isoidide-2,5-dibenzoate (IIDB)

^{1}H-NMR ($CDCl_3$, 300 MHz) δ (ppm): 8.03 (d, 4H, *J*=8.4 Hz), 7.58 (t, 2H, *J*=7.5 Hz), 7.43 (t, 4H, *J*=7.8 Hz), 5.50 (s, 2H), 4.87 (s, 2H), 4.12 (s, 2H); ^{13}C-NMR ($CDCl_3$,

75 MHz) δ (ppm): 165.6, 133.5, 129.9, 129.6, 128.6, 85.7, 78.1, 72.8; FTIR (ATR, cm^{-1}): 3064, 2966, 2879, 1718, 1585, 1095.

4.3.7 The FTIR, ^{1}H-NMR, and ^{13}C-NMR of isoidide-2-monobenzoate (IIMB)

^{1}H-NMR ($CDCl_3$, 400 MHz) δ (ppm): 8.01 (d, 2H, *J*=8.0 Hz), 7.57 (t, 1H, *J*=7.2 Hz), 7.43 (t, 2H, *J*=8.0 Hz), 5.41 (s, 1H), 4.82 (d, 1H, *J*=4.0 Hz), 4.65 (d, 1H, *J*=4.0 Hz), 4.39 (s, 1H), 4.02-3.90 (m, 4H), 2.35 (bs, 1H); ^{13}C-NMR ($CDCl_3$, 100 MHz) δ (ppm): 165.7, 133.5, 129.8, 129.5, 128.5, 87.9, 85.2, 78.2, 76.0, 74.8, 72.6; FTIR (ATR, cm^{-1}): 3430, 3066, 2929, 2877, 1719, 1601, 1079, 1030.

4.3.8 The FTIR, ^{1}H-NMR, and ^{13}C-NMR of isosorbide-2,5-difuroate (ISDF)

^{1}H-NMR ($CDCl_3$, 300 MHz) δ (ppm): 7.60 (s, 2H), 7.25-7.20 (m, 2H), 6.52 (s, 2H), 5.45-5.30 (m, 2H), 5.03 (d, 1H, *J*=4.8 Hz), 4.66 (s, 1H), 4.15-4.02 (m, 4H); ^{13}C-NMR ($CDCl_3$, 75 MHz, δ ppm): 157.9, 157.7, 146.9, 146.8, 144.07, 144.01, 118.9, 118.8, 112.0, 86.1, 81.1, 78.5, 74.3, 73.5, 70.7; FTIR (ATR, cm^{-1}): 3138, 2983, 2879, 1722, 1578, 1014.

4.3.9 The FTIR, ^{1}H-NMR, and ^{13}C-NMR of isosorbide *exo*-monofuroate (*exo*-ISMF)

^{1}H-NMR ($CDCl_3$, 300 MHz) δ (ppm): 7.58 (s, 1H), 7.19 (s, 1H), 6.50 (s, 1H), 5.41 (s, 1H), 4.69-4.59 (m, 2H), 4.31 (m, 2H), 4.08 (q, 1H, *J*=5.7 Hz), 3.89 (q, 1H, *J*=6.9 Hz), 3.58 (q, 1H, *J*=2.7 Hz), 2.72 (bs, 1H); ^{13}C-NMR ($CDCl_3$, 75 MHz) δ (ppm): 157.5, 146.8, 143.9, 118.8, 112.0, 85.6, 82.0, 78.8, 72.3; FTIR (ATR, cm^{-1}): 3439, 3139, 2926, 2857, 1715, 1578, 1074, 1012.

4.3.10 The FTIR, ^{1}H-NMR, and ^{13}C-NMR of isosorbide *endo*-monofuroate (*endo*-ISMF)

^{1}H-NMR ($CDCl_3$, 300 MHz) δ (ppm): 7.59 (s, 1H), 7.22 (s, 1H), 6.50 (s, 1H), 5.34 (t, 1H, *J*=2.7 Hz), 4.95 (s, 1H), 4.42-4.34 (m, 2H), 3.95-3.88 (m, 4H), 2.70 (bs, 1H); ^{13}C-NMR ($CDCl_3$, 75 MHz) δ (ppm): 158.1, 146.8, 144.0, 118.7, 112.0, 88.4, 80.6, 76.1, 75.6, 74.5, 70.5; FTIR (ATR, cm^{-1}): 3448, 3141, 2926, 2859, 1724, 1578, 1086, 1015.

4.3.11 The FTIR, ^{1}H-NMR, and ^{13}C-NMR of isomannide difuroate (IMDF)

^{1}H-NMR ($CDCl_3$, 300 MHz) δ (ppm): 7.60 (d, 2H, *J*=3.0 Hz), 7.27 (d, 2H, *J*=2.7 Hz), 6.53 (t, 2H, *J*=3.0 Hz), 5.32 (s, 2H), 4.85 (s, 2H), 4.12-4.00 (m, 4H); ^{13}C-NMR

($CDCl_3$, 75 MHz) δ (ppm): 158.0, 146.9, 144.0, 118.9, 112.1, 80.7, 74.1, 70.6; FTIR (ATR, cm^{-1}): 3165, 3108, 2989, 2886, 1721, 1577, 1097, 1011.

4.3.12 The FTIR, ^{1}H-NMR, and ^{13}C-NMR of isomannide monofuroate (IMMF)

^{1}H-NMR ($CDCl_3$, 300 MHz) δ (ppm): 7.60 (d, 1H, *J*=3.0 Hz), 7.25 (d, 1H, *J*=2.4 Hz), 6.52 (d, 1H, *J*=1.5 Hz), 5.37 (t, 1H, *J*=3.0 Hz), 4.81 (t, 1H, *J*=3.0 Hz), 4.52 (t, 1H, *J*=2.7 Hz), 4.31 (s, 1H), 4.17-4.15 (m, 1H), 4.04-3.97 (m, 2H), 3.62 (t, 1H, *J*=8.4 Hz), 2.74 (bs, 1H); ^{13}C-NMR ($CDCl_3$, 75 MHz) δ (ppm): 157.9, 146.8, 143.9, 118.9, 112.0, 81.6, 80.7, 74.5, 73.9, 72.2, 71.1; FTIR (ATR, cm^{-1}): 3457, 3133, 2956, 2855, 1716, 1580, 1076, 1011.

4.3.13 The FTIR, ^{1}H-NMR, and ^{13}C-NMR of isoidide difuroate (IIDF)

^{1}H-NMR ($CDCl_3$, 300 MHz) δ (ppm): 7.59 (d, 2H, *J*=3.0 Hz), 7.20 (d, 2H, *J*=2.4 Hz), 6.51 (t, 2H, *J*=2.7 Hz), 5.44 (s, 2H), 4.83 (s, 2H), 4.07 (d, 4H, *J*=2.7 Hz); ^{13}C-NMR ($CDCl_3$, 75 MHz) δ (ppm): 157.6, 146.9, 144.0, 118.9, 112.1, 85.5, 78.0, 72.7; FTIR (ATR, cm^{-1}): 3139, 2956, 2852, 1723, 1578, 1117, 1016.

4.3.14 The FTIR, ^{1}H-NMR, and ^{13}C-NMR of isoidide monofuroate (IIMF)

^{1}H-NMR ($CDCl_3$, 300 MHz) δ (ppm): 7.58 (d, 1H, *J*=3.3 Hz), 7.19 (d, 1H, *J*=2.7 Hz), 6.50 (t, 1H, *J*=2.1 Hz), 5.37 (s, 1H), 4.79 (s, 1H), 4.63 (s, 1H), 4.36 (s, 1H), 4.10 (t, 2H, *J*=4.2 Hz), 3.99 (t, 1H, *J*=2.4 Hz); ^{13}C-NMR ($CDCl_3$, 75 MHz) δ (ppm): 157.7, 146.9, 144.0, 118.9, 112.1, 87.9, 85.1, 78.2, 76.0, 74.8, 72.4; FTIR (ATR, cm^{-1}): 3443, 3012, 2923, 2855, 1724, 1577, 1121, 1083.

4.3.15 The FTIR, ^{1}H-NMR, and ^{13}C-NMR of isosorbide dioleate (ISDO)

^{1}H-NMR ($CDCl_3$, 300 MHz) δ (ppm): 5.33 (t, 4H, *J*=5.7 Hz), 5.18-5.12 (m, 2H), 4.81 (t, 1H, *J*=5.1 Hz), 4.45 (d, 1H, *J*=4.8 Hz), 3.96-3.90 (m, 3H), 3.77 (q, 1H, *J*=6.0 Hz), 2.38-2.27 (m, 4H), 2.03-1.96 (m, 8H), 1.61 (q, 4H, *J*=3.0 Hz), 1.29-1.24 (m, 40H), 0.87 (t, 6H, *J*=6.6 Hz); ^{13}C-NMR ($CDCl_3$, 75 MHz) δ (ppm): 173.2, 173.0, 130.1, 130.0, 129.8, 129.7, 86.1, 80.8, 77.8, 73.6, 70.4, 34.2, 32.0, 29.9, 29.8, 29.7, 29.6, 29.5, 29.4, 29.3, 29.27, 29.24, 29.2, 29.18, 29.16, 27.3, 27.2, 24.98, 24.94, 22.8, 14.2; FTIR (ATR, cm^{-1}): 3004, 2925, 2855, 1739, 1579, 1088.

4.3.16 The FTIR, ^{1}H-NMR, and ^{13}C-NMR of isosorbide *exo*-monooleate (*exo*-ISMO)

^{1}H-NMR ($CDCl_3$, 300 MHz) δ (ppm): 5.31 (t, 2H, *J*=5.7 Hz), 5.20 (s, 1H), 4.59 (t, 1H, *J*=4.8 Hz), 4.44 (d, 1H, *J*=4.5 Hz), 4.28 (q, 1H, *J*=5.7 Hz), 3.98 (d, 1H, *J*=2.4

Hz), 3.86 (dd, 1H, *J*=6.0, 6.3 Hz), 3.54 (dd, 1H, *J*=6.0, 6.0 Hz), 2.32-2.27 (m, 2H), 2.03-1.95 (m, 4H), 1.59 (t, 2H, *J*=7.2 Hz), 1.28 (t, 20H, *J*=4.2 Hz), 0.85 (t, 3H, *J*=6.0 Hz); ^{13}C-NMR ($CDCl_3$, 75 MHz) δ (ppm): 172.8, 130.1, 129.7, 85.7, 82.0, 78.2, 73.7, 73.4, 72.4, 34.1, 31.9, 29.8, 29.7, 29.5, 29.3, 29.2, 29.14, 29.11, 27.2, 24.8, 22.7, 14.1; FTIR (ATR, cm^{-1}): 3490, 3006, 2925, 2855, 1741, 1463, 1088.

4.3.17 The FTIR, ^{1}H-NMR, and ^{13}C-NMR of isosorbide *endo*-monooleate *(endo*-ISMO)

^{1}H-NMR ($CDCl_3$, 300 MHz) δ (ppm): 5.31 (t, 2H, *J*=5.7 Hz), 5.10 (q, 1H, *J*=5.4 Hz), 4.81 (t, 1H, *J*=4.8 Hz), 4.36 (q, 1H, *J*=3.0 Hz), 4.27 (s, 1H), 3.90-3.84 (m, 3H), 3.73 (q, 1H, *J*=3.0 Hz), 2.32 (q, 2H, *J*=7.5 Hz), 2.03-1.94 (m, 4H), 1.62-1.55 (m, 2H), 1.32-1.22 (m, 20H), 0.85 (t, 3H, *J*=6.6 Hz); ^{13}C-NMR ($CDCl_3$, 75 MHz) δ (ppm): 173.4, 130.0, 129.7, 88.2, 80.3, 76.0, 75.4, 73.9, 70.3, 33.9, 31.9, 29.77, 29.7, 29.5, 29.3, 29.18, 29.1, 29.0, 27.1, 24.7, 22.6, 14.1; FTIR (ATR, cm^{-1}): 3458, 3006, 2924, 2854, 1740, 1462, 1089.

4.3.18 The FTIR, ^{1}H-NMR, and ^{13}C-NMR of isomannide dioleate (IMDO)

^{1}H-NMR ($CDCl_3$, 300 MHz) δ (ppm): 5.33 (m, 4H), 5.08 (q, 2H, *J*=4.8 Hz), 4.67 (d, 2H, *J*=4.2 Hz), 4.01 (dd, 2H, *J*=4.8, 4.8 Hz), 3.78 (dd, 2H, *J*=5.1, 5.1 Hz), 2.36 (dd, 4H, *J*=4.2, 5.7 Hz), 2.05-1.97 (m, 8H), 1.63 (t, 4H, *J*=5.7 Hz), 1.29-1.24 (m, 40H), 0.874 (t, 6H, *J*=5.1 Hz); ^{13}C-NMR ($CDCl_3$, 75 MHz) δ (ppm): 173.3, 130.1, 129.8, 80.5, 73.6, 70.5, 34.0, 32.0, 29.9, 29.8, 29.6, 29.4, 29.3, 29.2, 29.1, 27.3, 27.2, 24.9, 22.8, 14.2; FTIR (ATR, cm^{-1}): 3004, 2924, 2854, 1743, 1462, 1119.

4.3.19 The FTIR, ^{1}H-NMR, and ^{13}C-NMR of isomannide monooleate (IMMO)

^{1}H-NMR ($CDCl_3$, 300 MHz) δ (ppm): 5.32 (t, 2H, *J*=2.1 Hz), 5.13 (q, 1H, *J*=4.2 Hz), 4.68 (t, 1H, *J*=3.9 Hz), 4.46 (t, 1H, *J*=3.9 Hz), 4.28 (q, 1H, *J*=5.1 Hz), 4.09 (dd, 1H, *J*=4,8, 4.5 Hz), 3.95 (dd, 1H, *J*=4.5, 4.5 Hz), 3.82 (dd, 1H, *J*=4.8, 4.8 Hz), 3.56 (dd, 1H, *J*=5.4, 5.4 Hz), 2.38-2.30 (m, 2H), 2.04-1.97 (m, 4H), 1.61 (q, 2H, *J*=5.7 Hz), 1.29-1.24 (m, 20H), 0.86 (t, 3H, *J*=3.0 Hz); ^{13}C-NMR ($CDCl_3$, 75 MHz) δ (ppm): 173.3, 130.1, 129.8, 81.6, 80.5, 74.0, 72.3, 70.9, 34.3, 32.0, 29.9, 29.8, 29.6, 29.4, 29.28, 29.22, 29.1, 27.3, 27.2, 24.9, 22.8, 14.2; FTIR (ATR, cm^{-1}): 3473, 3004, 2923, 2853, 1740, 1462, 1081.

4.3.20 The FTIR, ^{1}H-NMR, and ^{13}C-NMR of isosorbide dilevulinate (ISDL)

^{1}H-NMR ($CDCl_3$, 400 MHz) δ (ppm): 5.18-5.10 (m, 2H), 4.80 (t, 1H, *J*=3.6 Hz), 4.46 (d, 1H, *J*=3.6 Hz), 4.10 (q, 1H, *J*=5.4 Hz), 3.95-3.88 (m, 2H), 3.78 (q, 1H, *J*=3.9 Hz), 2.78-2.54 (m, 8H), 2.18 (s, 3H), 2.17 (s, 3H); ^{13}C-NMR ($CDCl_3$, 100 MHz) δ (ppm): 206.5, 172.3, 172.0, 85.9, 80.9, 78.3, 74.3, 73.4, 70.4, 38.0, 37.9, 29.98, 29.93, 29.8, 28.0, 27.8; FTIR (ATR, cm^{-1}): 2956, 2851, 1773, 1732, 1464, 1187.

4.3.21 The FTIR, ^{1}H-NMR, and ^{13}C-NMR of isosorbide *exo*-monolevulinate (*exo*-ISML)

^{1}H-NMR ($CDCl_3$, 400 MHz) δ (ppm): 5.19 (s, 1H), 4.60 (t, 1H, *J*=4.8 Hz), 4.44 (d, 1H, *J*=4.4 Hz), 4.27 (q, 1H, *J*=5.6 Hz), 3.98 (t, 2H, *J*=4.4 Hz), 3.85 (dd, 1H, *J*=6.0, 5.6 Hz), 3.53 (dd, 1H, *J*=6.0, 5.6 Hz), 2.79 (t, 2H, *J*=6.0 Hz), 2.54 (t, 2H, *J*=6.4 Hz), 2.16 (s, 3H); ^{13}C-NMR ($CDCl_3$, 100 MHz) δ (ppm): 206.6, 171.9, 85.6, 82.0, 78.5, 73.53, 73.51, 72.3, 37.8, 29.8, 27.9; FTIR (ATR, cm^{-1}): 3436, 2955, 2856, 1712, 1460, 1080.

4.3.22 The FTIR, ^{1}H-NMR, and ^{13}C-NMR of isosorbide *endo*-monolevulinate (*endo*-ISML)

^{1}H-NMR ($CDCl_3$, 400 MHz) δ (ppm): 5.12 (q, 1H, *J*=1.6 Hz), 4.82 (t, 1H, *J*=4.8 Hz), 4.38-4.30 (m, 2H), 4.10 (q, 1H, *J*=1.6 Hz), 3.90-3.86 (m, 2H), 3.78-3.74 (m, 1H), 2.77-2.68 (m, 4H), 2.17 (s, 3H); ^{13}C-NMR ($CDCl_3$, 100 MHz) δ (ppm): 206.5, 171.4, 86.1, 80.7, 73.5, 70.0, 65.0, 60.6, 35.1, 29.7, 27.6; FTIR (ATR, cm^{-1}): 3435, 2956, 2854, 1736, 1715, 1462, 1087, 1014.

4.3.23 The FTIR, ^{1}H-NMR, and ^{13}C-NMR of isomannide dilevulinate (IMDL)

^{1}H-NMR ($CDCl_3$, 400 MHz) δ (ppm): 5.13-5.05 (m, 2H), 4.65 (q, 2H, *J*=5.2 Hz), 4.11-3.95 (m, 4H), 2.77-2.55 (m, 8H), 2.17 (s, 6H); ^{13}C-NMR ($CDCl_3$, 100 MHz) δ (ppm): 206.6, 172.3, 80.4, 73.9, 70.4, 37.9, 29.3, 27.7; FTIR (ATR, cm^{-1}): 2954, 2920, 2853, 1770, 1723, 1375, 1189, 1083.

4.3.24 The FTIR, ^{1}H-NMR, and ^{13}C-NMR of isomannide monolevulinate (IMML)

^{1}H-NMR ($CDCl_3$, 400 MHz) δ (ppm): 5.04-4.99 (m, 1H), 4.57 (t, 1H, *J*=5.2 Hz), 4.35 (t, 1H, *J*=5.2 Hz), 4.18 (q, 1H, *J*=6.4 Hz), 3.99-3.83 (m, 2H), 3.76-3.66 (m, 1H), 3.45 (dd, 1H, *J*=1.6. 1.6 Hz), 2.73-2.64 (m, 2H), 2.56-2.52 (m, 2H), 2.60 (bs, 1H), 2.08 (s, 3H); ^{13}C-NMR ($CDCl_3$, 100 MHz) δ (ppm): 206.6, 172.1, 81.4, 80.3, 74.1,

73.2, 72.0, 70.6, 37.6, 29.6, 27.5; FTIR (ATR, cm^{-1}): 3456, 2955, 2924, 2856, 1736, 1713, 1410, 1078, 1019.

4.3.25 The FTIR, ^{1}H-NMR, and ^{13}C-NMR of isosorbide diacrylate (ISDAr)

^{1}H-NMR ($CDCl_3$, 300 MHz) δ (ppm): 6.33-6.24 (m, 2H), 6.03-5.91 (m, 2H), 5.74 (q, 2H, *J*=2.1 Hz), 5.12-5.07 (m, 2H), 4.74 (t, 1H, *J*=5.1 Hz), 4.39 (d, 1H, *J*=4.8 Hz), 3.97 (q, 1H, *J*=7.2 Hz), 3.87-3.84 (m, 2H), 3.71 (q, 1H, *J*=5.1 Hz); ^{13}C-NMR ($CDCl_3$, 75 MHz) δ (ppm): 165.0, 164.7, 131.5, 131.4, 127.59, 127.5, 85.7, 80.6, 77.8, 73.8, 73.0, 70.1; FTIR (ATR, cm^{-1}): 3031, 2951, 2879, 1729, 1630, 1094.

4.3.26 The FTIR, ^{1}H-NMR, and ^{13}C-NMR of isomannide diacrylate (IMDAr)

^{1}H-NMR ($CDCl_3$, 300 MHz) δ (ppm): 6.45 (dd, 2H, *J*=1.6, 1.0 Hz), 6.16 (dd, 2H, *J*=7.2, 5.4 Hz), 5.86 (dd, 2H, *J*=1.0, 1.0 Hz), 5.17 (q, 2H, *J*=4.2, 4.2 Hz), 4.74 (t, 2H, *J*=3.6 Hz), 4.14-4.12 (m, 2H), 4.10-3.99 (m, 2H); ^{13}C-NMR ($CDCl_3$, 75 MHz) δ (ppm): 165.1, 137.7, 127.8, 80.6, 73.6, 70.3; FTIR (ATR, cm^{-1}): 3031, 2951, 2879, 1729, 1630, 1094.

4.3.27 The FTIR, ^{1}H-NMR, and ^{13}C-NMR of isosorbide-5-benzoate-2-acetate (5-ISBA)

^{1}H-NMR ($CDCl_3$, 300 MHz) δ (ppm): 8.04 (d, 2H, *J*=5.1 Hz), 7.56 (t, 1H, *J*=5.7 Hz), 7.43 (t, 2H, *J*=6.0 Hz), 5.37 (q, 1H, *J*=4.2, 3.9 Hz), 5.21 (d, 1H, *J*=2.7 Hz), 4.95 (t, 1H, *J*=3.6 Hz), 4.52 (d, 1H, *J*=3.6 Hz), 4.02-3.92 (m, 4H), 2.05 (s, 3H); 13C-NMR ($CDCl_3$, 75 MHz) δ (ppm): 170.2, 166.0, 133.4, 129.8, 129.6, 128.5, 86.2, 81.1, 78.2, 74.5, 73.6, 70.8, 21.0; FTIR (ATR, cm^{-1}): 2924, 2854, 1721, 1602, 1065.

4.3.28 The FTIR, ^{1}H-NMR, and ^{13}C-NMR of isosorbide-2-benzoate-5-acetate (2-ISBA)

^{1}H-NMR ($CDCl_3$, 300 MHz) δ (ppm): 8.02 (d, 2H, *J*=6.3 Hz), 7.57 (t, 1H, *J*=5.7 Hz), 7.43 (t, 2H, *J*=6.0 Hz), 5.44 (s, 1H), 5.17 (dd, 1H, *J*=3.9, 3.9 Hz), 4.91 (t, 1H, *J*=3.3 Hz), 4.63 (d, 1H, *J*=3.3 Hz), 4.11 (d, 2H, *J*=1.8 Hz), 3.98 (dd, 1H, *J*=2.7, 2.7 Hz), 3.83 (dd, 1H, *J*=4.2, 4.2 Hz); ^{13}C-NMR ($CDCl_3$, 75 MHz) δ (ppm): 170.2, 166.0, 133.4, 129.8, 129.6, 128.5, 86.2, 81.1, 78.2, 74.5, 73.5, 70.8, 20.9; FTIR (ATR, cm^{-1}): 2922, 2853, 1721, 1602, 1066.

4.3.29 The FTIR, ^{1}H-NMR, and ^{13}C-NMR of isomannide-2-benzoate-5-acetate (IMBA)

^{1}H-NMR ($CDCl_3$, 300 MHz) δ (ppm): 8.06 (d, 2H, *J*=7.8 Hz), 7.56 (t, 1H, *J*=7.5 Hz), 7.43 (t, 2H, *J*=7.5 Hz), 5.32 (q, 1H, *J*=6.0 Hz), 5.08 (q, 1H, *J*=6.3, 6.6 Hz), 4.83 (t, 1H, *J*=5.1 Hz), 4.72 (t, 1H, *J*=5.1 Hz), 4.12 (q, 1H, *J*=6.3 Hz), 4.03 (m, 2H), 3.81 (q, 1H, *J*=8.1 Hz), 2.13 (s, 3H); 13C-NMR ($CDCl_3$, 75 MHz) δ (ppm): 170.5, 166.0, 133.4, 129.9, 129.5, 128.5, 80.8, 80.4, 74.3, 73.7, 71.0, 70.2, 20.7; FTIR (ATR, cm^{-1}): 3065, 2983, 2882, 1718, 1601, 1068.

4.4 RESULTS AND DISCUSSION

Initially, the reaction duration was optimized by keeping other reaction parameters unaltered. When the reaction was carried out for 12 h at 160 °C, the isolated yield of ISDB and ISMBs were 78.4% and 18.2%, respectively. Furthermore, the decrease in reaction duration (ca. 6 h) resulted in 78.5% of ISDB and 20.8% ISMBs. The decrease in reaction duration to 6 h from 12 h has not changed the overall yield. Therefore, 6 h of reaction duration was held constant for optimizing other reaction parameters. The reaction temperature is a key parameter that determines the extent of conversion of the starting material, selectivity, and yield of product(s). Therefore, the reaction temperature for synthesizing mono- and di-esters of IS have been studied. When the reaction temperature was raised to 180 °C, the yield of ISDB reached up to 94% in 6 h. Decreasing the reaction temperature to 140 °C significantly lowered the ISDB yield to 54% and increased the combined yield of ISMBs to 45% (Figure 4.4). Further decrease in reaction temperature increased the yield of *endo*- and *exo*-ISMB, in expense of ISDB.

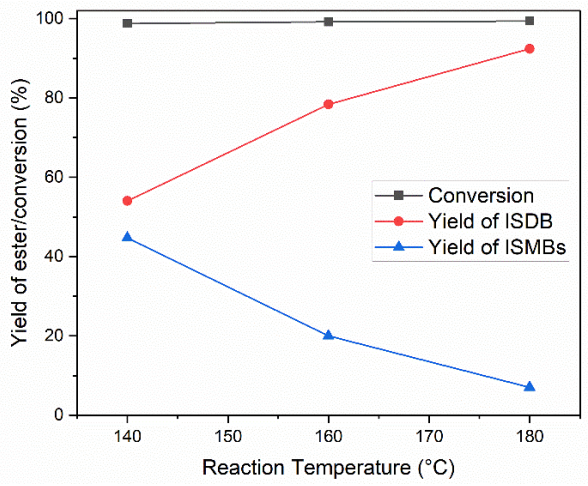

Figure 4.4 The effect of reaction temperature on isosorbide dibenzoate yield. *Reaction Conditions:* IS (0.5 g, 3.42 mmol), ethyl benzoate (5 equiv., 2.57 g, 17.113 mmol), anhyd. K_2CO_3 (50 mol%, 0.237 g), 6 h.

The amount of catalyst was varied between 25, 50, and 75 mol% for the synthesis of ISDB. The use of 25 mol% of K_2CO_3 gave an 83.4% yield of ISDB and 16% of ISMBs at 180 °C for 6 h. Increasing catalyst loading to 75 mol% gave a 93% yield of ISDB under identical reaction conditions. When the loading of anhydrous K_2CO_3 catalyst was increased to 50 mol%, ISDB was isolated in a 94% isolated yield (Scheme 4.2).

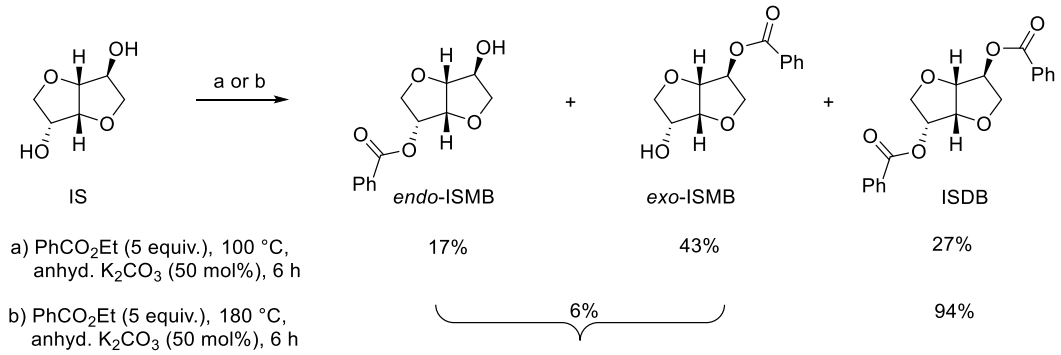

Scheme 4.2 Preparation of ISMBs and ISDB as a model reaction for process optimization.

Interestingly, when the reaction was carried out at a lower temperature, the selectivity of monoesters increased noticeably. Among all the monoesters of IS, the *exo*-product was formed in noticeably more quantity than the *endo*-product. The base catalyst did not seem to affect the selectivity to any noticeable extent. In the case of ISMB, both *exo*- and *endo*-product started to form simultaneously, and attempts to

manipulate the selectivity by altering the reaction parameters (e.g., temperature, duration, and equivalents of reagent) was not successful.

When the amount of ethyl benzoate was varied between 3-5 equivalents, the conversion, selectivity, and yield of ISDB and ISMBs were affected (Figure 4.5a). When the reaction was carried out at a lower temperature, the isolated yield ISDB decreased considerably, whereas the yields of ISMBs increased (Figure 4.5b).

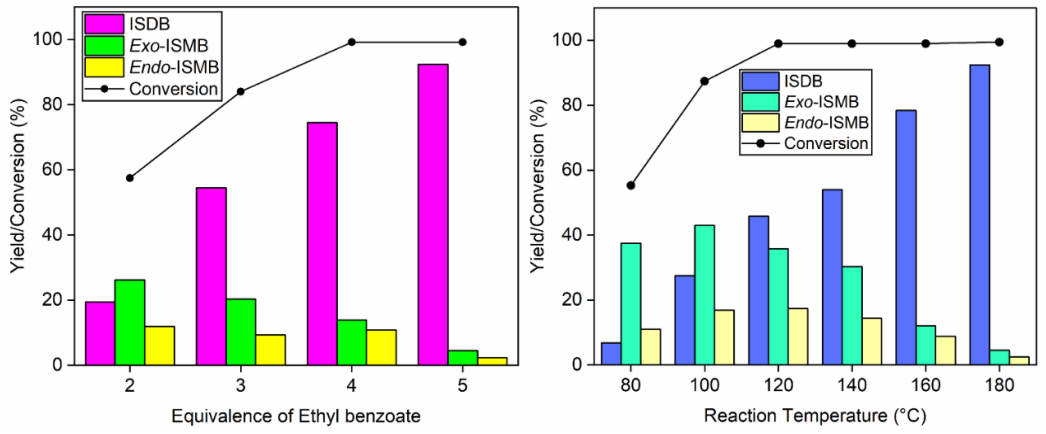

Figure 4.5 The effects of (a) equivalence of ethyl benzoate and (b) reaction temperature on the conversion of IS and selectivity toward ISDB, *exo*-ISMB, and *endo*-ISMB.

A series of aliphatic and aromatic diesters of IS was synthesized using a base-catalyzed transesterification protocol (Table 4.1). All esters were isolated in satisfactory yields, which were improved further by optimizing the reaction parameters of individual esters. The use of higher temperatures favored the formation of diester, and lower temperatures favored the monoesters formation.

Table 4.1 Synthesis of the various monoesters and diesters of isosorbide.

Entry	**Reagent**	**Reaction conditions**	**Diester**	***exo*-monoester**	***endo*-monoester**
1	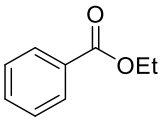		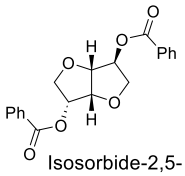 Isosorbide-2,5-dibenzoate (**ISDB**)	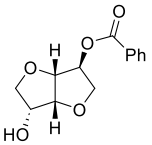 Isosorbide *exo*-mono benzoate(***exo*-ISMB**)	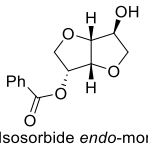 Isosorbide *endo*-mono benzoate (***endo*-ISMB**)
		(a)	27%	43%	17%
		(b)	94%	6%	

2	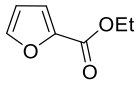		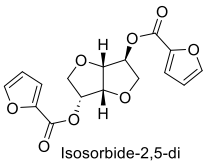 Isosorbide-2,5-di furoate (**ISDF**)	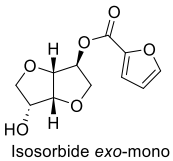 Isosorbide *exo*-mono furoate (***exo*-ISMF**)	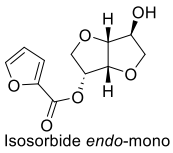 Isosorbide *endo*-mono furoate (***endo*-ISMF**)
		(a)	36.2%	28%	15.7%
		(b)	88%	7.2%	4.2%
3	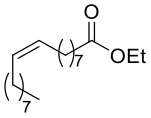		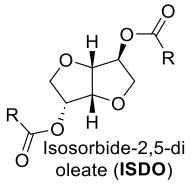 Isosorbide-2,5-di oleate (**ISDO**) R = $C_{17}H_{33}$	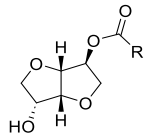 Isosorbide *exo*-mono oleate (***exo*-ISMO**) R = $C_{17}H_{33}$	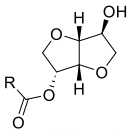 Isosorbide *endo*-mono oleate (***endo*-ISMO**) R = $C_{17}H_{33}$
		(b)	30	22.3	9
4			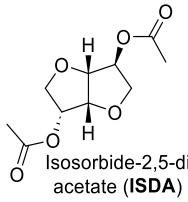 Isosorbide-2,5-di acetate (**ISDA**)	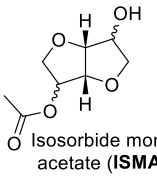 Isosorbide mono acetate (**ISMA**)	
		(b)	50%	10%	
		(c)	80%	5%	
5	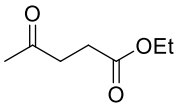		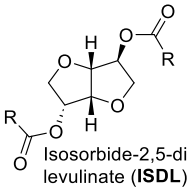 Isosorbide-2,5-di levulinate (**ISDL**) R = $-CH_2CH_2COCH_3$	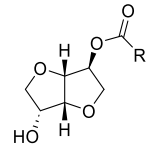 Isosorbide *exo*-mono levulinate (***exo*-ISML**) R = $-CH_2CH_2COCH_3$	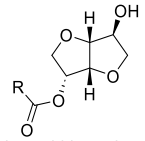 Isosorbide *endo*-mono levulinate(***endo*-ISML**) R = $-CH_2CH_2COCH_3$
		(d)	30%	27%	12%
6	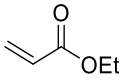		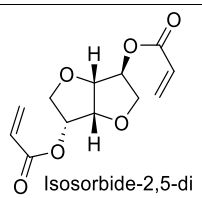 Isosorbide-2,5-di acrylate (**ISDAr**)	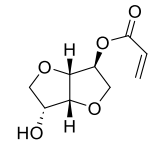 Isosorbide *exo*-mono acrylate (***exo*-ISMAr**)	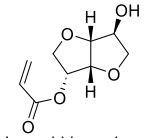 Isosorbide *endo*-mono acrylate (***endo*-ISMAr**)
		(e)	60%	16%	4%

Reaction conditions: a) ester reagent (5 equiv.), 100 °C, anhyd. K_2CO_3 (50 mol%, 0.237 g), 6 h; b) ester reagent (5 equiv.), 180 °C, anhyd. K_2CO_3 (50 mol%, 0.237 g), 6 h; c) ethyl acetate (excess), 220 °C, anhyd. K_2CO_3 (50 mol%, 0.237 g), 6 h (pressure reactor); d) ethyl levulinate

(5 equiv.), 150 °C, anhyd. K_2CO_3 (50 mol%, 0.237 g), 12 h; e) ethyl acrylate (10 equiv.), 110 °C, anhyd. K_2CO_3 (50 mol%, 0.237 g), 12 h.

Furthermore, the synthetic protocol optimized for IS was then extended to the synthesis of various mono- and diesters of IM and II (Table 4.2). Since IM and II have symmetrically oriented hydroxyl groups, the *exo*- and *endo*-substitutions are not relevant. When IM was reacted with ethyl benzoate at 180 °C for 6 h using 50 mol% anhyd. K_2CO_3, IMDB was obtained exclusively in a 97% isolated yield. When the reaction temperature was dropped to 100 °C, IMMB was obtained in a 35% isolated yield along with 12% IMDB. However, when II was reacted with ethyl benzoate at 180 °C, only a 67% yield of IIDB was obtained. The process coproduced 17% IIMB.

Table 4.2 Synthesis of the various monoesters and diesters of IM and II.

Entry	**Isohexide**	**Reagent**	**Reaction conditions** #	**Diester**	**Monoester**
1	IM	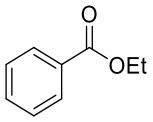		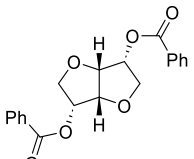 Isomannide-2,5-di benzoate (**IMDB**)	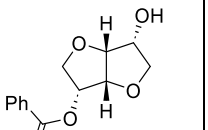 Isomannide mono benzoate (**IMMB**)
			(a)	12%	35%
			(b)	97%	-
2	II	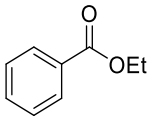		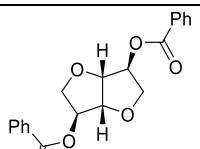 Isoidide-2,5-di benzoate (**IIDB**)	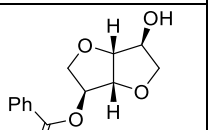 Isoidide mono benzoate (**IIMB**)
			(b)	67%	17%
3	IM	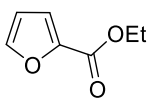		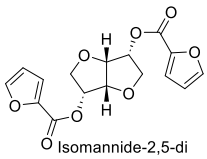 Isomannide-2,5-di furoate (**IMDF**)	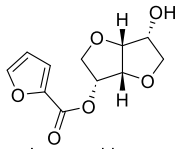 Isomannide mono furoate (**IMMF**)
			(a)	24.2%	43.7%
			(b)	73.2%	17.3%

4	II	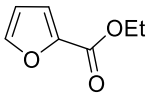		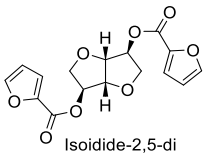 Isoidide-2,5-di furoate (**IIDF**)	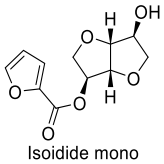 Isoidide mono furoate (**IIMF**)
			(a)	4%	23%
			(b)	50.4%	17.8%
5	IM			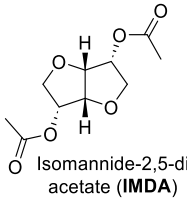 Isomannide-2,5-di acetate (**IMDA**)	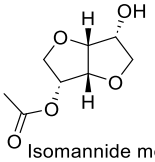 Isomannide mono acetate (**IMMA**)
			(b)	45%	5%
			(c)	72%	-
6	II			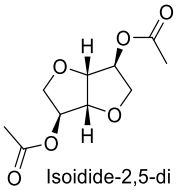 Isoidide-2,5-di acetate (**IIDA**)	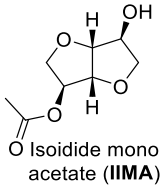 Isoidide mono acetate (**IIMA**)
			(c)	53%	-
7	IM	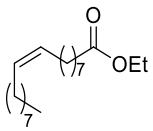		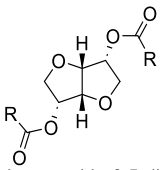 Isomannide-2,5-di oleate (**IMDO**) R = $C_{17}H_{33}$	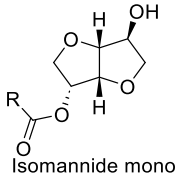 Isomannide mono oleate (**IMMO**) R = $C_{17}H_{33}$
			(b)	21%	20%
8	IM	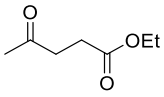		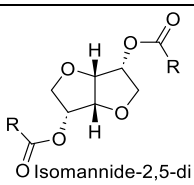 Isomannide-2,5-di levulinate (**IMDL**) R = $-CH_2CH_2COCH_3$	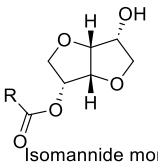 Isomannide mono levulinate (**IMML**) R = $-CH_2CH_2COCH_3$
			(d)	40%	32%

9	IM	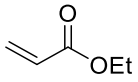		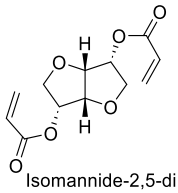 Isomannide-2,5-di acrylate (**IMDAr**)	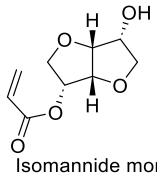 Isomannide mono acrylate (**IMMAr**)
			(e)	40%	26%

Reaction Conditions: a) ester reagent (5 equiv.), 100 °C, anhyd. K_2CO_3 (50 mol%, 0.237 g), 6 h; b) ester reagent (5 equiv.), 180 °C, anhyd. K_2CO_3 (50 mol%, 0.237 g), 6 h; c) ethyl acetate (excess), 220 °C, anhyd. K_2CO_3 (50 mol%, 0.237 g), 6 h (pressure reactor); d) ethyl levulinate (5 equiv.), 150 °C, anhyd. K_2CO_3 (50 mol%, 0.237 g), 12 h; e) ethyl acrylate (10 equiv.), 110 °C, anhyd. K_2CO_3 (50 mol%, 0.237 g), 12 h.

Furthermore, the asymmetric esters of isomannide were prepared as a model substrate to demonstrate the synthesis of asymmetric esters. Isomannide-2-benzoate-5-acetate was isolated in moderate yield (ca. 35%) starting from IMMB and ethyl acetate using potassium carbonate as a base.

Even though anhyd. K_2CO_3 is inexpensive and available in bulk, recyclability of the catalyst was studied to understand the reactivity of recycled catalyst, to ensure process economics, and to improve the environmental suitability of the process. Recyclability of the anhyd. K_2CO_3 catalyst was studied on the transesterification of IS with ethyl benzoate. After the reaction, the reaction mixture was diluted with ethyl acetate and filtered under vacuum to separate the solid residue. The solid was then washed with fresh ethyl acetate and dried at 60 °C for 6 h. After that, the recovered K_2CO_3 catalyst was dried at 120 °C for 6 h to remove volatiles and then subjected to the next catalytic cycle. The fresh anhyd. K_2CO_3 catalyst afforded 92% ISDB along with trace amounts of the monoesters (i.e., *exo*-ISMB and *endo*-ISMB) under the optimized reaction conditions (180 °C, 6 h, 50 mol% K_2CO_3, 5 equiv. $PhCO_2Et$) (Figure 4.6). The catalyst was separated from the reaction mixture by filtration, washed with ethyl acetate to remove organics, and dried in an oven (120 °C) before using in the next catalytic cycle. The yield of ISDB noticeably decreased to 86% with the recycled K_2CO_3 catalyst.

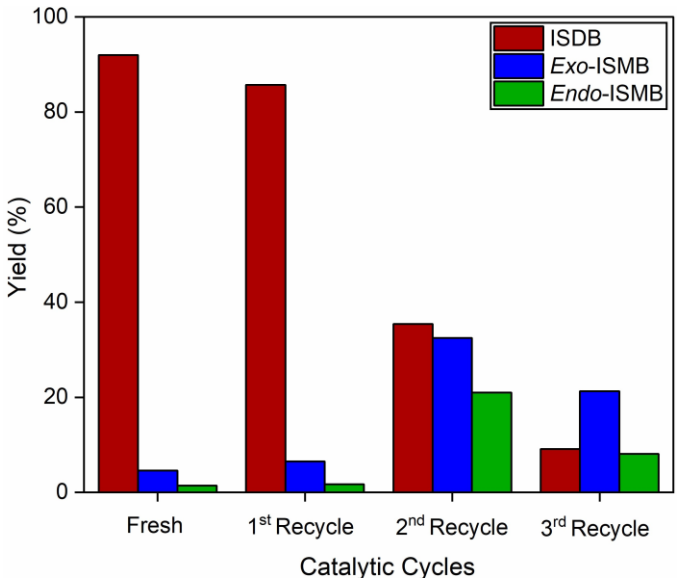

Figure 4.6 Product distribution during the recycling of anhydrous K_2CO_3 for the transesterification of IS with ethyl benzoate.

Reaction Conditions: IS (0.5 g, 3.42 mmol), ethyl benzoate (5 equiv., 2.57 g, 17.113 mmol), anhyd. K_2CO_3 (50 mol%, 0.237 g), 180 °C, 6 h.

The yield of *exo*-ISMB increased to 7%, whereas the yield of *endo*-ISDB was only around 2%. Interestingly, selectivity of the two monoesters followed the same trend observed during the targeted synthesis of monoesters of IS. In the second recycle, there was sharp decline in the yield of ISDB to 35%. The yield of *exo*-ISMB and endo-ISMB increased significantly to 33% and 21%, respectively. In the third recycle, ISDB became a minor product with an isolated yield of only 9%. The overall yield of the esters was significantly diminished. Interestingly, the higher selectivity toward *exo*-ISMB compared to *endo*-ISMB was still pronounced. The lowering of catalytic activity can be due to absorption of moisture by anhyd. K_2CO_3 during the work up and partial decomposition.

4.5 CONCLUSION

In summary, various monoesters and diesters of biomass-derived isohexides have been synthesized by base-catalyzed transesterification under organic solvent-free conditions. The preparation was performed on several grams scale, and the products were isolated in excellent yields. The inexpensive K_2CO_3 catalyst was conveniently separated and successfully reused. Alkyl, aryl, and vinyl esters of isohexides were synthesized with equal ease, and even unsymmetrical diesters were produced in

sequential transesterification steps. In the case of IS, noticeable selectivity was observed towards the *exo*-monoester. In some cases, entirely biorenewable esters of isohexides were obtained using renewable ester reagents. This work will help expand the commercial applications and markets of these commercially relevant esters.

CHAPTER 5

RENEWABLE SYNTHESIS OF γ-BUTYROLACTONE FROM BIOMASS-DERIVED 2-FURANONE USING PALLADIUM SUPPORTED ON HUMIN-DERIVED ACTIVATED CARBON (Pd/HAC) AS A HETEROGENEOUS CATALYST

Abstract

This work reports a high-yielding synthesis of γ-butyrolactone (GBL), a promising biofuel, industrial solvent, and chemical feedstock, by the catalytic hydrogenation of 2-furanone. 2-Furanone can be synthesized over two catalytic steps starting from hemicellulose. Humin, produced during the preparation of furfural (FF) from xylose, was carbonized to form humin-derived activated carbon (HAC). Palladium supported on humin-derived activated carbon (Pd/HAC) was used as an efficient and recyclable catalyst for hydrogenating 2-furanone into GBL. The process was optimized on temperature, catalyst loading, and solvent. Under optimized conditions (RT, 0.5 MPa H_2, 3 h), the 4%Pd/HAC (5 wt.% loading) catalyst afforded GBL in 89% isolated yield. Under identical conditions, an 85% isolated yield of γ-valerolactone (GVL) was obtained starting from biomass-derived angelica lactone. Moreover, the 4%Pd/HAC catalyst was conveniently recovered after the reaction and successfully recycled for five cycles with only a marginal decrease in the yield of GBL.

Graphical abstract

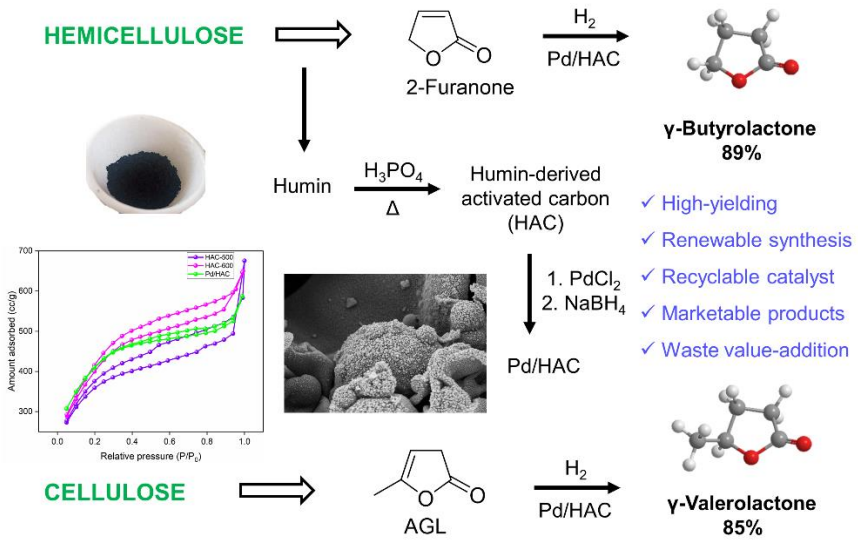

5.1 INTRODUCTION

Catalysis is a cornerstone of green chemistry and an integral part of a modern biorefinery for the selective conversion of biomass components into bulk and specialty organic chemicals under commercially feasible and environmentally acceptable conditions (Alonso et al. 2010). Acid hydrolysis of lignocellulosic biomass is an established catalytic strategy that not only allows the biopolymers to separate from each

other but also deconstructs the biopolymers into organic small molecules (Jönsson and Martín 2016). For example, the hemicellulose fraction leads to furfural (FF), whereas the cellulose fraction forms levulinic acid (LA) under acid catalysis at elevated temperatures (Boonyakarn et al. 2019; Luo et al. 2019). FF and LA have been established as carbohydrate-derived chemical platforms for producing bulk- and specialty chemicals that are otherwise sourced from petroleum (Sajid et al. 2021; Shen et al. 2020; Song et al. 2020). FF can be catalytically oxidized to 2-furanone using innocuous oxidants, such as gaseous O_2 and aqueous H_2O_2 (Bhat et al. 2023; Yu et al. 2021). Catalytic hydrogenation of the olefinic group in 2-furanone leads to γ-butyrolactone (GBL) (Li et al. 2019). GBL has applications as an industrial solvent, potential biofuel, and chemical feedstock in several industries, such as polymers, cosmetics, and pharmaceuticals (Centi et al. 1988; Ichikawa et al. 2004). GBL is commercially produced by dehydrogenating 1,4-butanediol over a copper catalyst or by partially reducing maleic anhydride over a nickel catalyst (Schwarz et al. 2019). Even though the processes mentioned above can utilize both petroleum and biomass resources, the synthetic routes involve multiple synthetic steps and demanding reaction conditions.

The intramolecular dehydrative lactonization of LA leads to angelica lactones (AGLs), a combination of three positional isomers (Lima et al. 2018; Mascal et al. 2014). Catalytic hydrogenation of the olefin group in AGLs leads to γ-valerolactone (GVL) (Mamun et al. 2017). GVL has received interest as a diesel additive, renewable solvent, and chemical feedstock (Alonso et al. 2013). Among the various noble metals and non-noble metal catalysts examined, palladium is one of the most active metals for the catalytic hydrogenation of 2-furanone to GBL, and AGLs to GVL, respectively (Cao et al. 2014; Li et al. 2016). Activated carbon (AC), possessing high surface area and hierarchical pore structures, is a commonly employed supporting material for metal-based heterogeneous catalysts (Das et al. 2023). In this regard, humin is a complex furanic resin that forms inadvertently during the production of FF and LA from sugars and polymeric carbohydrates (Wang et al. 2016). Humin, in principle, could act as an inexpensive precursor for deriving AC for catalyst support. At present, humin is typically combusted as a solid fuel to generate process heat for other biorefinery processes or to produce synthesis gas (Hoang et al. 2015). Alternative

value-addition pathways for humin, such as reinforcing materials, adsorbent, and catalyst support, have attracted significant interest recently (Jesus et al. 2011; Mija et al. 2017; Yang et al. 2020). In this work, water-insoluble humin produced during the dehydration of xylose into FF was used as the starting material to form the carbon-based catalyst support. Humin was carbonized and activated by treating with orthophosphoric acid (H_3PO_4) at 600 °C. Palladium metal was supported on humin-derived activated carbon (HAC) by the wet impregnation method. The Pd/HAC catalyst was employed as a heterogeneous catalyst for hydrogenating 2-furanone and AGL into GBL and GVL, respectively (Scheme 5.1).

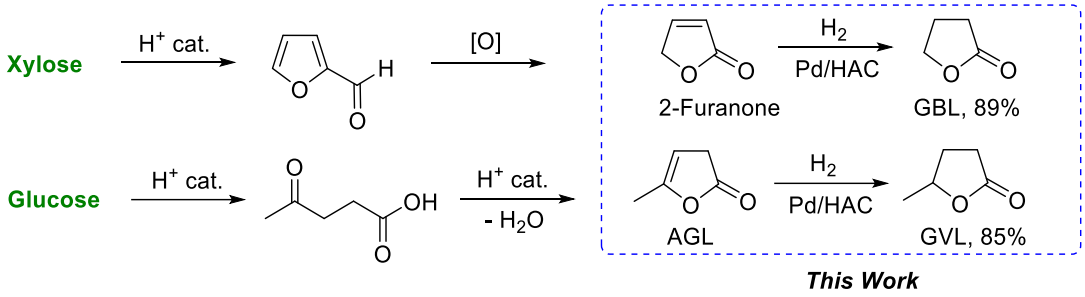

Scheme 5.1 Catalytic synthesis of γ-butyrolactone and γ-valerolactone from carbohydrates.

5.2 EXPERIMENTAL SECTION

5.2.1 Materials

Xylose (99%) and benzyltributylammonium chloride (BTBAC, 99%) were procured from Spectrochem. $PdCl_2$ was purchased from Sigma. $NaBH_4$, 1,2-dichloroethane (DCE, 98%), HCl (aq., 35-38%), and tetrahydrofuran (THF, 99.5%) were obtained from Molychem. Sodium sulfate (anhydrous, 99%), NaOH, and deionized (DI) water were purchased from Loba Chemie Pvt. Ltd. Methanol (99.5%) and chloroform (98%) were purchased from Finar. AGL (>95% α-isomer) was purchased from Alfa Aesar and purified by passing through a plug of silica gel (60-120 mesh) using chloroform as the eluent. Chloroform was then evaporated in a rotary evaporator under reduced pressure to obtain pure AGL as a faint-yellow oil. 2-Furanone was synthesized according to the literature procedure (Bhat et al. 2023).

5.2.2 Characterization methods

Fourier-transform infrared spectroscopy (FTIR) spectra of the HAC support and 4%Pd/HAC catalyst were recorded on a Bruker Alpha 400 FTIR spectrometer using

the KBr pellet technique. Powder X-ray diffraction (PXRD) patterns were recorded on Rigaku MiniFlex 600 (Japan) X-ray Powder Diffractometer using Cu Kα radiation as the source. The surface morphology of the samples was investigated using field emission scanning electron microscopy (FESEM), Gemini 300, Carl Zeiss, operating at an accelerating voltage of 15 kV, and the high-resolution transmission electron microscopy (HR-TEM) images were recorded on the FEI Tecnai G2 F30 S-Twin instrument. Brunauer-Emmett-Teller (BET) surface area of the catalysts was measured using Autosorb IQ-XR-XR, Anton Paar, employing N_2 adsorption at 77.35 K. The pore size distribution of the samples was determined from nitrogen desorption isotherms using the Barrett-Joyner-Halenda (BJH) method. Thermogravimetric analysis (TGA) was recorded on a TGA 4000 (PerkinElmer) instrument under nitrogen atmosphere at a temperature ramp of 10 °C/min.

5.2.3 Preparation of humin and HAC

Humin and HAC were prepared by following the same preparation methods described in *Chapter 3*.

5.2.4 Preparation of 4%Pd/HAC catalyst

The catalyst was prepared by the wet impregnation method (Solanki and Rode 2019). In this method, HAC-600 (0.5 g) was dispersed by ultrasonication in HPLC-grade water (20 mL) for 15 min. Palladium(II) chloride (0.042 g) was dissolved in a minimum quantity of HCl (5%, aq.) and added dropwise into suspended HAC-600 at RT under vigorous stirring. After complete addition, the stirring was continued for an additional 2 h. An aqueous solution of NaOH (10 M) was then added slowly while stirring to adjust the pH in the range of 8-9. The mixture was stirred for 0.5 h, and $NaBH_4$ (0.5 g) was added slowly. The solution was stirred again for 1 h, filtered, and washed with DI water until the pH level dropped to 7. The catalyst was dried in a hot-air oven for 5 h at 110 °C before using it in the hydrogenation reactions.

5.2.5 Catalytic hydrogenation of renewable lactones

The Hastelloy-made high-pressure reactor was charged with 2-furanone (0.5 g, 5.9 mmol), catalyst (0.025 g, 5 wt.%), and THF (55 mL). The reactor was closed, purged with H_2 three times, and pressurized to 0.5 MPa of H_2 pressure. The reaction was carried out at RT for 3 h. After the reaction, the reaction mixture was centrifuged to separate the suspended Pd/HAC catalyst. The THF solvent was evaporated under

reduced pressure to get crude GBL as a colorless liquid. The crude product was then passed through a small plug of silica gel (60-120 mesh) to get pure GBL (0.469 g, 89%). The identity and purity of synthesized GBL (Jin et al. 2020) were confirmed by spectroscopic techniques.

The same synthetic procedure was employed for the hydrogenation of AGL to GVL, except that the catalyst loading was increased to 8 wt.% (compared to starting AGL). An 85% isolated yield of spectroscopically GVL (Khajone et al. 2023) was obtained as a clear liquid.

5.3 CHARACTERIZATION OF SYNTHESIZED COMPOUNDS

5.3.1The FTIR, ^{1}H-NMR, and ^{13}C-NMR spectra of γ-Butyrolactone (GBL)

^{1}H-NMR ($CDCl_3$, 300 MHz) δ (ppm): 4.35 (t, 2H, *J*=6.6 Hz), 2.49 (t, 2H, *J*=7.8 Hz), 2.28 (m, 2H); ^{13}C-NMR ($CDCl_3$, 75 MHz) δ (ppm): 178.3, 68.7, 27.81, 22.1; FTIR (ATR, cm^{-1}): 2957, 2921, 1763, 1033.

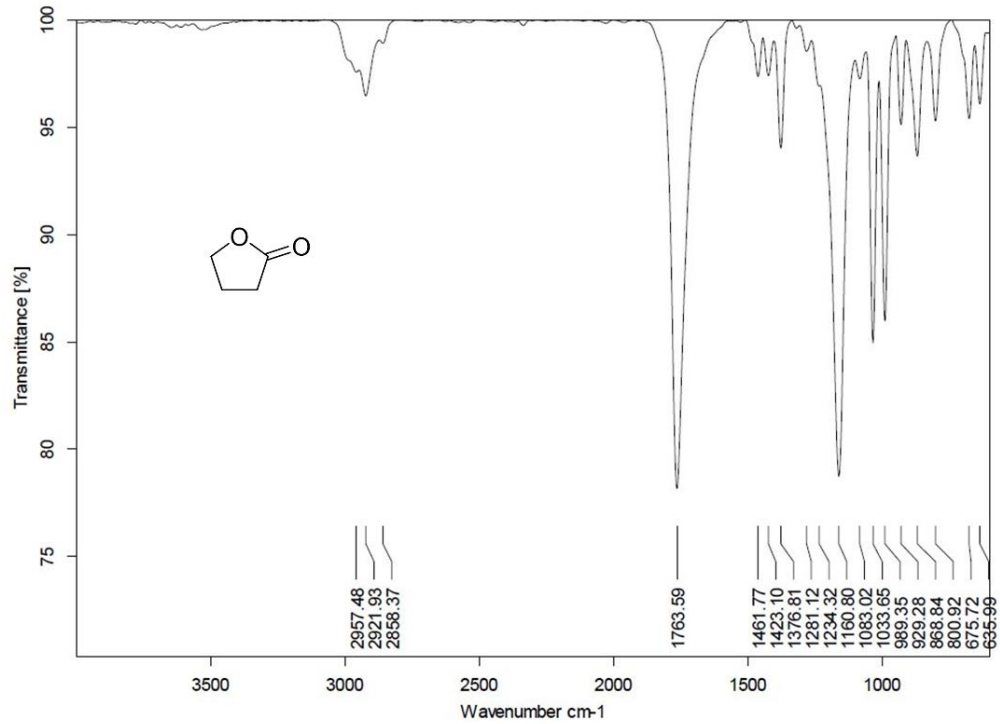

Figure 5.1 The FTIR spectrum of γ-butyrolactone (GBL).

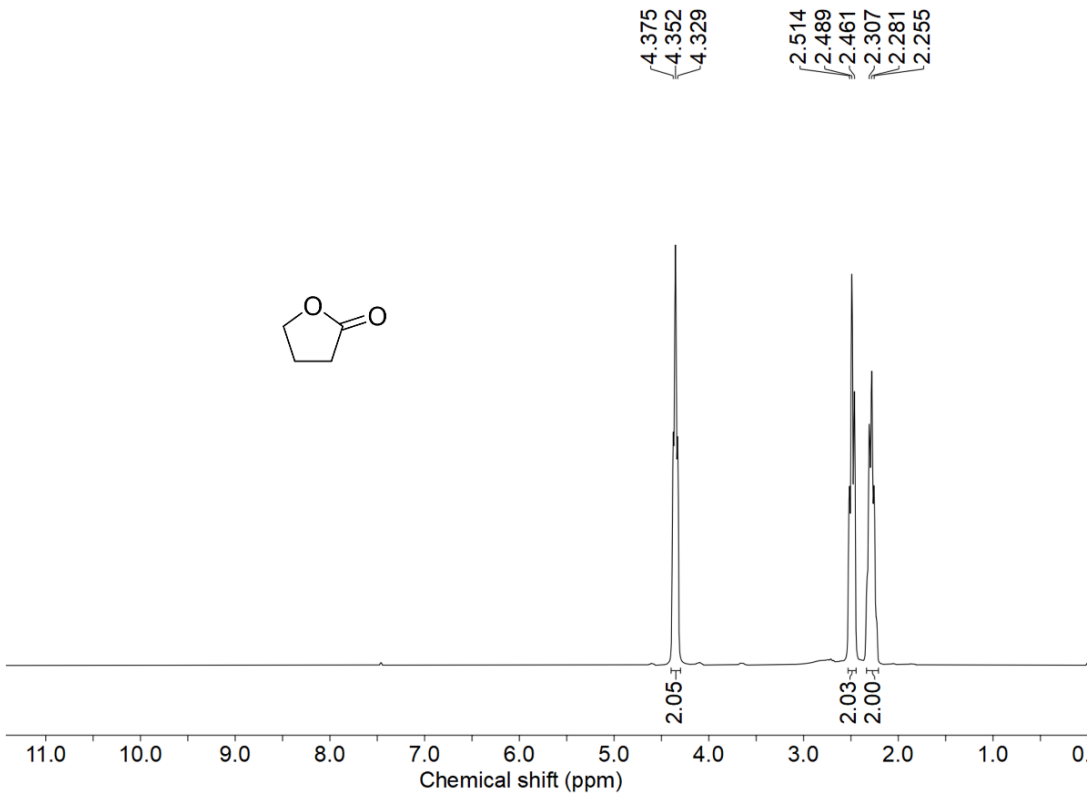

Figure 5.2 The ^{1}H NMR spectrum of γ-butyrolactone (GBL).

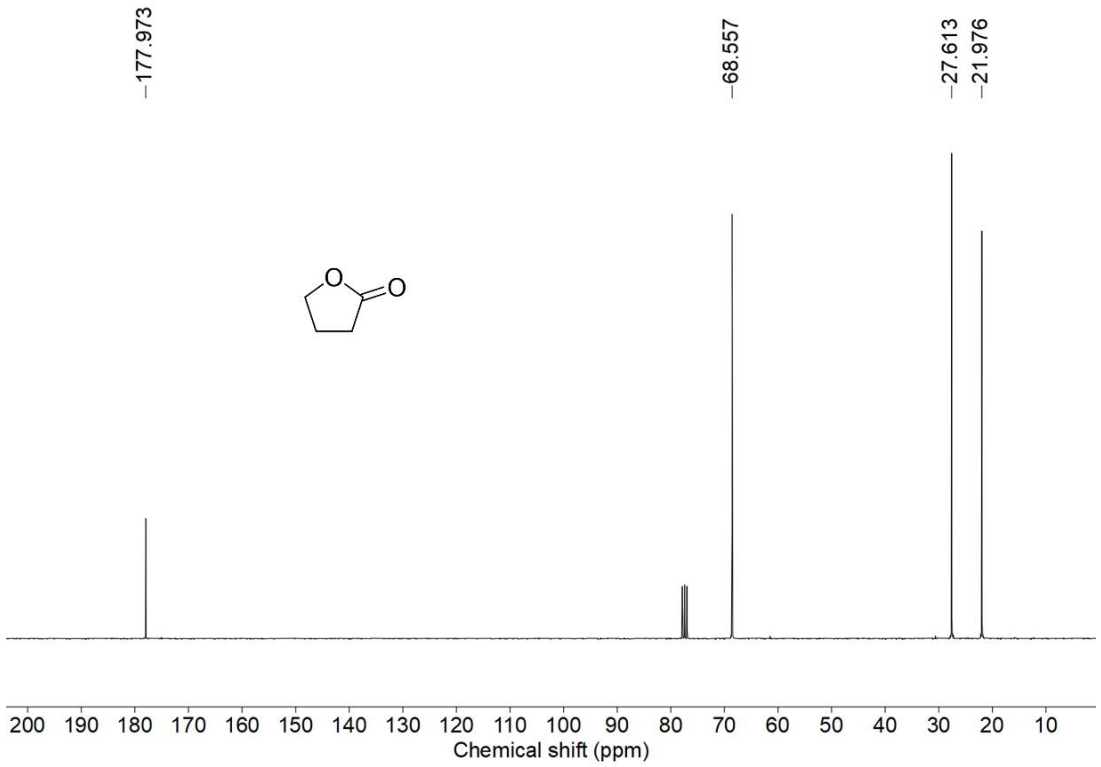

Figure 5.3 The ^{13}C NMR spectrum of γ-butyrolactone (GBL).

5.3.2 The FTIR, ^{1}H-NMR, and ^{13}C-NMR spectra of γ-Valerolactone (GVL)

^{1}H-NMR ($CDCl_3$, 300 MHz) δ (ppm): 4.58 (m, 1H), 2.47 (m, 2H), 2.31 (m, 2H), 1.33 (d, 3H, *J*=6.6 Hz); ^{13}C-NMR ($CDCl_3$, 75 MHz): δ (ppm): 173.3, 77.2, 29.6, 29, 20.9; FTIR (ATR, cm^{-1}): 2973, 2934, 1765, 1119.

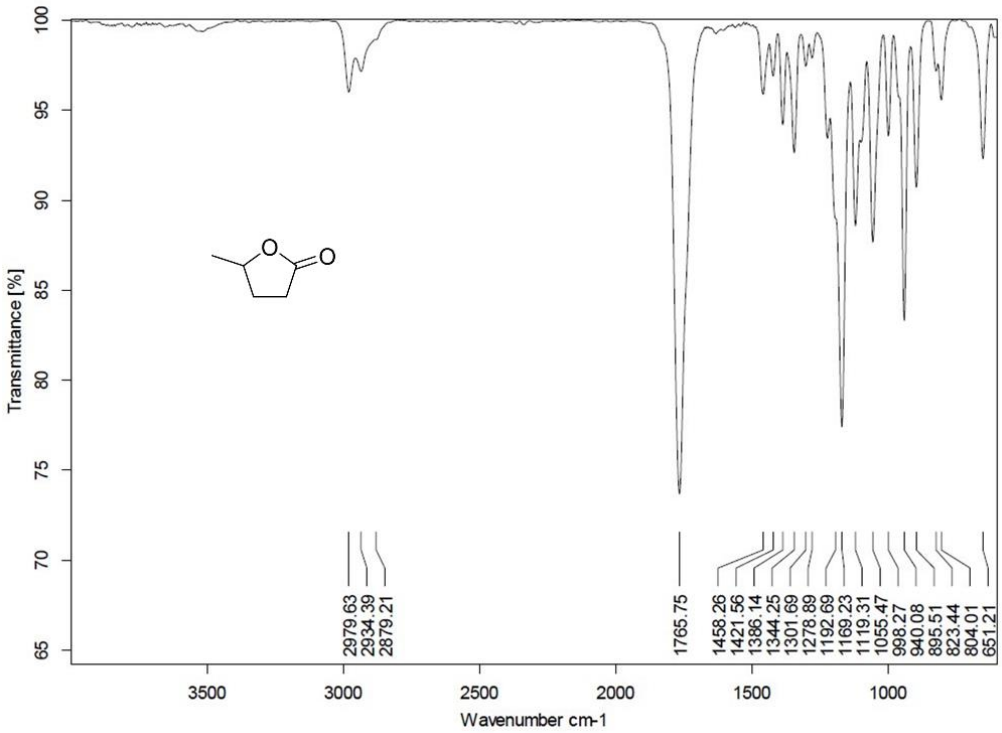

Figure 5.4 The FTIR spectrum of γ-valerolactone (GVL).

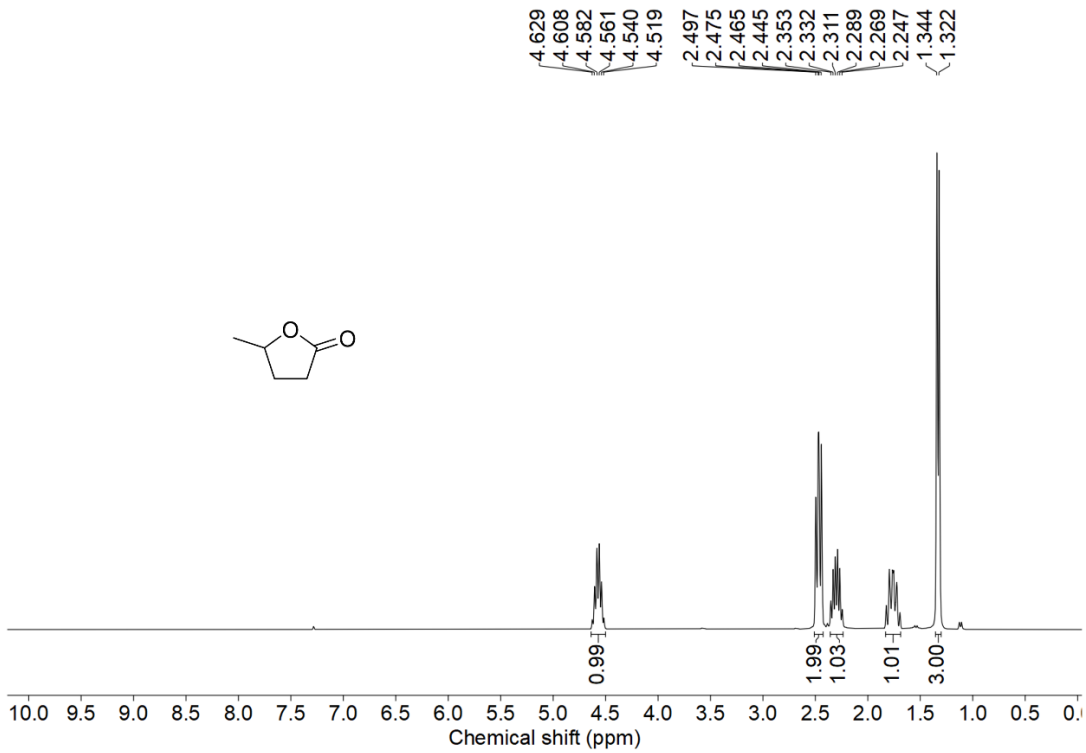

Figure 5.5 The ^{1}H NMR spectrum of γ-valerolactone (GVL).

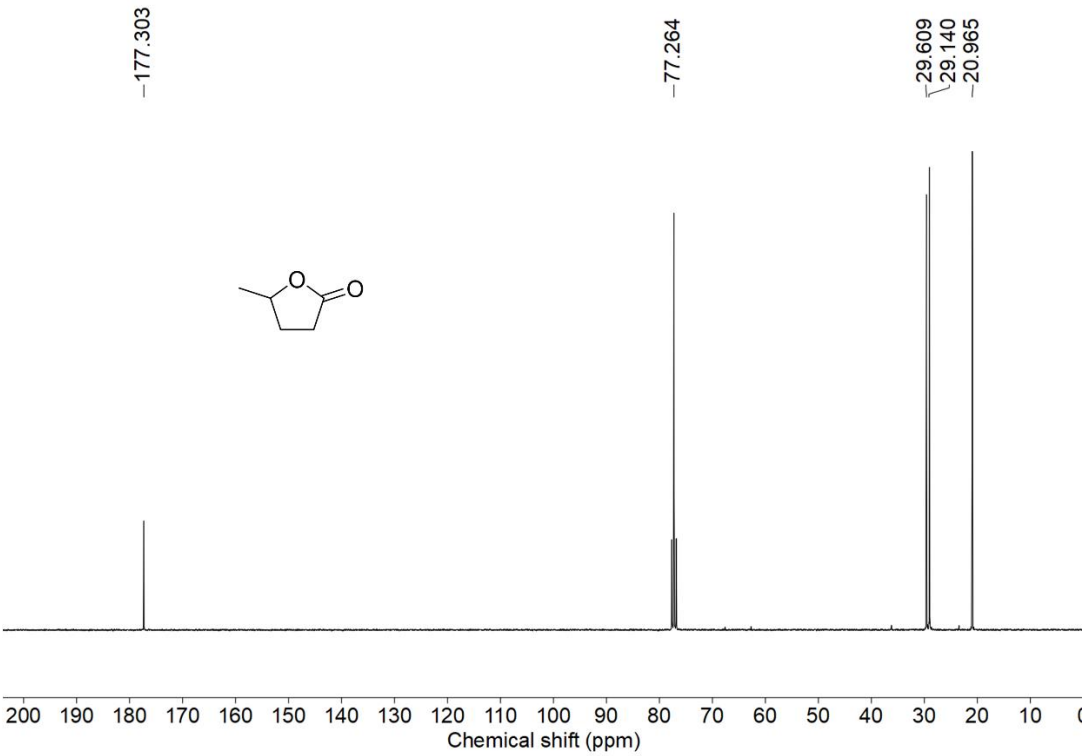

Figure 5.6 The ^{13}C NMR spectrum of γ-valerolactone (GVL).

5.4 RESULTS AND DISCUSSION

5.4.1 Physicochemical characterization

Iodine number (IN) is routinely measured to determine the adsorption capacity of AC. The IN of the synthesized HACs was determined according to ASTM standards (Table 5.1) (ASTM-D4607-14R21). The IN of HAC-500 and 600 were calculated to be 727 mg/g and 853 mg/g, respectively. A high IN typically indicates a high surface area of AC involving large micro-and mesoporous structures.

The textural characterization of the synthesized HACs was studied using nitrogen adsorption-desorption analysis. From the BJH pore size distribution curves, the pore size ranged between 2 nm and 40 nm. A distinct peak at 4.25 nm confirms that the materials are mesoporous with uniform pore size distribution (Figure 5.7). HAC-600 exhibited type IV adsorption isotherm, and was used for the catalyst preparation because of its higher IN and BET surface area values (Table 5.1). The surface area of the catalyst decreased marginally owing to the impregnation of Pd NPs on the HAC support.

Table 5.1 Pore structure parameters of HAC-500, HAC-600, and 4%Pd/HAC.

Sample	IN (mg/g)	S_{BET} (m^2/g)	V_{total} (cc/g)	D_{avg} (nm)
HAC-500	727	1203	0.32	3.4
HAC-600	853	1425	0.33	2.8
4%Pd/HAC	-	1401	0.24	2.6

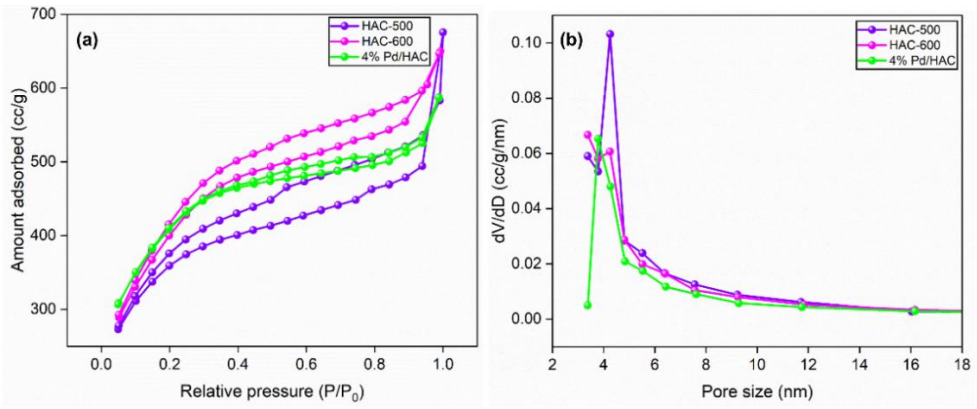

Figure 5.7 (a) N_2 adsorption isotherms, (b) BJH pore size distribution curves of HAC-500, HAC-600, and 4%Pd/HAC.

The surface morphology of the materials was determined using field-emission scanning electron microscopy (FESEM). Figure 5.8 shows the presence of cup-shaped structures in HAC. The distribution of Pd over the support can be seen from the FESEM images, which was further validated by HR-TEM. The HR-TEM image of the recycled Pd/HAC catalyst (5^{th} cycle) suggests agglomeration of Pd NPs and leaching from the HAC support (Figure 5.9). The selected area electron diffraction (SAED) pattern shows the amorphous nature of the catalyst. The presence of constituent elements in the Pd/HAC catalyst was confirmed by energy-dispersive X-ray analysis (EDX) (e-j, Figure 5.8). The elemental mapping of the catalyst further confirmed the uniform distribution of Pd NPs on the HAC support. The target of metal-on-carrier catalysts, such as the 4%Pd/HAC catalyst reported in this work, is to ensure maximum metal dispersion on the supporting material. The extent of metal dispersion depends on multiple factors, including the metal loading, duration and temperature of reduction of the metal salt precursor, and texture of the carrier material. The uniformity of metal dispersion and free-metal surface area is a guideline to check the quality and reproducibility of different catalysts. The catalytic behavior (e.g., activity, selectivity) of the metallic part of the catalyst relies on the texture, the structure, and the surface composition (Chen et al. 2020). For palladium catalysts, the extent of hydrogen adsorption depends on the metal dispersion.

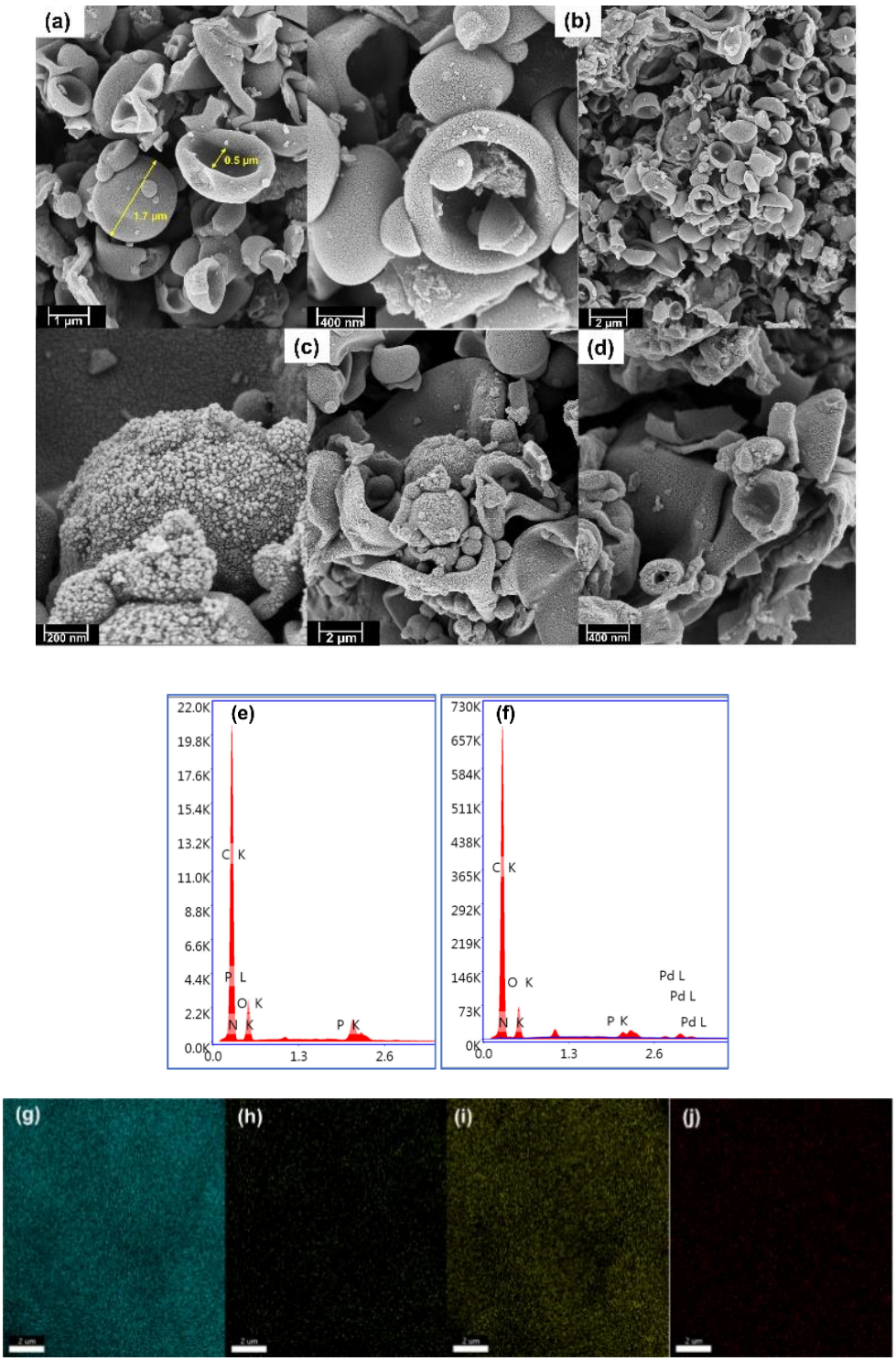

Figure 5.8 The FESEM images of (a) HAC-500, (b) HAC-600, (c) 4%Pd/HAC (fresh), and (d) Pd/HAC (recovered after the 4th cycle). The EDX pattern of (e) HAC-600, (f) Pd/HAC, and elemental mapping of Pd/HAC for (g) C, (h) N, (i) O, and (j) Pd.

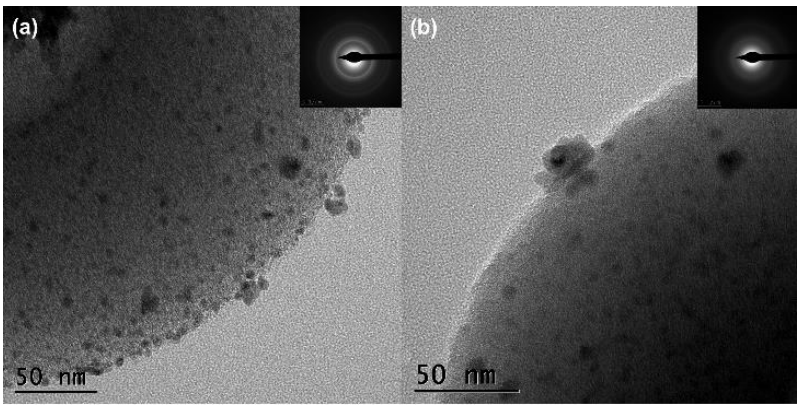

Figure 5.9 The HR-TEM images of (a) fresh 4%Pd/HAC, (b) recycled Pd/HAC (after the 5th catalytic cycle), and their corresponding SAED pattern (inset).

The powder X-ray diffraction (PXRD) patterns of the HACs and catalyst are shown in Figure 5.10. The scan was recorded in the 2θ range between 10-60º. A broad diffraction peak at 2θ = 23º confirms the amorphous nature of AC. It is evident from the literature that peaks located at 2θ = 23º and 43º for HAC-500 and 600 correspond to (002) and (101) planes of carbon. The PXRD pattern of the catalyst exhibit diffraction peaks at 40.1º, 46.5º, 67.8º, and 81.8º, corresponding to (111), (200), (220), and (311) planes of Pd, respectively (JCPDS card no. 46-1043). The peak at 40.1º suggests the formation of Pd nanoparticles. The FTIR spectra of the HACs and the catalyst are shown in Figure 5.11. The bands 2909 and 2838 cm^{-1} correspond to C-H asymmetric and symmetric stretching, whereas bands assigned 1612 and 1392 cm^{-1} correspond to C=C stretch and C-H bending vibrations. Figure 5.12 shows the thermal decomposition profiles of fresh and recycled Pd/HAC catalyst. A marginal weight loss till 90 °C corresponds to the loss in surface moisture content, and a gradual decomposition of the catalyst is observed at higher temperatures. Whereas in case of recycled Pd/HAC (5th cycle) catalyst, a faster weight loss was possibly due to evaporation of volatiles chemisorbed on the catalyst surface.

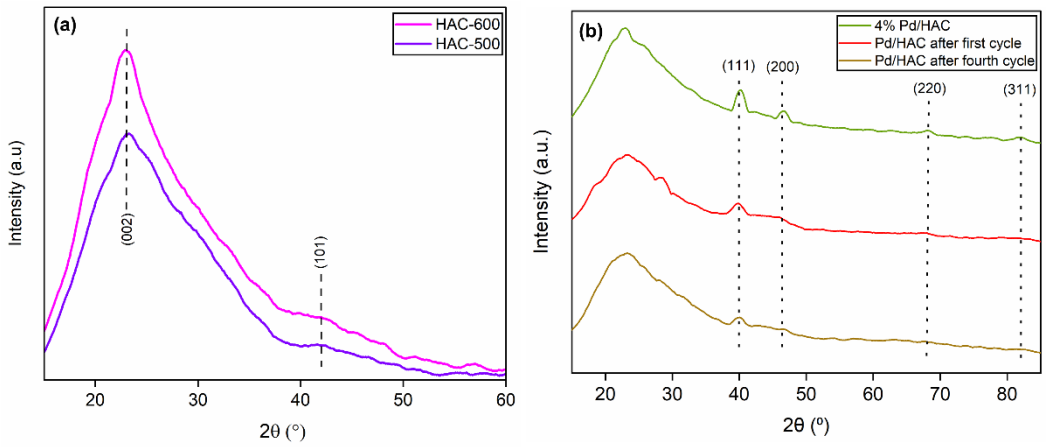

Figure 5.10 The PXRD patterns of (a) HAC-500 and HAC-600, (b) 4%Pd/HAC (fresh), recycled after the first catalytic cycle, and recycled after the fourth catalytic cycle.

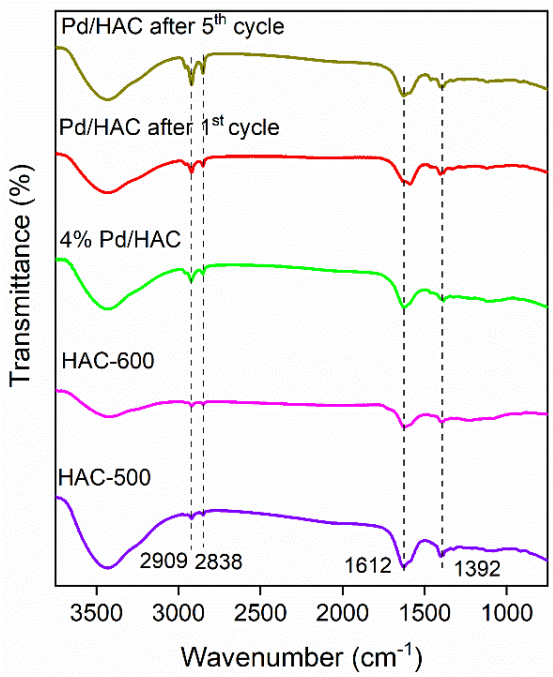

Figure 5.11 The FTIR spectra of HACs and the Pd/HAC catalysts (fresh and recycled).

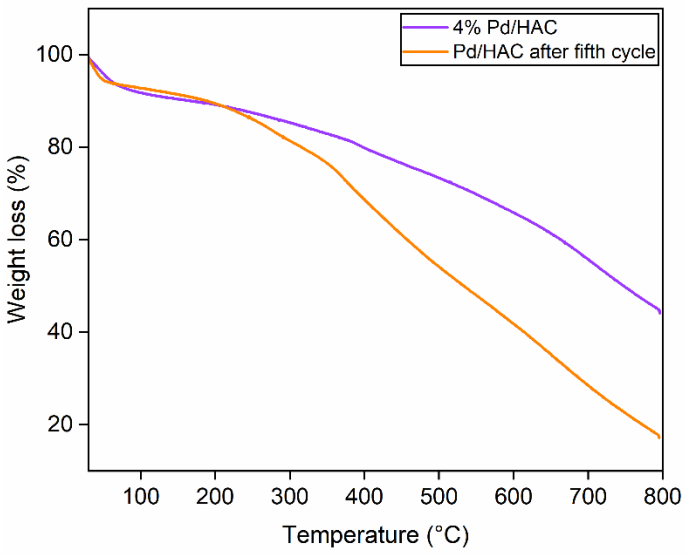

Figure 5.12 The TGA curves of fresh and recycled Pd/HAC catalyst.

5.4.2 Catalyst evaluation

The prepared catalyst was evaluated for the hydrogenation of 2-furanone GBL in a Hastelloy-made high-pressure reactor. A complete conversion of the substrate was obtained when the reaction was carried out at RT for 3 h under 0.5 MPa H_2 pressure. No conversion of 2-furanone was observed even after several hours when the reduction reaction was attempted using a hydrogen balloon. The yield of GBL remained the same when the reaction was carried out at 40 °C keeping all other reaction parameters constant. The hydrogenation reaction was studied in various organic solvents. The solubility of hydrogen gas in the organic solvent is known to influence the outcome of the hydrogenation reaction. Ethereal solvents like THF are known to solubilize gaseous hydrogen better than aliphatic and aromatic hydrocarbon solvents (Brunner 1985). Different solvents were screened for the catalytic hydrogenation reaction, and a maximum GBL yield (ca. 89%) was obtained in the presence of THF (Figure 5.13). The high yield of GBL in THF may be explained by the higher solubility of gaseous hydrogen in the solvent. Water was also examined as a green solvent for the catalytic hydrogenation reaction, and GBL was obtained in a 77% isolated yield. However, the high solubility of GBL and GVL in water somewhat defeats the purpose of using water as a sustainable reaction medium since an organic solvent is warranted to extract the product. When the reaction was carried out using commercially available 5%Pd/AC, GBL was obtained in 77% yield.

The catalyst was further evaluated for the hydrogenation of AGL to GVL. Interestingly, the conversion of AGL was incomplete under optimized reaction conditions, which may be attributed to the lesser reactivity of the olefinic group in AGL compared to 2-furanone towards catalytic hydrogenation. A complete conversion of the substrate was obtained by doubling the catalyst loading (10 wt.%). Further optimizations on the catalyst loading showed that an 8 wt.% catalyst loading was enough to ensure quantitative conversion of AGL and a high isolated yield of GVL. The synthesized GBL and GVL were characterized using FTIR, ^{1}H NMR, and ^{13}C NMR spectroscopic techniques.

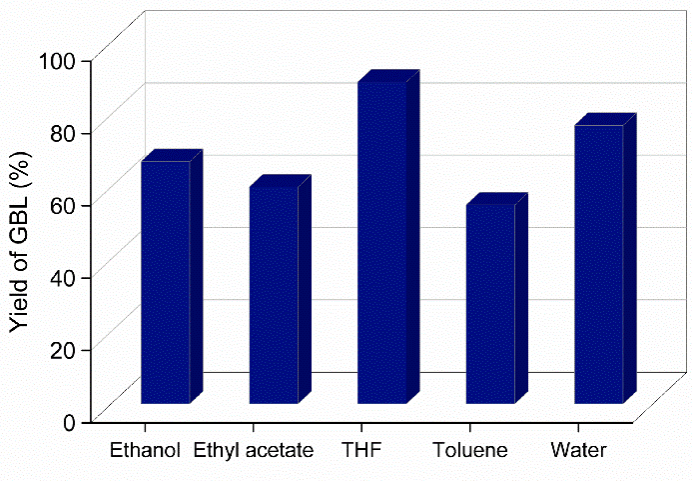

Figure 5.13 Effect of different solvents on the yield of GBL.
Reaction conditions: 2-Furanone (0.5 g), 4%Pd/HAC catalyst (5 wt.%, 0.025 g), solvent (55 mL), RT, 0.5 MPa H_2, 3 h.

5.4.3 Recyclability of the catalyst

After the reaction, the catalyst was centrifuged and reused for the next catalytic cycle after washing it with THF and dried in a hot-air oven at 80 ˚C for 12 h. The spent catalyst was characterized using FESEM, EDX, HR-TEM, TGA, and PXRD techniques. The stability of the catalyst was excellent, with only a marginal drop in the catalytic activity after the fifth cycle. It is evident from the EDX data that the loss in catalyst activity was due to the leaching of the palladium metal particles (the amount of Pd decreased from 4% to 1.5%) and chemisorption of organic contaminants on the HAC support (Figure 5.14). The authors envision that a glass-lined pressure reactor could

slow down the leaching of Pd NPs from the HAC support and decrease the physical loss of the catalyst.

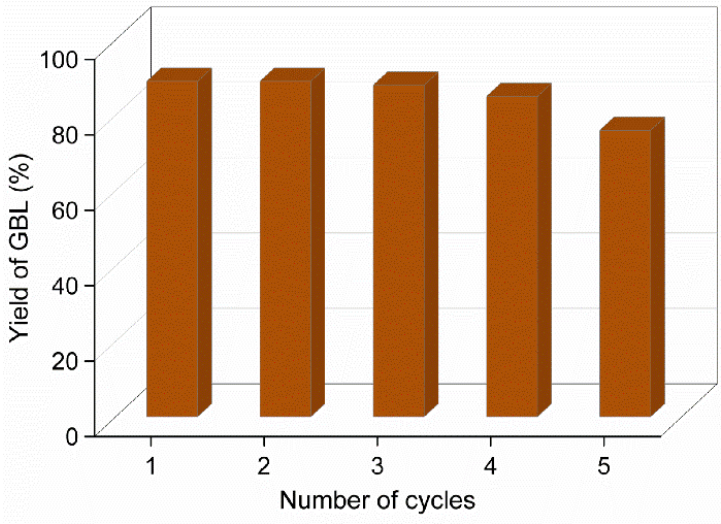

Figure 5.14 Catalytic recyclability test for the conversion of 2-Furanone to GBL. *Reaction conditions:* 2-Furanone (0.5 g), 4%Pd/HAC catalyst (5 wt.%, 0.025 g), THF (55 mL), RT, 0.5 MPa H_2, 3 h.

5.5 CONCLUSION

Palladium metal supported on humin-derived activated carbon showed excellent catalytic activity for the catalytic hydrogenation of furfural-derived 2-furanone in a batch reactor, providing an 89% isolated yield of GBL. The Pd/HAC catalyst also successfully hydrogenated angelica lactones into GVL, affording an 85% isolated yield. The starting materials, i.e., AGL and 2-furanone, are known to form many reduced products in the presence of Pd-based catalysts under appropriate reaction conditions. However, in this work, the hydrogenation reaction was performed under mild conditions (i.e., RT-40 °C, 5 bar H_2) so that only the olefin group in 2-furanone and AGL get reduced. The activation energy for the other competing mechanistic pathways is not reached under these conditions. The catalyst showed excellent recyclability and retained its activity till the third cycle. The yield of GBL decreased marginally to 76% after the fifth consecutive cycle. Deactivation of the catalyst is due to the partial leaching of Pd NPs from the HAC support and also chemisorption of organic contaminants on the catalyst surface. Future research will employ this catalyst for synthesizing other biorenewable fuels and chemicals by catalytic hydrogenation.

CHAPTER 6

ONE-POT TRANSFORMATION OF LEVULINIC ACID TO γ-VALEROLACTONE USING HETEROGENEOUS CATALYSTS

Abstract

Humin, waste from biomass hydrolysis, are the main factor limiting the utilization efficiency of biomass carbon. In this study, humin-derived activated carbon (HAC) was used as catalyst support for the hydrogenation of levulinic acid (LA) to γ-valerolactone (GVL). The HAC formed possesses a high surface area and pore volume. The Ru-supported HAC was employed for the hydrogenation of levulinic acid to γ-valerolactone. The incorporation acid groups in the catalyst increased the selectivity of GVL. Under optimized conditions (60 ℃, 1 MPa H_2, 3 h), the 5%Ru/HAC (5 wt.% loading) catalyst afforded GVL in 81.5% isolated yield and 5%Ru-20%PTA/HAC afforded 87% of GVL under similar reaction conditions.

Graphical abstract

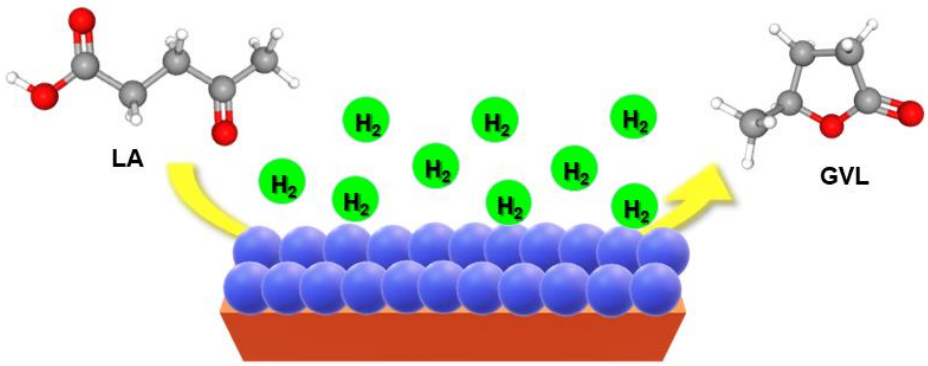

6.1 INTRODUCTION

The formation of 5-(hydroxymethyl)furfural (HMF) and levulinic acid (LA) by the acid-catalyzed deconstruction of biomass-derived sugars and carbohydrates has been known for more than a hundred years. HMF and LA were selected as sugar-derived renewable chemical platforms based on their extensive derivative chemistry and potential industrial applications. Both HMF and LA have reactive functionalities, which may be exploited individually or together to synthesize a wide range of products of desired structures and properties. Recognizing its significance in biorefinery, the National Renewable Energy Laboratory listed LA among the top 10 renewable chemicals based on its commercial potential. With two reactive functionalities (i.e., ketone and carboxylic acid), LA participates in various redox reactions involving either one or both of its functional groups. Catalytic hydrogenation of the ketone group in LA, followed by intramolecular lactonization, forms γ-valerolactone (GVL) (Scheme 6.1)

(Yu et al. 2020c). GVL has potential applications as a renewable solvent, fuel oxygenate, and chemical intermediate for making hydrocarbon fuels and olefins (Kamble et al. 2023). GVL is a promising fuel additive, green solvent, fragrance ingredient, and renewable chemical intermediate for further value addition. The property of those derivatives can be fine-tuned by modifying the functionality introduced in the GVL moiety.

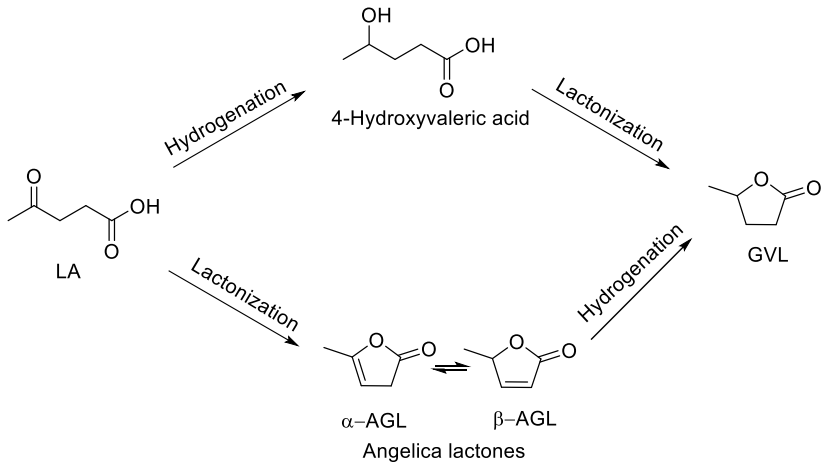

Scheme 6.1 The synthesis of GVL from LA.

GVL is typically synthesized by the liquid- or vapor-phase hydrogenation of LA in a hydrogen-donor solvent or an overpressure of hydrogen gas in the presence of a suitable metal catalyst (Huang et al. 2023). Catalysts used in this transformation include noble metals, non-noble metals, and bimetallic catalysts. The reaction can proceed by hydrogenating the ketone functionality, followed by the intramolecular lactonization of the alcohol intermediate (Zhang et al. 2021a). Alternatively, GVL can be formed by the hydrogenation of the angelica lactones formed by the intramolecular lactonization of LA (Scheme 6.1). Although numerous heterogeneous catalysts have been screened for the hydrogenation of LA to GVL, developing a stable, active heterogeneous catalyst remains challenging. The Ru-based catalytic systems are extensively employed for the hydrogenation of LA to GVL due to the ability of Ru to hydrogenate the carbonyl functionality of LA selectively to hydroxyl functionality under mild reaction conditions (Bounoukta et al. 2023b).

In the current work, humin derived during the acid-catalyzed hydrolysis of xylose was used to prepare HACs as potential catalyst support for the direct transformation of LA to GVL (Scheme 6.2). The gram-scale synthesis afforded high

isolated GVL yields at near quantitative substrate conversion under optimized reaction conditions.

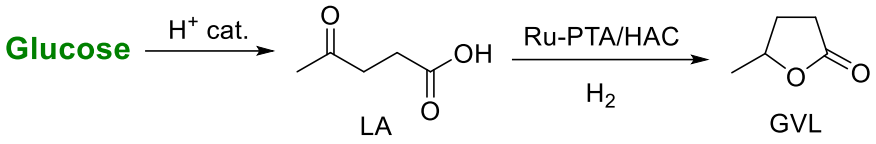

Scheme 6.2 Catalytic conversion of levulinic acid to γ-valerolactone.

6.2 EXPERIMENTAL PROCEDURE

6.2.1 Materials

Xylose (99%) and benzyltributylammonium chloride (BTBAC, 99%) were procured from Spectrochem. Ruthenium (III) chloride hydrate was purchased from TCI. $NaBH_4$, 1,2-dichloroethane (DCE) (98%), and HCl (aq., 35-38%) were obtained from Molychem. Sodium sulfate (anhydrous, 99%), NaOH, and deionized (DI) water were purchased from Loba Chemie Pvt. Ltd. Methanol (99.5%) was purchased from Finar.

6.2.2 Preparation of humin and HAC

Humin and HAC were prepared following the same preparation methods described in *Chapter 3*.

6.2.3 Preparation of Ru/HAC and Ru-PTA/HAC catalyst

The catalyst (5%Ru/HAC-600) was prepared following the literature procedure (Ohyama et al. 2013). HAC (0.500 g) was dispersed in 20 mL HPLC water under ultrasonication for 15 min. The required amount of $RuCl_3$ was dissolved in water and added dropwise into the above solution at RT under vigorous stirring. The mixture was stirred for 2 h, followed by adding 0.1 M NaOH solution to maintain the pH in the range of 7-8. The mixture was stirred for 0.5 h, and $NaBH_4$ (15 mL, 10 mmol) was added slowly. The solution was stirred for 1 h, filtered, washed with 500 mL of DI water, and dried at 110 ℃ for 6 h.

To the 5%Ru/HAC-600 suspended in dry methanol (50 mL), a calculated amount of phosphotungstic acid dissolved in methanol (25 mL) was added and stirred for 6 h. Methanol was evaporated under reduced pressure, and the 5%Ru-20%PTA/HAC-600 catalyst was dried for 6 h at 110 ℃.

6.2.4 Characterization methods

Fourier-transform infrared spectroscopy (FTIR) spectra of the synthesized materials were recorded on a Bruker Alpha 400 FTIR spectrometer using the KBr pellet technique. Powder X-ray diffraction (PXRD) patterns were recorded on Rigaku MiniFlex 600 (Japan) X-ray Powder Diffractometer using Cu Kα radiation as the source. The surface morphology of the samples was investigated using field emission scanning electron microscopy (FESEM), Gemini 300, Carl Zeiss, operating at an accelerating voltage of 15 kV. Brunauer-Emmett-Teller (BET) surface area of the samples was measured using Autosorb IQ-XR-XR, Anton Paar, employing N_2 adsorption at 77.35 K. The pore size distribution of the samples was determined from nitrogen desorption isotherms using the Barrett-Joyner-Halenda (BJH) method. The temperature-programmed desorption (TPD) measurement was performed using Quantachrome TPRWin v3.52 instrument. The sample was activated in helium gas with a flow rate of 30 mL min^{-1} at 200 ℃ for 110 min. After cooling, the sample was saturated with 10% NH_3 blended in He with a flow rate of 30 mL min^{-1} for 60 min. The analysis was carried out in the temperature range of 100-800 ℃ with a heating rate of 10 ℃ min^{-1}.

6.2.5 Catalytic conversion of LA to GVL

LA (1.002 g, 8.62 mmol), catalyst (5 wt.%, 0.05 g), and water (55 mL) were charged into a Hastelloy-made high-pressure reactor. The reactor was closed, purged with H_2 three times, and pressurized to 1.0 MPa of H_2 pressure. The reaction was carried out at 60 ℃ for 3 h. After the reaction, the reaction mixture was centrifuged to separate the suspended 5%Ru/HAC-600 catalyst. The reaction mixture was extracted with ethyl acetate and evaporated under reduced pressure to get crude GVL (Khajone et al. 2023) as a colorless liquid. The crude product was then passed through a small plug of silica gel (60-120 mesh) to get pure GVL (0.703 g, 81.5%).

6.3 CHARACTERIZATION OF SYNTHESIZED COMPOUNDS

6.3.1The FTIR, ^{1}H-NMR, and ^{13}C-NMR spectra of γ-valerolactone (GVL)

^{1}H-NMR ($CDCl_3$, 300 MHz) δ (ppm): 4.58 (m, 1H), 2.47 (m, 2H), 2.31 (m, 2H), 1.33 (d, 3H, , *J*=6.6 Hz); ^{13}C-NMR ($CDCl_3$, 75 MHz): δ (ppm): 173.3, 77.2, 29.6, 29, 20.9; FTIR (ATR, cm^{-1}): 2973, 2934, 1765, 1119.

6.4 RESULTS AND DISCUSSION

6.4.1 Physicochemical characterization

Chapter 3 discussed the detailed characterization data for HAC-600.

FTIR spectrum of the catalyst shows a broad peak at 3443 cm^{-1}, corresponding to -OH stretching frequency. Peaks at 2923 cm^{-1} and 2852 cm^{-1} are responsible for the antisymmetric and symmetric C–H stretching vibrations. Similarly, peaks at 1620 cm^{-1}, 1385 cm^{-1}, and 1115 cm^{-1} correspond to -C=O stretch, -C=C vibration, and -C-H bending vibrations, respectively (Figure 6.1a). The powder X-ray diffraction (PXRD) patterns of the catalysts show diffraction peaks at 41.7º, 42.5º, 68.0º, and 78.0º, corresponding to (100), (002), (110), and (103) planes of ruthenium, respectively (Figure 6.1b).

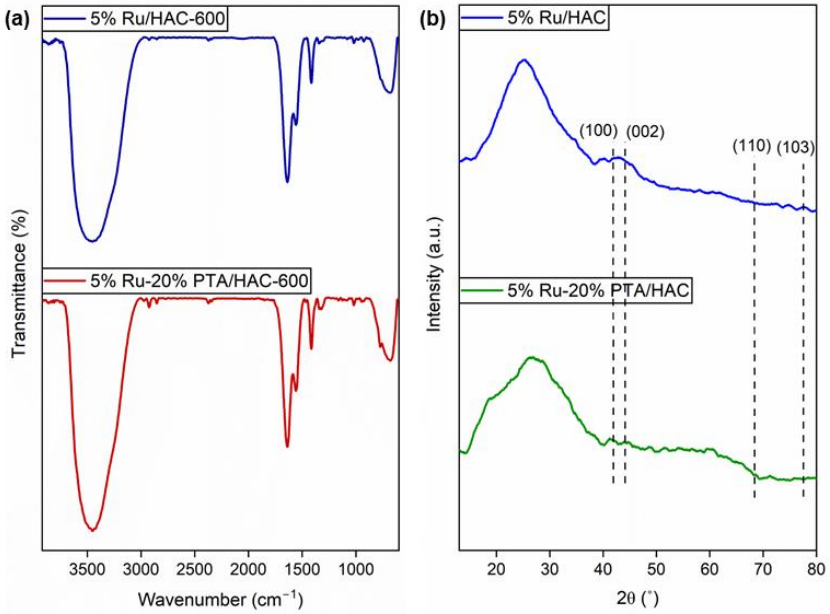

Figure 6.1 (a) FTIR spectra (b) PXRD patterns of 5%Ru/HAC-600 and 5%Ru-PTA/HAC-600.

The porous features of the prepared catalysts were studied using nitrogen adsorption-desorption analysis. A decrease in surface area from nitrogen adsorption-desorption analysis implies that the Ru nanoparticles occupy the surface of the support (Figure 6.2a). The isotherms match with type IV, and the hysteresis loops indicate that both possess mesoporous structures. The size of the mesopores, as shown in Figure 6.2b, is 2.6 nm for 5%Ru/HAC-600 and 2.5 nm for 5%Ru-PTA/HAC-600 catalysts, which confirms a uniform pore size distribution. The surface morphology of the

materials was determined using field-emission scanning electron microscopy (FESEM). The catalyst possesses cup-shaped structures with an average diameter of 1.4 μm inherited from the HAC support. The Ru nanoparticles are well dispersed over the HAC support. The acidity of 5%Ru-20%PTA/HAC-600 was calculated using NH_3-TPD analysis Figure 6.5. Based on the temperature at which adsorbed ammonia molecules desorb, acidic sites in catalysts can be divided into three groups. Weak acidic sites desorb ammonia around 200-300 °C, moderate acidic sites around 300-450 °C, and strong acidic sites above 450 °C. It is evident from the figure that the catalyst possesses moderate acidic sites.

Table 6.1 Pore structure parameters of HAC-600, 5%Ru/HAC-600, and 5%Ru-20%PTA/HAC-600.

Sample	IN (mg/g)	S_{BET} (m^2/g)	V_{total} (cc/g)	D_{avg} (nm)
HAC-600	853	1425	0.33	2.8
5%Ru/HAC-600	-	1139	0.11	2.4
5%Ru-20%PTA/HAC-600	-	577	0.05	2.4

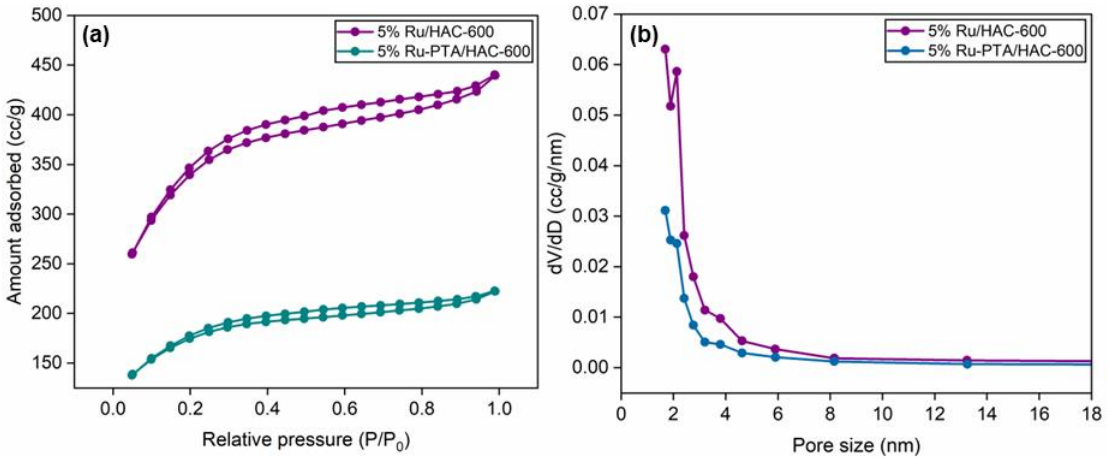

Figure 6.2 (a) N_2 adsorption isotherms, (b) BJH pore size distribution curves of 5%Ru/HAC-600 and 5%Ru-PTA/HAC-600.

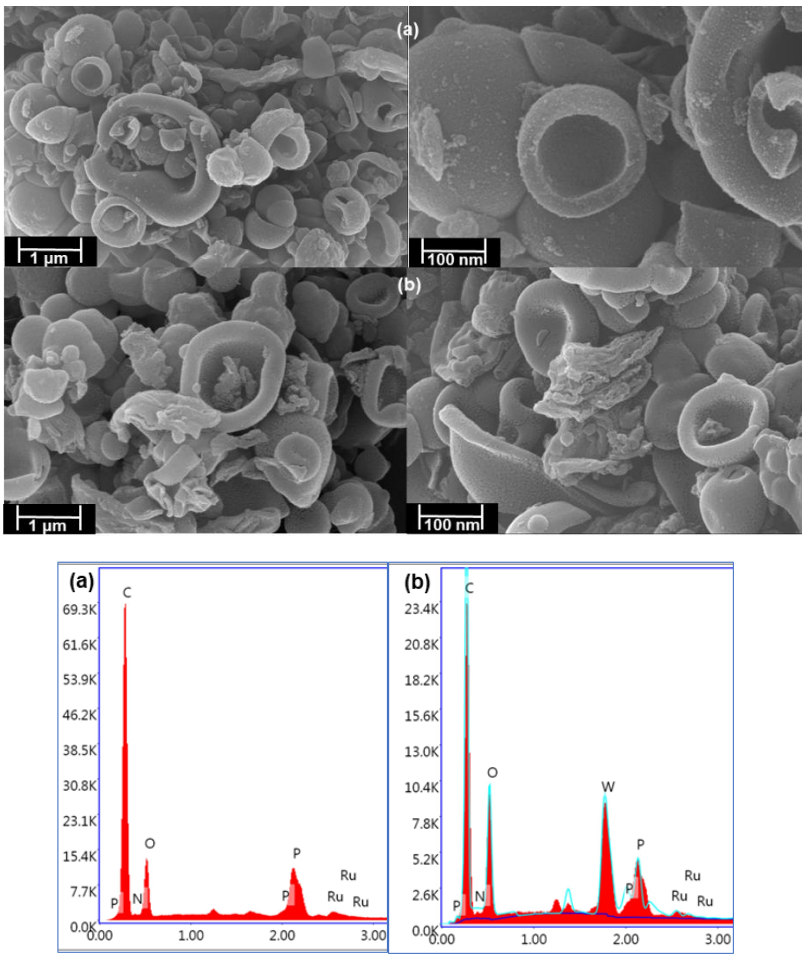

Figure 6.3 The FESEM images and EDX pattern of 5%Ru/HAC-600 and 5%Ru-20%PTA/HAC-600.

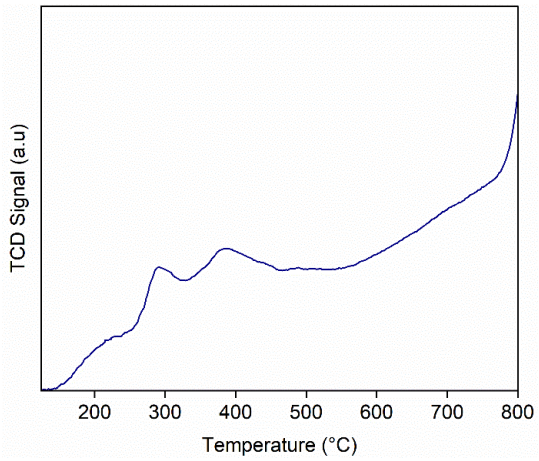

Figure 6.4 NH_3-TPD pattern of the 5%Ru-PTA/HAC-600 catalyst.

6.4.2 Catalyst evaluation

The prepared catalyst was evaluated for the hydrogenation of LA to GVL in a Hastelloy-made high-pressure reactor. A quantitative conversion of LA was observed when the reaction was carried out at 60 ℃ for 3 h using 1.0 MPa hydrogen pressure. The effect of various reaction parameters such as reaction temperature, duration, and hydrogen pressure on the yield of GVL was studied. The effect of reaction temperature was investigated at 40-120 ℃ (Figure 6.5). Quantitative conversion of the substrate was not observed, when the reaction was carried out at lower temperatures (<40 ℃), but the selectivity increased at 60 ℃. Further increase of temperature to 100 and 120 ℃, resulted in marginal decrease in GVL yield.

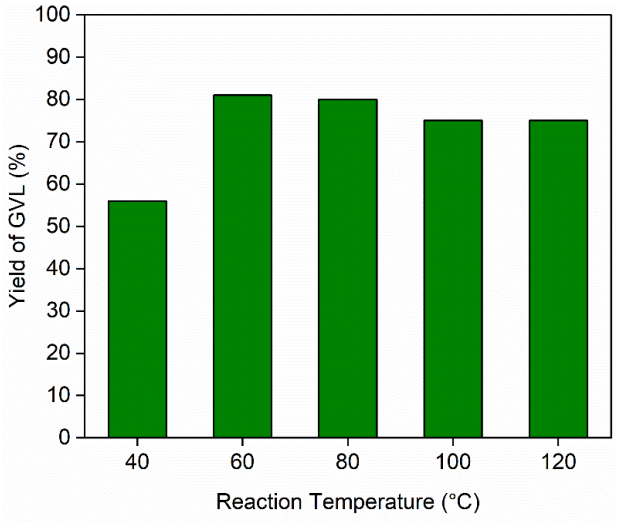

Figure 6.5 Effect of reaction temperature on the yield of GVL.
Reaction conditions: LA (1.002 g, 8.62 mmol), water (55 mL), 5%Ru/HAC-600 (5 wt.%, 0.05 g), 1.0 MPa H_2, 3 h.

The effect of reaction duration was studied by varying the time between 1-4 h (Figure 6.6a). When the reaction was carried out for 3 h, a maximum GVL yield (ca. 81.5%) was obtained with quantitative conversion of LA. However, lowering the duration to 1-2 h decreased the isolated yield of GVL. With prolonged reaction time, GVL yield remained constant, indicating that the GVL was stable under these reaction conditions. The influence of hydrogen pressure (0.5-1.5 MPa) on the yield of GVL was also studied (Figure 6.6b). A hydrogen pressure of 1 MPa furnished 81.5% yield of GVL, further increase in the hydrogen pressure have no effect on the yield.

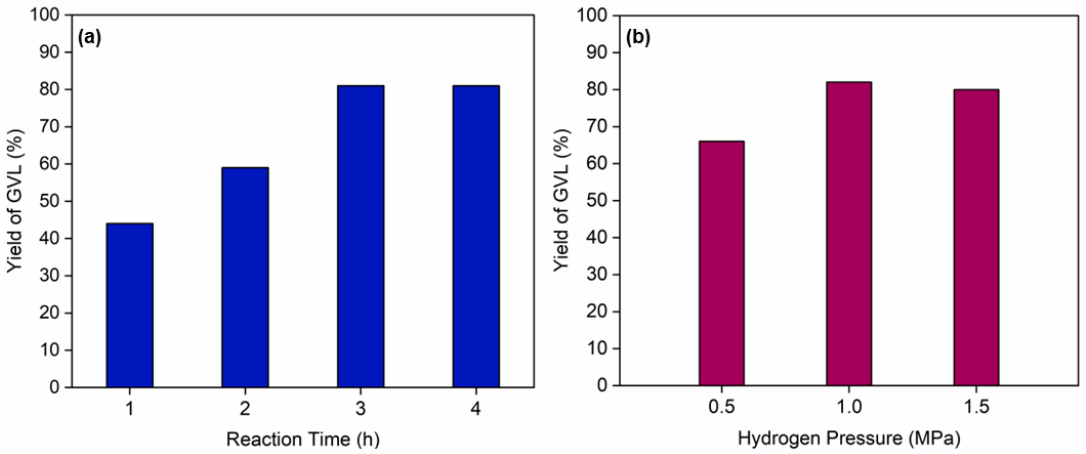

Figure 6.6 Effect of (a) reaction time and (b) hydrogen pressure on the yield of GVL. *Reaction conditions:* (a) LA (1.002 g, 8.62 mmol), water (55 mL), 5%Ru/HAC-600 (5 wt.%, 0.05 g), 60 ℃, and 1.0 MPa H_2, and (b) LA (1.002 g, 8.62 mmol), water (55 mL), 5%Ru/HAC-600 (5 wt.%, 0.05 g), 60 ℃, and 3 h.

The use acid additive for LA to GVL conversion was reported in the literature. In this regard, the catalytic activity of 5%Ru/HAC-600 was compared with bifunctional 5%Ru-20%PTA/HAC catalyst under optimized reaction conditions. The presence of acid enhanced the dehydration of LA, and furnished GVL in 87% yield.

6.5 CONCLUSION

Ruthenium supported on humin-derived activated carbon served as a best catalyst for the hydrogenation of LA to GVL using water as the solvent. Under optimized conditions (60 ℃, 1 MPa H_2, 3 h), the 5%Ru/HAC (5 wt.% loading) catalyst afforded GVL in 81.5% isolated yield. The introduction of PTA on the catalyst further improved the yield of GVL, owing to the enhanced dehydration of LA. The effect of various reaction parameters (temperature, time, and hydrogen pressure) on the yield of GVL was studied.

CHAPTER 7

SUMMARY AND CONCLUSION

This chapter includes the summary and important conclusions of the present research work. It also consists of a brief account of the scope for future work.

7.1 SUMMARY

- The present work attempted the synthesis of renewable lactones and esters from carbohydrate-derived chemical platforms via hydrogenation and esterification reactions. The humin-derived activated carbon (HAC) was employed as a catalyst support for the above transformations. The synthesis of monoesters and diesters of glucose-derived isosorbide (IS) via base-catalyzed transesterification is also reported.
- Several efficient catalysts have been developed for synthesizing alkyl levulinates (ALs) under economically amenable reaction parameters. Catalysts that function equally well with multiple feedstocks to form ALs following a general synthetic protocol are limited. The present work reported the straightforward and high-yielding synthesis of ALs by the acid-catalyzed esterification of LA and by the alcoholysis of carbohydrate-derived chemical platforms, such as furfuryl alcohol (FAL) and α-angelica lactone (AGL). Phosphotungstic acid (PTA) was chosen as the solid acid catalyst for the transformation, which was heterogenized on HAC for superior recyclability. Using HAC as catalyst support expands the scope of valorizing humin, a complex furanic resin produced inevitably as a side product (often considered waste) during the acid-catalyzed hydrolysis/dehydration of sugars and polymeric carbohydrates.
- A systematic study of the base-catalyzed transesterification of isohexides under straightforward and scalable process conditions is warranted. The present work reports the solvent-free, high-yielding, and scalable pathway for producing the monoesters and diesters of IS by transesterification reaction using K_2CO_3 as an efficient, inexpensive, and recyclable base catalyst. The monoesters and diesters of glucose-derived IS have a number of applications, such as dispersants in pigments, surfactants in detergents, emulsifiers in cosmetics, monomers for

biopolymers, and plasticizers in vinyl polymers. The methodology was successfully extended to synthesize the monoesters and diesters of the other two isohexides, i.e., isomannide and isoidide. The gram-scale preparation of alkyl, vinyl, and aryl esters of isohexides was optimized on the reaction temperature, duration, equivalence of the ester reagent, and catalyst loading. The unsymmetrical diesters of isohexides have also been produced using step-wise transesterification.

- The value-addition pathways of humin as an adsorbent, reinforcing material, and catalyst support is known. Humin, produced during the preparation of furfural (FF) from xylose, was carbonized to form humin-derived activated carbon (HAC). Palladium supported on HAC (Pd/HAC) was used as an efficient and recyclable catalyst for hydrogenating 2-furanone into GBL. The process was optimized on temperature, catalyst loading, and solvent. Moreover, the catalyst was conveniently recovered after the reaction and successfully recycled for five cycles with only a marginal decrease in the yield of GBL.
- Furthermore, the catalytic hydrogenation followed by cyclization of levulinic acid to GVL is paramount due to huge potential market of GVL. Ruthenium based heterogeneous catalyst (Ru-HAC) using HAC as a support was synthesized and their catalytic activity was studied. The reaction parameters such as temperature, time, and hydrogen pressure were studied. Finally, PTA and Ru-based bifunctional catalyst was prepared, characterized, and catalytic activity was compared with monofunctional catalyst.

7.2 CONCLUSION

The main objectives of the thesis were the preparation and value addition of renewable chemical intermediates from carbohydrates. Based on experimental results, the following conclusions were drawn.

- Humin worked as a promising feedstock for deriving activated carbon with high surface area with micro- and mesoporosity. HAC was successfully used as a supporting material for PTA to produce a heterogeneous acid catalyst. The

PTA/HAC-600 catalyst produced alkyl levulinates in good to excellent isolated yields starting from carbohydrate-derived chemical intermediates, such as LA, FAL, and α-AGL. The catalyst was successfully recovered and recycled for five catalytic cycles. This work will create interest in the high-value application of humin, a waste product produced in the biorefinery. Future work will explore the efficiency of the PTA/HAC-600 catalyst towards other acid-catalyzed reactions for the catalytic value addition of biomass and sustainable organic synthesis in general.

- Various monoesters and diesters of biomass-derived isohexides have been synthesized by base-catalyzed transesterification under organic solvent-free conditions. The preparation was performed on several grams scale, and the products were isolated in excellent yields. The inexpensive K_2CO_3 catalyst was conveniently separated and successfully reused. Alkyl, aryl, and vinyl esters of isohexides were synthesized with equal ease, and even unsymmetrical diesters were produced in sequential transesterification steps. In the case of IS, noticeable selectivity was observed towards the *exo*-monoester. In some cases, entirely biorenewable esters of isohexides were obtained using renewable ester reagents. This work will help expand the commercial applications and markets of these commercially relevant esters.
- Palladium metal supported on humin-derived activated carbon showed excellent catalytic activity for the catalytic hydrogenation of furfural-derived 2-furanone in a batch reactor, providing an 89% isolated yield of GBL. The Pd/HAC catalyst also successfully hydrogenated angelica lactones into GVL, affording an 85% isolated yield. The starting materials, i.e., α-AGL and 2-furanone, are known to form many reduced products in the presence of Pd-based catalysts under appropriate reaction conditions. However, in this work, the hydrogenation reaction was performed under mild conditions (i.e., RT-40 °C, 5 bar H_2) so that only the olefin group in 2-furanone and α-AGL get reduced. The activation energy for the other competing mechanistic pathways is not reached under these conditions. The catalyst showed excellent recyclability and retained its activity

till the third cycle. The yield of GBL decreased marginally to 76% after the fifth consecutive cycle. Deactivation of the catalyst is due to partial leaching of Pd NPs from the HAC support and also chemisorption of organic contaminants on the catalyst surface. Future research will employ this catalyst for synthesizing other biorenewable fuels and chemicals by catalytic hydrogenation.

- Ruthenium supported on humin-derived activated carbon served as a best catalyst for the hydrogenation of LA to GVL using water as the solvent. Under optimized conditions (60 ℃, 1 MPa H_2, 3 h), the 5%Ru/HAC (5 wt.% loading) catalyst afforded GVL in 81.5% isolated yield. The introduction of PTA on the catalyst further improved the yield of GVL, owing to the enhanced dehydration of LA. The effect of various reaction parameters (temperature, time, and hydrogen pressure) on the yield of GVL was studied.

7.3 FUTURE SCOPE

The present work described the chemocatalytic upgradation of carbohydrate-derived renewable chemical intermediates into value-added chemicals using abundant, inexpensive, efficient, and eco-friendly heterogeneous catalysts. More dedicated research is warranted to design and develop state-of-the-art heterogeneous catalysts that will provide the targeted biorenewable product(s) in the desired selectivity and yield under economically viable and environmentally acceptable conditions. HAC has been used as an inexpensive and sustainable heterogeneous support for acid and metal catalysts. Esterification and alcoholysis have been described as model reactions using PTA/HAC as the heterogeneous acid catalyst. Future research should focus on using this catalyst for other acid-catalyzed reactions, such as dehydration, aldol reaction, and acetalization. For example, the production of furfural and HMF can be attempted starting from xylose and glucose, respectively, using the PTA/HAC catalyst. Moreover, HAC can be functionalized with sulfonic acid using suitable reagents (e.g., conc. H_2SO_4) so that no solid acids need to be supported on it. The novel sulfonic acid-functionalized HAC can then be used as heterogeneous acid catalyst for various acid-catalyzed reactions for synthesizing renewable chemicals. Noble metal nanoparticles

supported on HAC have been employed for catalytic hydrogenation reaction, such as preparing GVL and GBL from the corresponding olefinic starting material, as potential fuel oxygenate, solvent, and sustainable chemical feedstock. The catalysts can also be tried for other catalytic transformations, such as hydrogenolysis and hydrodeoxygenation reactions. For example, the Pd/HAC can be used for synthesizing DMF by hydrogenating HMF or its hydrophobic analogs. The catalyst worked well for the reduction of olefins (e.g., ethyl oleate was hydrogenated quantitatively to ethyl stearate). This can be used as a model reaction to stabilize biodiesel that contains polyaromatic compounds. Several existing and novel mono- and diesters of carbohydrate-derived isohexides have been synthesizing by transesterification reaction catalyzed by anhydrous K_2CO_3. The process scalability should be studied next, and the compounds should be prepared in several grams scale. The physicochemical properties of the esters should be studied in detail to explore their potential applications and markets.

REFERENCES

Ahmad, E., Kishore Pant, K., and Ali Haider, M. (2022a). "Synthesis and application of TiO_2-supported phosphotungstic acid for ethyl levulinate production." *Mater. Sci. Energy Technol.*, 5, 189–196.

Ahmad, K. A., Siddiqui, M. H., Alam, Md. I., Haider, M. A., and Ahmad, E. (2022b). "Keggin heteropolyacid catalysts: Synthesis, heterogenization, and application in conversion of biomass-derived molecules." *Catalysis*, J. Spivey, Y.-F. Han, and D. Shekhawat, eds., Cambridge: Royal Society of Chemistry, 206–247.

Alonso, D. M., Bond, J. Q., and Dumesic, J. A. (2010). "Catalytic conversion of biomass to biofuels." *Green Chem.*, 12(9), 1493.

Alonso, D. M., Wettstein, S. G., and Dumesic, J. A. (2013). "Gamma-valerolactone, a sustainable platform molecule derived from lignocellulosic biomass." *Green Chem.*, 15(3), 584.

Al-Shaal, M. G., Hausoul, P. J. C., and Palkovits, R. (2014). "Efficient, solvent-free hydrogenation of α-angelica lactone catalysed by Ru/C at atmospheric pressure and room temperature." *Chem. Commun.*, 50(71), 10206.

Anjali, K., Vijayan, A., Venkatesha, N. J., and Sakthivel, A. (2021). "Niobium based macromolecule preparation and its potential application in biomass derived levulinic acid esterification." *Inorg. Chem. Commun.*, 123, 108302.

Appaturi, J. N., Andas, J., Ma, Y.-K., Lee Phoon, B., Muazu Batagarawa, S., Khoerunnisa, F., Hazwan Hussin, M., and Ng, E.-P. (2022). "Recent advances in heterogeneous catalysts for the synthesis of alkyl levulinate biofuel additives from renewable levulinic acid: A comprehensive review." *Fuel*, 323, 124362.

ASTM-D4607-14R21 Standard test method for determination of iodine number of activated carbon, ASTM International, West Conshohocken, PA, 2021.

Ayashi, N., Najafi Chermahini, A., and Saraji, M. (2022). "Biomass conversion to alkyl levulinates using heteropoly acid carbon mesoporous composites." *Process Saf. Environ. Prot.*, 160, 988–1000.

Badgujar, K. C., Badgujar, V. C., and Bhanage, B. M. (2020). "A review on catalytic synthesis of energy rich fuel additive levulinate compounds from biomass derived levulinic acid." *Fuel Process. Technol.*, 197, 106213.

Badgujar, K. C., Badgujar, V. C., and Bhanage, B. M. (2023). "Synthesis of alkyl levulinate as fuel blending agent by catalytic valorization of carbohydrates via alcoholysis: Recent advances and challenges." *Catal. Today*, 408, 9–21.

Bai, J., Cheng, C., Liu, Y., Wang, C., Liao, Y., Chen, L., and Ma, L. (2021). "Selective hydrogenation of levulinic acid to γ-valerolactone on Ni-based catalysts." *Mol. Catal.*, 516, 112000.

Bazoti, S. F., Bonatto, C., Scapini, T., Camargo, A. F., Treichel, H., and De Oliveira, D. (2023). "Recent advances, perspectives and challenges on levulinic acid production from residual biomass." *Biofuels, Bioprod. Bioref.*, 17(4), 1068–1084.

Bhat, N. S., Kumar, R., Jana, A., Mal, S. S., and Dutta, S. (2023). "Selective oxidation of biomass-derived furfural to 2(5H)-furanone using trifluoroacetic acid as the catalyst and hydrogen peroxide as a green oxidant." *Biomass Conver. Biorefin.*, 13(2), 1029–1034.

Bhat, N. S., Mal, S. S., and Dutta, S. (2021). "Recent advances in the preparation of levulinic esters from biomass-derived furanic and levulinic chemical platforms using heteropoly acid (HPA) catalysts." *Mol. Catal.*, 505, 111484.

Bhat, N. S., Vinod, N., Onkarappa, S. B., and Dutta, S. (2020). "Hydrochloric acid-catalyzed coproduction of furfural and 5-(chloromethyl)furfural assisted by a phase transfer catalyst." *Carbohydr. Res.*, 496, 108105.

Boonyakarn, T., Wataniyakul, P., Boonnoun, P., Quitain, A. T., Kida, T., Sasaki, M., Laosiripojana, N., Jongsomjit, B., and Shotipruk, A. (2019). "Enhanced levulinic acid production from cellulose by combined Brønsted hydrothermal carbon and Lewis acid catalysts." *Ind. Eng. Chem. Res.*, 58(8), 2697–2703.

Bounoukta, C. E., Megías-Sayago, C., Navarro, J. C., Ammari, F., Ivanova, S., Centeno, M. Á., and Odriozola, J. A. (2023a). "Functionalized biochars as supports for Ru/C catalysts: Tunable and efficient materials for γ-valerolactone production." *Nanomaterials*, 13(6), 1129.

Bounoukta, C. E., Megías-Sayago, C., Rendón, N., Ammari, F., Penkova, A., Ivanova, S., Centeno, M. Á., and Odriozola, J. A. (2023b). "Selective hydrodeoxygenation of levulinic acid to γ-valerolactone over Ru supported on functionalized carbon nanofibers." *Sustainable Energy Fuels*, 7(3), 857–867.

Brunner, E. (1985). "Solubility of hydrogen in 10 organic solvents at 298.15, 323.15, and 373.15 K." *J. Chem. Eng. Data*, 30(3), 269–273.

Cai, B., Zhang, Y., Feng, J., Huang, C., Ma, T., and Pan, H. (2021). "Highly efficient g-C_3N_4 supported ruthenium catalysts for the catalytic transfer hydrogenation of levulinic acid to liquid fuel γ-valerolactone." *Renewable Energy*, 177, 652–662.

Cao, R., Xin, J., Zhang, Z., Liu, Z., Lu, X., Ren, B., and Zhang, S. (2014). "Efficient conversion of α-angelica lactone into γ-valerolactone with ionic liquids at room temperature." *ACS Sustainable Chem. Eng.*, 2(4), 902–909.

Centi, G., Trifiro, F., Ebner, J. R., and Franchetti, V. M. (1988). "Mechanistic aspects of maleic anhydride synthesis from C4 hydrocarbons over phosphorus vanadium oxide." *Chem. Rev.*, 88(1), 55–80.

Chen, H., Goodarzi, F., Mu, Y., Chansai, S., Mielby, J. J., Mao, B., Sooknoi, T., Hardacre, C., Kegnæs, S., and Fan, X. (2020). "Effect of metal dispersion and support structure of Ni/silicalite-1 catalysts on non-thermal plasma (NTP) activated CO_2 hydrogenation." *Appl. Catal., B*, 272, 119013.

Chen, M., Zhong, Q., Ma, J., Zhang, Z., Liu, Y., Wei, Z., and Deng, S. (2023). "Highly efficient Ni–Mn/SiO_2 catalyst for the selective hydrogenation of biomass-derived levulinic acid to γ-valerolactone under mild conditions." *New J. Chem.*, 47(21), 10455–10462.

Chen, Z., Wang, Y., Cheng, H., and Zhou, H. (2022). "Hemicellulose degradation: An overlooked issue in acidic deep eutectic solvents pretreatment of lignocellulosic biomass." *Ind. Crops Prod.*, 187, 115335.

Chernyshev, V. M., Kravchenko, O. A., and Ananikov, V. P. (2017). "Conversion of plant biomass to furan derivatives and sustainable access to the new generation of polymers, functional materials and fuels." *Russ. Chem. Rev.*, 86(5), 357–387.

Chernysheva, D. V., Chus, Y. A., Klushin, V. A., Lastovina, T. A., Pudova, L. S., Smirnova, N. V., Kravchenko, O. A., Chernyshev, V. M., and Ananikov, V. P. (2018). "Sustainable utilization of biomass refinery wastes for accessing activated carbons and supercapacitor electrode materials." *ChemSusChem*, 11(20), 3599–3608.

Chhabra, T., Rohilla, J., and Krishnan, V. (2022). "Nanoarchitectonics of phosphomolybdic acid supported on activated charcoal for selective conversion of furfuryl alcohol and levulinic acid to alkyl levulinates." *Mol. Catal.*, 519, 112135.

Chung, S., De Haart, S., Parton, R., and Raveendran Shiju, N. (2022). "Conversion of furfuryl alcohol into alkyl–levulinates using solid acid catalysts." *Sustain. Chem. Clim. Act.*, 1, 100004.

Ciptonugroho, W., Mensah, J. B., Al-Shaal, G., and Palkovits, R. (2023). "WO_x/ZrO_2 catalysts for the conversion of α-angelica lactone with butanol to butyl levulinates." *Chem. Pap.*, 77(7), 3769–3778.

Cui, C., Zhang, Z., Zeng, Q., and Chen, B. (2016). "Insight into the synthesis of isosorbide diester plasticizer using immobilized lipases." *RSC Adv.*, 6(110), 108180–108186.

Da Silva, M. J., Chaves, D. M., Teixeira, M. G., and Oliveira Bruziquesi, C. G. (2021). "Esterification of levulinic acid over Sn(II) exchanged Keggin heteropolyacid salts: An efficient route to obtain bioaditives." *Mol. Catal.*, 504, 111495.

Das, A., Mondal, S., Hansda, K. M., Adak, M. K., and Dhak, D. (2023). "A critical review on the role of carbon supports of metal catalysts for selective catalytic hydrogenation of chloronitrobenzenes." *Appl. Catal., A*, 649, 118955.

Démolis, A., Essayem, N., and Rataboul, F. (2014). "Synthesis and applications of alkyl levulinates." *ACS Sustainable Chem. Eng.*, 2(6), 1338–1352.

Devi, A., Bajar, S., Kour, H., Kothari, R., Pant, D., and Singh, A. (2022). "Lignocellulosic biomass valorization for bioethanol production: A circular bioeconomy approach." *Bioenerg. Res.*, 15(4), 1820–1841.

Di Bucchianico, D. D. M., Wang, Y., Buvat, J.-C., Pan, Y., Casson Moreno, V., and Leveneur, S. (2022). "Production of levulinic acid and alkyl levulinates: A process insight." *Green Chem.*, 24(2), 614–646.

Dosarapu, V., Bandalla, S., Ravula, M., Bathula, G. B., Mavurapu, S., Shee, D., Varkolu, M., Baithy, M., and Vasam, C. S. (2023). "Insights into structure–activity relationships in efficient silica-supported Ni catalysts for selective hydrogenation of levulinic acid." *Sustainable Energy Fuels*, 7(15), 3609–3624.

Dusselier, M., Mascal, M., and Sels, B. F. (2014). "Top chemical opportunities from carbohydrate biomass: A chemist's view of the biorefinery." *Selective Catalysis for Renewable Feedstocks and Chemicals*, Topics in Current Chemistry, K. M. Nicholas, ed., Cham: Springer International Publishing, 1–40.

Dussenne, C., Delaunay, T., Wiatz, V., Wyart, H., Suisse, I., and Sauthier, M. (2017). "Synthesis of isosorbide: An overview of challenging reactions." *Green Chem.*, 19(22), 5332–5344.

Dutta, S., and Bhat, N. S. (2021). "Recent advances in the value addition of biomass-derived levulinic acid: A review focusing on its chemical reactivity patterns." *ChemCatChem*, 13(14), 3202–3222.

Dutta, S., Yu, I. K. M., Tsang, D. C. W., Ng, Y. H., Ok, Y. S., Sherwood, J., and Clark, J. H. (2019). "Green synthesis of gamma-valerolactone (GVL) through hydrogenation of biomass-derived levulinic acid using non-noble metal catalysts: A critical review." *Chem. Eng. J.*, 372, 992–1006.

Enumula, S. S., Gurram, V. R. B., Chada, R. R., Burri, D. R., and Kamaraju, S. R. R. (2017a). "Clean synthesis of alkyl levulinates from levulinic acid over one pot synthesized WO_3-SBA-16 catalyst." *J. Mol. Catal. A: Chem.*, 426, 30–38.

Enumula, S. S., Koppadi, K. S., Babu Gurram, V. R., Burri, D. R., and Rao Kamaraju, S. R. (2017b). "Conversion of furfuryl alcohol to alkyl levulinate fuel additives over Al_2O_3/SBA-15 catalyst." *Sustainable Energy Fuels*, 1(3), 644–651.

Eseyin, A., E., and Steele, P., H. (2015). "An overview of the applications of furfural and its derivatives." *Int. J. Adv. Chem*, 3(2), 42.

Fenouillot, F., Rousseau, A., Colomines, G., Saint-Loup, R., and Pascault, J.-P. (2010). "Polymers from renewable 1,4:3,6-dianhydrohexitols (isosorbide, isomannide and isoidide): A review." *Prog. Polym. Sci.*, 35(5), 578–622.

Fraile, J. M., and Saavedra, C. J. (2017). “Synthesis of isosorbide esters from sorbitol with heterogeneous catalysts.” *ChemistrySelect*, 2(3), 1013–1018.

Gao, Z., Zhou, Z., Wang, M., Shang, N., Gao, W., Cheng, X., Gao, S., Gao, Y., and Wang, C. (2023). “Highly dispersed Pd anchored on heteropolyacid modified ZrO_2 for high efficient hydrodeoxygenation of lignin-derivatives.” *Fuel*, 334, 126768.

Gautam, P., Barman, S., and Ali, A. (2022). “A comparative study on the performance of acid catalysts in the synthesis of levulinate ester using biomass-derived levulinic acid: a review.” *Biofuels, Bioprod. Biorefin.*, 16(4), 1095–1115.

Geboers, J. A., Van De Vyver, S., Ooms, R., Op De Beeck, B., Jacobs, P. A., and Sels, B. F. (2011). “Chemocatalytic conversion of cellulose: Opportunities, advances and pitfalls.” *Catal. Sci. Technol.*, 1(5), 714.

Gong, H., Zhang, J., Li, Q., Wei, L., Hu, Y., Rui, Y., and Shi, X.-L. (2023). “Catalytic conversion of levulinic acid or furfural alcohol into ethyl levulinate using a sulfonic acid-functionalized coffee biochar.” *Fuel*, 352, 129059.

Grochowski, M. R., Yang, W., and Sen, A. (2012). “Mechanistic study of a one-step catalytic conversion of fructose to 2,5-dimethyltetrahydrofuran.” *Chem. Eur. J.*, 18(39), 12363–12371.

Halliday, G. A., Young, R. J., and Grushin, V. V. (2003). “One-pot, two-step, practical catalytic synthesis of 2,5-diformylfuran from fructose.” *Org. Lett.*, 5(11), 2003–2005.

Haq, I., Qaisar, K., Nawaz, A., Akram, F., Mukhtar, H., Zohu, X., Xu, Y., Mumtaz, M., Rashid, U., Ghani, W., and Choong, T. (2021). “Advances in valorization of lignocellulosic biomass towards energy generation.” *Catalysts*, 11(3), 309.

Hara, M., Nakajima, K., and Kamata, K. (2015). “Recent progress in the development of solid catalysts for biomass conversion into high value-added chemicals.” *Sci. Technol. Adv. Mater.*, 16(3), 034903.

Hayes, D. J., Fitzpatrick, S., Hayes, M. H. B., and Ross, J. R. H. (2005). “The biofine process – Production of levulinic acid, furfural, and formic acid from lignocellulosic feedstocks.” *Biorefineries-Industrial Processes and Products*, B. Kamm, P. R. Gruber, and M. Kamm, eds., Wiley, 139–164.

He, L., Tao, M., Liu, Z., Cao, Z., Zhu, J., Gao, J., Bergh, W. V. D., Chailleux, E., Huang, Y., Vasconcelos, K., Cannone Falchetto, A., Balieu, R., Grenfell, J., Wilson, D. J., Valentin, J., Kowalski, K. J., Rzek, L., Gaspar, L., Ling, T., and Ma, Y. (2023). "Biomass valorization toward sustainable asphalt pavements: Progress and prospects." *Waste Management*, 165, 159–178.

He, M., Guo, J., Wang, X., Song, Y., Liu, S., Wang, H., and Li, C. (2020). "Direct conversion of cellulose into isosorbide over Ni doped $NbOPO_4$ catalysts in water." *New J. Chem.*, 44(25), 10292–10299.

Hoang, T. M. C., Van Eck, E. R. H., Bula, W. P., Gardeniers, J. G. E., Lefferts, L., and Seshan, K. (2015). "Humin based by-products from biomass processing as a potential carbonaceous source for synthesis gas production." *Green Chem.*, 17(2), 959–972.

Hu, L., Lin, L., and Liu, S. (2014). "Chemoselective hydrogenation of biomass-derived 5-hydroxymethylfurfural into the liquid biofuel 2,5-dimethylfuran." *Ind. Eng. Chem. Res.*, 53(24), 9969–9978.

Huang, R., Cheng, Y., Liu, H., Peng, L., and Zhang, J. (2023). "Catalytic transfer hydrogenation of levulinic acid to gamma-valerolactone over a zirconium-based FDCA hybrid: Insights into the effect of heteropoly acids." *Sustainable Energy Fuels*, 7(11), 2645–2652.

Huang, X., Liu, K., Vrijburg, W. L., Ouyang, X., Iulian Dugulan, A., Liu, Y., Tiny Verhoeven, M. W. G. M., Kosinov, N. A., Pidko, E. A., and Hensen, E. J. M. (2020). "Hydrogenation of levulinic acid to γ-valerolactone over Fe-Re/TiO_2 catalysts." *Appl. Catal., B*, 278, 119314.

Ibrahim, A., Liu, X., Uguna, C. N., and Sun, C. (2023). "Selective hydrogenation of levulinic acid to γ-valerolactone over copper based bimetallic catalysts derived from metal-organic frameworks." *Mat. Today Sustain.*, 23, 100424.

Ichikawa, N., Sato, S., Takahashi, R., Sodesawa, T., and Inui, K. (2004). "Dehydrogenative cyclization of 1,4-butanediol over copper-based catalyst." *J. Mol. Catal. A: Chem.*, 212(1–2), 197–203.

Inayat, A., Van Assche, A., Clark, J. H., and Farmer, T. J. (2018). "Greening the esterification between isosorbide and acetic acid." *Sustainable Chem. Pharm.*, 7, 41–49.

İzgi, M. S., Saka, C., Baytar, O., Saraçoğlu, G., and Şahin, Ö. (2019). "Preparation and characterization of activated carbon from microwave and conventional heated almond shells using phosphoric acid activation." *Anal. Lett.*, 52(5), 772–789.

Jaswal, A., Singh, P. P., and Mondal, T. (2022). "Furfural – A versatile, biomass-derived platform chemical for the production of renewable chemicals." *Green Chem.*, 24(2), 510–551.

Jayakumari, M. T., and Krishnan, C. K. (2023). "Tuning Al sites in Y-zeolite for selective production of γ-valerolactone from levulinic acid." *Appl. Catal., A,* 663, 119318.

Jesus, A. M. D., Romão, L. P. C., Araújo, B. R., Costa, A. S., and Marques, J. J. (2011). "Use of humin as an alternative material for adsorption/desorption of reactive dyes." *Desalination*, 274(1–3), 13–21.

Jiang, L., Xu, G., and Fu, Y. (2021). "A nitrogen-doped carbon modified nickel catalyst for the hydrogenation of levulinic acid under mild conditions." *Green Chem.*, 23(18), 7065–7073.

Jin, S., Ning, X., Cao, J., and Wang, Y. (2020). "Food safety risk assessment of γ-butyrolactone transformation into dangerous γ-hydroxybutyric acid in beverages by quantitative ^{13}C-NMR technique." *J. Food Qual.*, 2020, 1–7.

Jönsson, L. J., and Martín, C. (2016). "Pretreatment of lignocellulose: Formation of inhibitory by-products and strategies for minimizing their effects." *Bioresour. Technol.*, 199, 103–112.

Kadraoui, M., Maunoury, T., Derriche, Z., Guillarme, S., and Saluzzo, C. (2015). "Isohexides as versatile scaffolds for asymmetric catalysis." *Eur. J. Org. Chem.*, 2015(3), 441–457.

Kamble, P. A., Vinod, C. P., Rathod, V. K., and Kantam, M. L. (2023). "Hydrogenation of levulinic acid to gamma-valerolactone over nickel supported organoclay catalyst." *Catal. Today*, 408, 36–49.

Kang, S., Fu, J., Deng, Z., Jiang, S., Zhong, G., Xu, Y., Guo, J., and Zhou, J. (2018a). "Valorization of biomass hydrolysis waste: Activated carbon from humins as exceptional sorbent for wastewater treatment." *Sustainability*, 10(6), 1795.

Kang, S., Jiang, S., Peng, Z., Lu, Y., Guo, J., Li, J., Zeng, W., and Lin, X. (2018b). "Valorization of humins by phosphoric acid activation for activated carbon production." *Biomass Convers. Biorefin.*, 8(4), 889–897.

Khajone, V. B., Raut, S. U., Deshmukh, S. A., Bhansali, K. J., Balinge, K. R., Muskawar, P. N., and Bhagat, P. R. (2023). "Recyclable polymer-supported carboxyl functionalized Zn–porphyrin photocatalyst for transfer hydrogenation of levulinic acid to γ-valerolactone." *Biomass Convers. Biorefin.*, 13(10), 9107–9117.

Kim, J., and Han, J. (2021). "Bio-based process for the catalytic production of ethyl levulinate from cellulose." *Appl. Energy*, 300, 117430.

Kong, X., Zhang, X., Han, C., Li, C., Yu, L., and Liu, J. (2017). "Ethanolysis of biomass based furfuryl alcohol to ethyl levulinate over Fe modified USY catalyst." *Mol. Catal.*, 443, 186–192.

Kozhevnikov, I. V., Kloetstra, K. R., Sinnema, A., Zandbergen, H. W., and Van Bekkum, H. (1996). "Study of catalysts comprising heteropoly acid $H_3PW_{12}O_{40}$ supported on MCM-41 molecular sieve and amorphous silica." *J Mol Catal A: Chem*, 114(1–3), 287–298.

Kumaravel, S., Thiripuranthagan, S., Durai, M., Erusappan, E., and Vembuli, T. (2020). "Catalytic transfer hydrogenation of biomass-derived levulinic acid to γ-valerolactone over Sn/Al-SBA-15 catalysts." *New J. Chem.*, 44(20), 8209–8222.

Lam, E., and Luong, J. H. T. (2014). "Carbon materials as catalyst supports and catalysts in the transformation of biomass to fuels and chemicals." *ACS Catal.*, 4(10), 3393–3410.

Latos, P., Szelwicka, A., Boncel, S., Jurczyk, S., Swadźba-Kwaśny, M., and Chrobok, A. (2019). "Highly efficient synthesis of alkyl levulinates from α-angelica lactone, catalyzed with Lewis acidic trifloaluminate ionic liquids supported on carbon nanotubes." *ACS Sustainable Chem. Eng.*, 7(5), 5184–5191.

Li, B., Zhao, H., Fang, J., Li, J., Gao, W., Ma, K., Liu, C., Yang, H., Ren, X., and Dong, Z. (2022). "Ru nanoparticles anchored on porous N-doped carbon nanospheres for efficient catalytic hydrogenation of Levulinic acid to γ-valerolactone under solvent-free conditions." *J. Colloid Interface Sci.,* 623, 905–914.

Li, J., Zhao, S., Li, Z., Liu, D., Chi, Y., and Hu, C. (2021). "Efficient conversion of biomass-derived levulinic acid to γ-valerolactone over polyoxometalate@Zr-Based metal–organic frameworks: The synergistic effect of Brønsted and Lewis acidic sites." *Inorg. Chem.*, 60(11), 7785–7793.

Li, X., Lan, X., and Wang, T. (2016). "Highly selective catalytic conversion of furfural to γ-butyrolactone." *Green Chem.*, 18(3), 638–642.

Li, X., Li, Y., and Wang, T. (2019). "Effect of oxide supports on Pt-Ni bimetallic catalysts for the selective hydrogenation of biomass-derived 2(5H)-furanone." *Catal. Today*, 319, 93–99.

Li, X., Wan, W., Chen, J. G., and Wang, T. (2018). "Selective hydrogenation of biomass-derived 2(5H)-furanone to γ-butyrolactone over Ni-based bimetallic catalysts." *ACS Sustainable Chem. Eng.*, 6(12), 16039–16046.

Lima, C. G. S., Monteiro, J. L., de Melo Lima, T., Weber Paixão, M., and Corrêa, A. G. (2018). "Angelica lactones: From biomass-derived platform chemicals to value-added products." *ChemSusChem*, 11(1), 25–47.

Limousin, C., Cléophax, J., Loupy, A., and Petit, A. (1998). "Synthesis of benzoyl and dodecanoyl derivatives from protected carbohydrates under focused microwave irradiation." *Tetrahedron*, 54(44), 13567–13578.

Lin, Y., Yu, J., Zhang, X., Fang, J., Lu, G.-P., and Huang, H. (2022). "Carbohydrate-derived porous carbon materials: An ideal platform for green organic synthesis." *Chin. Chem. Lett.*, 33(1), 186–196.

Liu, S., Zhu, Y., Liao, Y., Wang, H., Liu, Q., Ma, L., and Wang, C. (2022a). "Advances in understanding the humins: Formation, prevention and application." *Appl. Energy Combust. Sci.*, 10, 100062.

Liu, X., Yang, W., Zhang, Q., Li, C., and Wu, H. (2020). "Current approaches to alkyl levulinates via efficient valorization of biomass derivatives." *Front. Chem.*, 8, 794.

Liu, Y., Liu, K., Zhang, M., Zhang, K., Ma, J., Xiao, S., Wei, Z., and Deng, S. (2022b). "Highly efficient selective hydrogenation of levulinic acid to γ-valerolactone over Cu–Re/TiO_2 bimetallic catalysts." *RSC Adv.*, 12(1), 602–610.

Liu, Z., Gao, X., and Song, G. (2023). "Synergy of ultra-low-loaded ruthenium with alumina stimulating the catalytic hydrogenation of levulinic acid into γ-valerolactone." *Chem. Eng. J.*, 470, 143869.

Lobato-Peralta, D. R., Duque-Brito, E., Villafán-Vidales, H. I., Longoria, A., Sebastian, P. J., Cuentas-Gallegos, A. K., Arancibia-Bulnes, C. A., and Okoye, P. U. (2021). "A review on trends in lignin extraction and valorization of lignocellulosic biomass for energy applications." *J. Cleaner Prod.*, 293, 126123.

Lu, Y., Wang, Y., Tang, Q., Cao, Q., and Fang, W. (2022). "Synergy in Sn-Mn oxide boosting the hydrogenation catalysis of supported Pt nanoparticles for selective conversion of levulinic acid." *Appl. Catal., B*, 300, 120746.

Lucas, N., Gurrala, L., and Athawale, A. (2019). "Heteropolyacids supported on mesoporous AlSBA-15 as efficient catalysts for esterification of levulinic acid." *J. Porous Mater.*, 26(5), 1335–1343.

Luo, X., Wu, H., Li, C., Li, Z., Li, H., Zhang, H., Li, Y., Su, Y., and Yang, S. (2020). "Heteropoly acid-based catalysts for hydrolytic depolymerization of cellulosic biomass." *Front. Chem.*, 8, 580146.

Luo, Y., Li, Z., Li, X., Liu, X., Fan, J., Clark, J. H., and Hu, C. (2019). "The production of furfural directly from hemicellulose in lignocellulosic biomass: A review." *Catal. Today*, 319, 14–24.

Mamun, O., Saleheen, M., Bond, J. Q., and Heyden, A. (2017). "Importance of angelica lactone formation in the hydrodeoxygenation of levulinic acid to γ-valerolactone over a Ru(0001) model surface." *J. Phys. Chem. C*, 121(34), 18746–18761.

Mariscal, R., Maireles-Torres, P., Ojeda, M., Sádaba, I., and López Granados, M. (2016). "Furfural: A renewable and versatile platform molecule for the synthesis of chemicals and fuels." *Energy Environ. Sci.*, 9(4), 1144–1189.

Marubayashi, H., Ushio, T., and Nojima, S. (2017). "Crystallization of polyesters composed of isohexides and aliphatic dicarboxylic acids: Effects of isohexide

stereoisomerism and dicarboxylic acid chain length." *Polym. Degrad. Stab.*, 146, 174–183.

Mascal, M., and Dutta, S. (2014). "Chemical-catalytic approaches to the production of furfurals and levulinates from biomass." *Selective Catalysis for Renewable Feedstocks and Chemicals*, Topics in Current Chemistry, K. M. Nicholas, ed., Cham: Springer International Publishing, 41–83.

Mascal, M., Dutta, S., and Gandarias, I. (2014). "Hydrodeoxygenation of the angelica lactone dimer, a cellulose-based feedstock: Simple, high-yield synthesis of branched C_7–C_{10} gasoline-like hydrocarbons." *Angew Chem. Int. Ed.*, 53(7), 1854–1857.

Matt, L., Parve, J., Parve, O., Pehk, T., Pham, T. H., Liblikas, I., Vares, L., and Jannasch, P. (2018). "Enzymatic Synthesis and polymerization of isosorbide-based monomethacrylates for high-T_g plastics." *ACS Sustainable Chem. Eng.*, 6(12), 17382–17390.

Maumela, M., Marx, S., and Meijboom, R. (2021). "Heterogeneous Ru catalysts as the emerging potential superior catalysts in the selective hydrogenation of bio-derived levulinic acid to γ-valerolactone: Effect of Particle size, solvent, and support on activity, stability, and selectivity." *Catalysts*, 11(2), 292.

Merenda, A., Orr, S. A., Liu, Y., Hernández Garcia, B., Osatiashtiani, A., Morales, G., Paniagua, M., Melero, J. A., Lee, A. F., and Wilson, K. (2023). "Continuous flow (sulfated) zirconia catalysed cascade conversion of levulinic acid to γ-valerolactone." *ChemCatChem*, 15(3), e202201224.

Mija, A., Van Der Waal, J. C., Pin, J.-M., Guigo, N., and De Jong, E. (2017). "Humins as promising material for producing sustainable carbohydrate-derived building materials." *Constr. Build. Mater.*, 139, 594–601.

Mohammadbagheri, Z., and Chermahini, A. N. (2019). "Catalytic conversion of furfuryl alcohol to n-hexyl levulinate using modified dendritic fibrous nanosilica." *Chem. Eng. J.*, 361, 450–460.

Nonque, F., Benlahoues, A., Audourenc, J., Sahut, A., Saint-Loup, R., Woisel, P., and Potier, J. (2021). "Study on polymerization of bio-based isosorbide monomethacrylate

for the formation of low-T and high-T sustainable polymers." *Eur. Polym. J.*, 160, 110799.

Nonque, F., Sahut, A., Jacquel, N., Saint-Loup, R., Woisel, P., and Potier, J. (2020). "Isosorbide monoacrylate: A sustainable monomer for the production of fully bio-based polyacrylates and thermosets." *Polym. Chem.*, 11(43), 6903–6909.

Ohyama, J., Sato, T., Yamamoto, Y., Arai, S., and Satsuma, A. (2013). "Size specifically high activity of Ru nanoparticles for hydrogen oxidation reaction in alkaline electrolyte." *J. Am. Chem. Soc.*, 135(21), 8016–8021.

Okolie, J. A., Epelle, E. I., Tabat, M. E., Orivri, U., Amenaghawon, A. N., Okoye, P. U., and Gunes, B. (2022). "Waste biomass valorization for the production of biofuels and value-added products: A comprehensive review of thermochemical, biological and integrated processes." *Process Saf. Environ. Prot.*, 159, 323–344.

Onkarappa, S. B., Bhat, N. S., and Dutta, S. (2020). "Preparation of alkyl levulinates from biomass-derived 5-(halomethyl)furfural (X = Cl, Br), furfuryl alcohol, and angelica lactone using silica-supported perchloric acid as a heterogeneous acid catalyst." *Biomass Convers. Biorefin.*, 10(4), 849–856.

Pachamuthu, M. P., Srinivasan, V. V., Karvembu, R., and Luque, R. (2019). "Preparation of mesoporous stannosilicates SnTUD-1 and catalytic activity in levulinic acid esterification." *Microporous Mesoporous Mater.*, 287, 159–166.

Patil, S. K. R., Heltzel, J., and Lund, C. R. F. (2012). "Comparison of structural features of humins formed catalytically from glucose, fructose, and 5-hydroxymethylfurfuraldehyde." *Energy Fuels*, 26(8), 5281–5293.

Patil, S. K. R., and Lund, C. R. F. (2011). "Formation and growth of humins via aldol addition and condensation during acid-catalyzed conversion of 5-hydroxymethylfurfural." *Energy Fuels*, 25(10), 4745–4755.

Pileidis, F. D., and Titirici, M. (2016). "Levulinic acid biorefineries: New challenges for efficient utilization of biomass." *ChemSusChem*, 9(6), 562–582.

Prajapati, R., Srivastava, S., Jadeja, G. C., and Parikh, J. (2023). "A novel SBA-15/H-ZSM-5 composite catalyst for conversion of furfuryl alcohol to ethyl levulinate." *Waste Biomass Valorization*, 14(2), 609–618.

Qian, W., Tan, X., Su, Q., Cheng, W., Xu, F., Dong, L., and Zhang, S. (2019). "Transesterification of isosorbide with dimethyl carbonate catalyzed by task-specific ionic liquids." *ChemSusChem*, 12(6), 1169–1178.

Ragno, D., Leonardi, C., Di Carmine, G., Bortolini, O., Brandolese, A., De Risi, C., and Massi, A. (2021). "Regiodivergent isosorbide acylation by oxidative N-heterocyclic carbene catalysis in batch and continuous flow." *ACS Sustainable Chem. Eng.*, 9(24), 8295–8305.

Raguindin, R. Q., Desalegn, B. Z., Gebresillase, M. N., and Seo, J. G. (2022). "Yolk-shell nickel–cobalt phosphides as bifunctional catalysts in the solvent-free hydrogenation of levulinic acid to gamma-valerolactone." *Renewable Energy*, 191, 763–774.

Rashid, U., and Anwar, F. (2008). "Production of biodiesel through base-catalyzed transesterification of safflower oil using an optimized protocol." *Energy Fuels*, 22(2), 1306–1312.

Ren, L., Yang, M.-M., Tung, C.-H., Wu, L.-Z., and Cong, H. (2017). "Visible-light photocatalysis employing dye-sensitized semiconductor: Selective aerobic oxidation of benzyl ethers." *ACS Catal.*, 7(12), 8134–8138.

Rosatella, A. A., Simeonov, S. P., Frade, R. F. M., and Afonso, C. A. M. (2011). "5-Hydroxymethylfurfural (HMF) as a building block platform: Biological properties, synthesis and synthetic applications." *Green Chem.*, 13(4), 754.

Rose, M., and Palkovits, R. (2012). "Isosorbide as a renewable platform chemical for versatile applications—Quo vadis?" *ChemSusChem*, 5(1), 167–176.

Sajid, M., Farooq, U., Bary, G., Azim, M. M., and Zhao, X. (2021). "Sustainable production of levulinic acid and its derivatives for fuel additives and chemicals: Progress, challenges, and prospects." *Green Chem.*, 23(23), 9198–9238.

Saska, J., Dutta, S., Kindler, A., Zuend, S. J., and Mascal, M. (2021). "Efficient and scalable production of isoidide from isosorbide." *ACS Sustainable Chem. Eng.*, 9(34), 11565–11570.

Schwarz, W., Schossig, J., Rossbacher, R., Pinkos, R., and Höke, H. (2019). "Butyrolactone." *Ullmann's Encyclopedia of Industrial Chemistry*, Wiley-VCH Verlag GmbH & Co. KGaA, ed., Wiley, 1–7.

Seretis, A., Diamantopoulou, P., Thanou, I., Tzevelekidis, P., Fakas, C., Lilas, P., and Papadogianakis, G. (2020). "Recent advances in ruthenium-catalyzed hydrogenation reactions of renewable biomass-derived levulinic acid in aqueous media." *Front. Chem.*, 8, 221.

Shao, S., Yang, Y., Guo, S., Hao, S., Yang, F., Zhang, S., Ren, Y., and Ke, Y. (2021). "Highly active and stable Co nanoparticles embedded in nitrogen-doped mesoporous carbon nanofibers for aqueous-phase levulinic acid hydrogenation." *Green Energy Environ.*, 6(4), 567–577.

Shen, F., Xiong, X., Fu, J., Yang, J., Qiu, M., Qi, X., and Tsang, D. C. W. (2020). "Recent advances in mechanochemical production of chemicals and carbon materials from sustainable biomass resources." *Renewable Sustainable Energy Rev.*, 130, 109944.

Shestakova, P., Popova, M., Szegedi, Á., Lazarova, H., Nga Luong, T. K., Trendafilova, I., Mihály, J., and Parac-Vogt, T. N. (2021). "Hybrid catalyst with combined Lewis and Brønsted acidity based on Zr^{IV} substituted polyoxometalate grafted on mesoporous MCM-41 silica for esterification of renewable levulinic acid." *Microporous Mesoporous Mater.*, 323, 111203.

Siddiqui, N., Pendem, C., Goyal, R., Khatun, R., Khan, T. S., Samanta, C., Chiang, K., Shah, K., Ali Haider, M., and Bal, R. (2022). "Study of γ-valerolactone production from hydrogenation of levulinic acid over nanostructured Pt-hydrotalcite catalysts at low temperature." *Fuel*, 323, 124272.

Solanki, B. S., and Rode, C. V. (2019). "Selective hydrogenolysis of 5-(hydroxymethyl)furfural over Pd/C catalyst to 2,5-dimethylfuran." *J. Saudi Chem. Soc.*, 23(4), 439–451.

Song, S., Fung Kin Yuen, V., Di, L., Sun, Q., Zhou, K., and Yan, N. (2020). "Integrating biomass into the organonitrogen chemical supply chain: Production of pyrrole and D-proline from furfural." *Angew Chem. Int. Ed.*, 59(45), 19846–19850.

Sorokina, S. A., Mikhailov, S. P., Kuchkina, N. V., Bykov, A. V., Vasiliev, A. L., Ezernitskaya, M. G., Golovin, A. L., Nikoshvili, L. Zh., Sulman, M. G., and Shifrina, Z. B. (2022). "Ru@hyperbranched polymer for hydrogenation of levulinic acid to gamma-valerolactone: The role of the catalyst support." *Int. J. Mol. Sci.*, 23(2), 799.

Srinivasa Rao, S. B., Krishna Kumari, P., Dhana Lakshmi, D., and Lingaiah, N. (2018). "One pot selective transformation of biomass derived chemicals towards alkyl levulinates over titanium exchanged heteropoly tungstate catalysts." *Catal. Today*, 309, 269–275.

Sych, N. V., Trofymenko, S. I., Poddubnaya, O. I., Tsyba, M. M., Sapsay, V. I., Klymchuk, D. O., and Puziy, A. M. (2012). "Porous structure and surface chemistry of phosphoric acid activated carbon from corncob." *Appl. Surf. Sci.*, 261, 75–82.

Takkellapati, S., Li, T., and Gonzalez, M. A. (2018). "An overview of biorefinery-derived platform chemicals from a cellulose and hemicellulose biorefinery." *Clean Technol. Environ. Policy*, 20(7), 1615–1630.

Tang, Y., Fu, J., Wang, Y., Guo, H., and Qi, X. (2023). "Bimetallic Ni-Zn@OMC catalyst for selective hydrogenation of levulinic acid to γ-valerolactone in water." *Fuel Process. Technol.*, 240, 107559.

Thiyagarajan, S., Wu, J., Knoop, R. J. I., Van Haveren, J., Lutz, M., and Van Es, D. S. (2014). "Isohexide hydroxy esters: Synthesis and application of a new class of biobased AB-type building blocks." *RSC Adv.*, 4(89), 47937–47950.

Thompson, P. (2012). "The agricultural ethics of biofuels: The food vs. fuel debate." *Agriculture*, 2(4), 339–358.

Tian, Y., Zhang, F., Wang, J., Cao, L., and Han, Q. (2021). "A review on solid acid catalysis for sustainable production of levulinic acid and levulinate esters from biomass derivatives." *Bioresour. Technol.*, 342, 125977.

Tiwari, M. S., Dicks, J. S., Keogh, J., Ranade, V. V., and Manyar, H. G. (2020). "Direct conversion of furfuryl alcohol to butyl levulinate using tin exchanged tungstophosphoric acid catalysts." *Mol. Catal.*, 488, 110918.

Tomishige, K., Yabushita, M., Cao, J., and Nakagawa, Y. (2022). "Hydrodeoxygenation of potential platform chemicals derived from biomass to fuels and chemicals." *Green Chem.*, 24(15), 5652–5690.

Vinod, N., Bandibairanahalli Onkarappa, S., Madhwaraj Girija, V., and Dutta, S. (2023). "A straightforward preparation of levulinic esters from biorenewable levulinic acid using methanesulfonic acid supported on silica gel (MSA-SG) as an efficient heterogeneous catalyst." *Mater. Today: Proc.*, 76, 18–24.

Wang, D., Luo, M., Yue, L., Wei, J., Zhang, X., and Cai, J. (2022). "Co-embedded N-doped hierarchical porous biocarbons: Facile synthesis and used as highly efficient catalysts for levulinic acid hydrogenation." *Fuel*, 329, 125364.

Wang, S., Cheng, A., Liu, F., Zhang, J., Xia, T., Zeng, X., Fan, W., and Zhang, Y. (2023a). "Catalytic conversion network for lignocellulosic biomass valorization: A panoramic view." *Ind. Chem. Mater.*, 1(2), 188–206.

Wang, S., Lin, H., Zhao, Y., Chen, J., and Zhou, J. (2016). "Structural characterization and pyrolysis behavior of humin by-products from the acid-catalyzed conversion of C6 and C5 carbohydrates." *J. Anal. Appl. Pyrolysis*, 118, 259–266.

Wang, T., Nolte, M. W., and Shanks, B. H. (2014). "Catalytic dehydration of C_6 carbohydrates for the production of hydroxymethylfurfural (HMF) as a versatile platform chemical." *Green Chem.*, 16(2), 548–572.

Wang, X., Qi, X., Qiu, M., Shen, F., Yang, J., and Shen, B. (2023b). "Bimetallic ordered mesoporous carbon from lignin for catalytic selective hydrogenation of levulinic acid to γ-valerolactone." *Fuel*, 341, 127720.

Wang, Y., Zhao, D., Triantafyllidis, K. S., Ouyang, W., Luque, R., and Len, C. (2020). "Microwave-assisted catalytic upgrading of bio-based furfuryl alcohol to alkyl levulinate over commercial non-metal activated carbon." *Mol. Catal.*, 480, 110630.

Wu, Y., Wang, H., Peng, J., and Ding, M. (2023). "Advances in catalytic valorization of cellulose into value-added chemicals and fuels over heterogeneous catalysts." *Catal. Today*, 408, 92–110.

Wu, Y., Ye, X., Yang, X., Wang, X., Chu, W., and Hu, Y. (1996). "Heterogenization of heteropolyacids: A general discussion on the preparation of supported acid catalysts." *Ind. Eng. Chem. Res.*, 35(8), 2546–2560.

Xiang, J., Yang, S., Zhang, J., Wu, J., Shao, Y., Wang, Z., and Yang, M. (2022). "The preparation of sorbitol and its application in polyurethane: A review." *Polym. Bull.*, 79(4), 2667–2684.

Xu, C., Paone, E., Rodríguez-Padrón, D., Luque, R., and Mauriello, F. (2020a). "Recent catalytic routes for the preparation and the upgrading of biomass derived furfural and 5-hydroxymethylfurfural." *Chem. Soc. Rev.*, 49(13), 4273–4306.

Xu, H., Hu, D., Lin, L., Zhang, M., Li, X., Zeng, Y., Amer, M., Luo, W., and Yan, K. (2023a). "MOF-derived bimetallic NiCo nanoalloys for the hydrogenation of biomass-derived levulinic acid to γ-valerolactone." *AIChE Journal*, 69(2), e17973.

Xu, Y., Liang, Y., Guo, H., and Qi, X. (2023b). "Catalytic hydrogenation of levulinic acid to γ-valerolactone over lignin-metal coordinated carbon nanospheres in water." *Int. J. Biol. Macromol.*, 240, 124451.

Xu, Z., Yang, Y., Yan, P., Xia, Z., Liu, X., and Zhang, Z. C. (2020b). "Mechanistic understanding of humin formation in the conversion of glucose and fructose to 5-hydroxymethylfurfural in [BMIM]Cl ionic liquid." *RSC Adv.*, 10(57), 34732–34737.

Yakout, S. M., and Sharaf El-Deen, G. (2016). "Characterization of activated carbon prepared by phosphoric acid activation of olive stones." *Arabian J. Chem.*, 9, S1155–S1162.

Yan, K., Wu, G., Lafleur, T., and Jarvis, C. (2014). "Production, properties and catalytic hydrogenation of furfural to fuel additives and value-added chemicals." *Renewable Sustainable Energy Rev*, 38, 663–676.

Yan, L., Yao, Q., and Fu, Y. (2017). "Conversion of levulinic acid and alkyl levulinates into biofuels and high-value chemicals." *Green Chem.*, 19(23), 5527–5547.

Yang, J., Niu, X., Wu, H., Zhang, H., Ao, Z., and Zhang, S. (2020). "Valorization of humin as a glucose derivative to fabricate a porous carbon catalyst for esterification and hydroxyalkylation/alkylation." *Waste Management*, 103, 407–415.

Yi, X., Al-Shaal, M. G., Ciptonugroho, W., Delidovich, I., Wang, X., and Palkovits, R. (2017). "Synthesis of butyl levulinate based on α-angelica lactone in the presence of easily separable heteropoly acid aatalysts." *ChemSusChem*, 10(7), 1494–1500.

Yong, K. J., Wu, T. Y., Lee, C. B. T. L., Lee, Z. J., Liu, Q., Jahim, J. M., Zhou, Q., and Zhang, L. (2022). "Furfural production from biomass residues: Current technologies, challenges and future prospects." *Biomass Bioenergy*, 161, 106458.

Yu, N., Lu, H., Yang, W., Zheng, Y., Hu, Q., Liu, Y., Wu, K., and Liang, B. (2022). "Transfer hydrogenation of levulinic acid to γ-valerolactone over acid site-modified CuNi alloy." *Biomass Convers. Biorefin., 1-12.*

Yu, X., Liu, H., Wang, Q., Jia, W., Wang, H., Li, W., Zheng, J., Sun, Y., Tang, X., Zeng, X., Xu, F., and Lin, L. (2021). "Selective oxidation of furfural to 2(5h)-furanone and maleic acid over $CuMoO_4$." *ACS Sustainable Chem. Eng.*, 9(39), 13176–13187.

Yu, Z., Lu, X., Bai, H., Xiong, J., Feng, W., and Ji, N. (2020a). "Effects of solid acid supports on the bifunctional catalysis of levulinic acid to γ-valerolactone: Catalytic activity and stability." *Chem. - Asian J.*, 15(8), 1182–1201.

Yu, Z., Lu, X., Xiong, J., Li, X., Bai, H., and Ji, N. (2020b). "Heterogeneous catalytic hydrogenation of levulinic acid to γ-valerolactone with formic acid as internal hydrogen source." *ChemSusChem*, 13(11), 2916–2930.

Yu, Z., Meng, F., Wang, Y., Sun, Z., Liu, Y., Shi, C., Wang, W., and Wang, A. (2020c). "Catalytic transfer hydrogenation of levulinic acid to γ-valerolactone over Ni_3P-$CePO_4$ catalysts." *Ind. Eng. Chem. Res.*, 59(16), 7416–7425.

Zainol, M. M., Asmadi, M., Iskandar, P., Wan Ahmad, W. A. N., Amin, N. A. S., and Hoe, T. T. (2021). "Ethyl levulinate synthesis from biomass derivative chemicals using iron doped sulfonated carbon cryogel catalyst." *J. Cleaner Prod.*, 281, 124686.

Zhang, K., Meng, Q., Wu, H., Yuan, T., Han, S., Zhai, J., Zheng, B., Xu, C., Wu, W., He, M., and Han, B. (2021a). "Levulinic acid hydrogenation to γ-valerolactone over single Ru atoms on a TiO_2@nitrogen doped carbon support." *Green Chem.*, 23(4), 1621–1627.

Zhang, M., Tu, Y., Zhou, Z., and Wu, G. (2020). "Balancing the transesterification reactivity of isosorbide with diphenyl carbonate: Preferential activation of *exo* -OH." *Polym. Chem.*, 11(34), 5512–5525.

Zhang, P., Yuan, Q., Chen, L., Xue, T., Guan, Y., and Wu, P. (2016). "Low temperature hydrogenation of α-angelica lactone on silica supported Pd–NiO catalysts with synergistic effect." *RSC Adv.*, 6(70), 65377–65382.

Zhang, Q., Luo, Q., Wu, Y., Yu, R., Cheng, J., and Zhang, Y. (2021b). "Construction of a Keggin heteropolyacid/Ni-MOF catalyst for esterification of fatty acids." *RSC Adv.*, 11(53), 33416–33424.

Zhao, D., Prinsen, P., Wang, Y., Ouyang, W., Delbecq, F., Len, C., and Luque, R. (2018). "Continuous flow alcoholysis of furfuryl alcohol to alkyl levulinates using zeolites." *ACS Sustainable Chem. Eng.*, 6(5), 6901–6909.

Zhou, S., Wu, L., Bai, J., Lei, M., Long, M., and Huang, K. (2022). "Catalytic esterification of levulinic acid into the biofuel n-butyl levulinate over nanosized TiO_2 particles." *Nanomaterials*, 12(21), 3870.

LIST OF PUBLICATIONS

Journal publications published/communicated from this thesis work

1. **Vinod, N.**, Dutta, S. (2023). "Production of alkyl levulinates from carbohydrate-derived chemical intermediates using phosphotungstic acid supported on humin-derived activated carbon (PTA/HAC) as a recyclable catalyst." *Chemistry*, 5(2), 800-812.
2. **Vinod, N.**, Dutta, S. (2023). "Renewable synthesis of γ-butyrolactone from biomass-derived 2-furanone using palladium supported on humin-derived activated carbon (Pd/HAC) as a heterogeneous catalyst." *RSC Adv.*, 13, 15141-15147.
3. **Vinod, N.**, Bhat, N. S., Nayak, M. K., Jana, A., Tarafder, K., Mal, S. S., Dutta, S. (2023). "Efficient preparation of the esters of biomass-derived isohexides by base-catalyzed transesterification under solvent-free conditions." *Ind. Eng. Chem. Res.*, 62(43), 17483-17492.
4. **Vinod, N.**, Dutta, S. (2023). "Humin-derived activated carbon integrated with acid- and metal-sites as bifunctional heterogeneous catalyst for the efficient preparation of γ-valerolactone starting from biomass-derived levulinic acid." Communicated.

Journal publications from other projects

1. **Vinod, N.**, Onkarappa, S.B., Girija, V.M., and Dutta, S. (2023). "A straightforward preparation of levulinic esters from biorenewable levulinic acid using methanesulfonic acid supported on silica gel (MSA-SG) as an efficient heterogeneous catalyst." *Mater. Today: Proc.*, 76, 18-24.
2. **Vinod, N.**, Anchan, H. N., Bhat, N. S., Prabhakar, P. S., Dutta, S. (2022). "Catalytic conversion of glucose and its biopolymers into renewable compounds by inducing C–C bond scission and formation." *Biomass Convers. Biorefin.*, DOI: 10.1007/s13399-022-03105-9.
3. **Vinod, N.**, and Dutta, S. (2021). "Energy Densification of Biomass-Derived Furfurals to Furanic Biofuels by Catalytic Hydrogenation and Hydrodeoxygenation Reactions." *Sustainable Chemistry*, 2(3), 521–549.

4. Bhat, N. S., **Vinod, N.**, Onkarappa, S. B., and Dutta, S. (2020). "Hydrochloric acid-catalyzed coproduction of furfural and 5-(chloromethyl)furfural assisted by a phase transfer catalyst." *Carbohydr. Res.*, 496, 108105.
5. **Vinod, N.**, Tiwari, R., Bhat, N. S., Mal, S. S., Dutta, S. (2020). "High-yielding synthesis of alkyl stearates from stearic acid within a closed batch reactor using heteropolyacids as efficient and recyclable catalyst." *AIP Conference Proceedings*, 2225(1), 070004.

PATENT

1. Bhat, N. S., Dutta, S., Tarafder, K. **Vinod, N.**, Transesterification of isohexides under solvent-free conditions (Published, Patent Application Number: IN202241069622).

BOOK CHAPTER

1. Dutta, S., Bhat, N. S., **Vinod, N.**, (2020). "Oxidation and reduction of biomass-derived 5-(hydroxymethyl)furfural and levulinic acid by nanocatalysis." In *Advanced Heterogeneous Catalysts Volume 1: Applications at the Nano-Scale*, American Chemical Society, pp. 239-259.

CONFERENCES ATTENDED

1. Presented oral presentation on TEQIP-III sponsored international conference on "**Energy and Environmental Technologies for Sustainable Development**" organized by Department of Chemical Engineering, MNNIT Allahabad, Prayagraj, India, during 14-16 February 2020.

2. Presented oral presentation on international conference on "**Advances in Chemical and Material Sciences-ACMS 2022**" organized by Indian Institute of Chemical Engineers, Kolkata, India during 14-16 April 2022.

Miss Nivedha Vinod

C.V House, Muringeri P.O, Kannur, Kerala-670612
Mo. +91-7034607693; Email: nivedhavinod@gmail.com

Personal Information:

Date of Birth: November 20, 1994

Sex: Female

Nationality: Indian

Languages: 1. English: Proficient, 2. Malayalam: Proficient (native), 3. Hindi: Basic, 4. Kannada: Basic

Mailing Address: 605 Science Block, Dept. of Chemistry, NITK, Surathkal, Mangaluru-575025, Karnataka, India.

Educational Qualifications:

Bachelor of Science (2013-2016) in Chemistry, Physics, and Mathematics from Nirmalagiri College, Kannur University, Kerala, India. CGPA: 3.42/4, First Class with distinction.

Master of Science (2016-2018) in Chemistry from National Institute of Technology Karnataka, Surathkal, India. CGPA: 7.74/10, First Class.

Previous Research Experience:

M. Sc. Research (major project) in National Institute of Technology Karnataka, Surathkal, India. (Dec, 2017- May, 2018)

Title of Thesis: *Heteropoly Acids as Green Catalyst for the Esterification of Stearic Acid*

Profile of Google Scholar:

https://scholar.google.com/citations?user=uMR5QFEAAAAJ&hl=en

Professional Skills:

- Multi-step organic synthesis, green chemistry and catalysis, high pressure and high temperature reactions.
- Hands-on experience in handling high pressure-glass reactors and Hastelloy-made High-pressure reactor.
- Hands-on experience in analytical instruments (FTIR, UV-Vis, and TGA).
- A regular compute operation in MS word, Excel, power point presentation, Chem Draw, Mestrelab Mestrenova, SciFinder, Bruker Topspin, Adobe products, etc.